

# **JUACEP Program 2017**

## **at University of Michigan & UCLA**



Japan-US Advanced Collaborative Education Program

Nagoya University

## Table of Contents

<1> About the Program	
(a) Overview.....	2
(b) Participants.....	3
(c) Schedule.....	4
<2> Research Reports.....	5
<3> Research Presentations.....	43
● For 2017 Short-term course.....	44
● For 2017 Medium-term course.....	45
<4> Findings through JUACEP.....	57
● Students' reviews .....	58
● Questionnaires (in Japanese).....	68



## <1> About the Program

- (a) Overview ...2
- (b) Participants ...3
- (c) Schedule ...4



With UCLA research group members



With UM research group members

## (a) Overview

JUACEP provides three program courses for students of the Graduate School of Engineering at Nagoya University to study abroad: a short-term (two months) course; a medium-term (six months) course; a long-term (eight months) course. Choosing one of those courses the selected students are offered an opportunity to work together with faculty and other researchers or students from all over the world at the world's top universities.

Each student works on a research project related to his/her own master's thesis topic while belonging to a specialized research group of the University of Michigan or UCLA. In addition to research implementation, the students are expected to attend lab seminars, lab discussions and other events. At the end of each course, the students are required to submit a research report to their mentors at the host institution, then give a research presentation based on their achievements in front of the faculty and peer students at JUACEP Workshop held in Nagoya University. The report and the presentation are primary requisites for course credits of the program.

This publication is compiling the activities of the following students.

- [a] One student of short-term course from August to September 2017 at Univ. Michigan
- [b] Six students of medium-term course from August 2017 to January 2018 at Univ. Michigan
- [c] Three student of medium-term course from August 2017 to January 2018 at UCLA

JUACEP 2017 Short and Medium-term Courses Flowchart

	Short-term course	Medium-term course
January 2017	Public announcement and accepting application (Jan. - Mar.)	
February		
March		
April	Screening of candidates	
May	Selected students approach UM/UCLA faculty to get post of 'Visiting Scholar' (called *VGR at UCLA). After acceptance by faculty, **DS-2019 procedure starts including examination of CV, English proficiency and other qualification.	
June		
July	J-1 Visa application	
August	[a] Short-term course study at UM from Aug. to Sep. 2017	[b, c] Medium-term course study at UM/UCLA from Aug. 2017 to Jan. 2018
September		
October	Research Presentation, Sep. 29 2017	
November		
January 2018		
February		
March		
April		

\*VGR: Visiting Graduate Researcher for UCLA

\*\*DS-2019: Certificate of eligibility to obtain J-1 Visa

## (b) Participants

### University of Michigan

#### Short-term course: August 8, 2017 - September 22, 2017

Name		Advisor at NU	Advisor at UM
Yoshiyuki Tange 丹下 祥之	M1	Prof. Takeo Matsumoto Mechanical Systems Engineering	Prof. Katsuo Kurabayashi Mechanical Engineering

#### Medium-term course: August 8, 2017 - January 26, 2018

Hiroki Fujiwara 藤原 弘貴	M1	Assoc. Prof. Akira Iwakawa Aerospace Engineering	Assoc.Prof. Mirko Gamba Aerospace Engineering
Makoto Takeuchi 竹内 惇	M1	Prof. Noritsugu Umehara Micro-Nano Mechanical Science and Engineering	Prof. Richard M. Laine Materials Science and Engineering
Taro Mizutani 水谷 太郎	M1	Prof. Eiji Shamoto Aerospace Engineering	Prof. S. Jack Hu Mechanical Engineering
Makoto Terada 寺田 真	M1	Prof. Noritsugu Umehara Micro-Nano Mechanical Science and Engineering	Prof. Albert J. Shih Mechanical Engineering
Tatsuya Okamoto 岡本 竜也	M1	Prof. Noritsugu Umehara Micro-Nano Mechanical Science and Engineering	Prof. L. Jay Guo Electrical Engineering and Computer Science
Yudai Suzuki 鈴木 雄大	M1	Assoc. Prof. Daisuke Tsubakino Aerospace Engineering	Assoc.Prof. Anouck Girard Aerospace Engineering

### UCLA

#### Medium-term course: August 8, 2017 - January 26, 2018

Yusuke Fukui 福井 雄佑	M1	Prof. Yoji Yamada Mechanical Systems Engineering	Prof. Jacob Rosen Mechanical and Aerospace Engineering
Fuga Matsubara 松原 風我	M1	Prof. Yang Ju Micro-Nano Mechanical Science and Engineering	Prof. Benjamin M. Wu Bioengineering
Kai Iio 飯尾 魁	M2	Prof. Katsutoshi Hori Biomolecular Engineering	Prof. Gerard C. L. Wong Bioengineering

#### Coordinators at Partner Universities

Prof. Katsuo Kurabayashi  
Prof. Jenn-Ming Yang

Mechanical Engineering, University of Michigan  
Materials Science and Engineering, UCLA

#### JUACEP Members

Prof. Noritsugu Umehara      Micro-Nano Mechanical Science and Engineering  
Prof. Yang Ju                      Micro-Nano Mechanical Science and Engineering  
Prof. Toshiro Matsumoto        Mechanical Systems Engineering  
Assoc. Prof. Yasumasa Ito        Mechanical Systems Engineering  
Assoc. Prof. Takayuki Tokoroyama      Micro-Nano Mechanical Science and Engineering  
Administrative Staff      Tomoko Kato

### (c) JUACEP Research Abroad 2017 Schedule

Period	Short-term course	Medium-term course
2017/08/08~2017/08/15	Departure from Japan and starting of JUACEP research activity at Univ. Michigan and UCLA	
~2017/09/17	Research activity at each lab	Research activity at each lab
2017/09/18~2017/09/22	Submitting research report to the advisor and receiving evaluation sheet from the advisor	
~2017/09/23	Departure from US/ arrival at Nagoya	
2017/09/25	Submission deadline for research report, JUACEP report, JASSO questionnaire and evaluation sheet to JUACEP Office	
2017/09/29	Workshop for Short-term course	
2017/10/07		
2017/11/07		
2017/12/07		
~2018/01/21		
2018/01/22~2018/01/26		Submitting research report to the advisor and receiving evaluation sheet from the advisor
~2018/01/31		Departure from US/ arrival at Nagoya
2018/02/02		Submission deadline for <u>research report</u> , <u>JUACEP report</u> , <u>JASSO questionnaire</u> and <u>evaluation sheet</u> to JUACEP Office
2018/02/27		The 21st Workshop for Medium-term course

## <2> Research Reports

### **Studies at University of Michigan**

- [S] Yoshiyuki Tange, *mentored by Prof. Katsuo Kurabayashi* (P.6)  
Design of Micro-Device to Implement in Micro-Piercing Method
- [M] Hiroki Fujiwara, *mentored by Assoc.Prof. Mirko Gamba* (P.9)  
Demonstration of Digital In-Line Holography for Primary Breakup of Water Column
- [M] Makoto Takeuchi, *mentored by Prof. Richard Laine* (P.13)  
Thin Alumina Films via Colloidal Processing of Flame Made Nanopowders
- [M] Taro Mizutani, *mentored by Prof. Jack Hu* (P.23)  
Analysis of Assembly Line with Learning Effects
- [M] Makoto Terada, *mentored by Prof. Albert Shih* (P.31)  
Forces: The Quantitative Values of Sharpened and Blunt Microwire for In-vivo Brain Insertion (*Undisclosed*)
- [M] Tatsuya Okamoto, *mentored by Prof. L. Jay Guo*  
Ab Initio Molecular Dynamics Simulation about Dielectric Properties of Boron-doped Diamond-like Carbon (P.32)
- [M] Yudai Suzuki, *mentored by Prof. Anouck Girard* (P.38)  
Failure Detection and Control of Distributed Electric Propulsion Aircraft Engines (*Undisclosed*)

### **Studies at UCLA**

- [M] Yusuke Fukui, *mentored by Prof. Jacob Rosen* (P.39)  
Developing Immersive Virtual Realities for Human Upper Limb Motor Recovery after Stroke (*Undisclosed*)
- [M] Fuga Matsubara, *mentored by Prof. Benjamin M. Wu* (P.40)  
Shelf-Life Testing of Bioink-Containing Pharmaceutical Tablets for 3D Pharming (*Undisclosed*)
- [M] Kai Iio, *mentored by Prof. Gerard C. L. Wong* (P.41)  
Artificial Bacterial Trail Influence Surface Movement (*Undisclosed*)

\*[S]; Short-term course, [M]; Medium-term course

# DESIGN OF MICRO-DEVICE TO IMPLEMENT IN *MICRO-PIERCING METHOD*

Yoshiyuki Tange

Department of Mechanical System Engineering, Graduate School of Engineering, Nagoya University  
tange.yoshiyuki@i.mbox.nagoya-u.ac.jp

Supervisor: Katsuo Kurabayashi

Department of Mechanical Engineering, Electrical Engineering and Computer Science,  
Graduate School of Engineering, University of Michigan  
katsuo@umich.edu

## ABSTRACT

Microfabrication technology has often been applied to experimental systems, in the field of biology, which focus on micro or nanometer order samples such as cells and molecules. However, there are not many applications of that technology to research investigating embryos. This study described the results of designing and manufacturing a micro-device to be implemented in *Micro-Piercing*, a new method that was constructed to estimate the mechanical properties inside of clawed African frog (*Xenopus laevis*) embryos. The device could hold a sample by negative pressure and consistently guide a fiber to the same point of the embryo. If executed correctly, the embryo handling time would be critically shortened, increasing the number of experimental data.

## 1. INTRODUCTION

Identifying what mechanisms realize morphogenetic movement has been one of the most difficult questions in developmental biology. Until now, developmental biology has focused on molecular interactions among cells. However, recent studies have suggested that mechanical properties, such as the magnitude of forces, and Young's modulus play significant roles. We are constructing a new method, *Micro-Piercing*, which estimates the stress direction inside of an embryo. Normally for this experiment, a *Xenopus laevis* embryo embedded in agarose gel is pierced by micro-pipet<sup>テキスト</sup> Ink, or other soft materials drawn by the pipet allows for visualization of the piercing hole. However, this process has many difficult steps. The main problems are poor reproducibility of the insertion point, long experiment times, and uncertainty of the piercing hole shape. In this study, we designed and manufactured a new device that could consistently reposition the needle at the same point, hold the embryo with negative pressure instead of embedding in agarose gel, and assist in drawing soft materials from within the embryo. Additionally, we ran experiments with a phantom

embryo to try to confirm whether this device could succeed in these processes.

## 2. MATERIALS AND METHODS

### 2.1 CONCEPT OF NEW DEVICE

The new device can hold the sample by negative pressure. In past *Micro-Piercing* methods, we have embedded the sample in agarose gel. However, this process would take up to 30 minutes, causing the pre-gel to cool down and solidify, making one third of the gel too stiff to insert the remaining embryos. Even if you missed the gelling moment by a few seconds, the result would have been critical. The embryos would also break when manipulating their orientation within the gel. Thus, we selected negative pressure as a holding method over embedding in agarose.

Moreover, the device could guide the route of the fiber to consistently pierce the same position of the embryo. Currently, we have manipulated the fiber under the microscope, however, it was difficult to insert the fiber at the same point in different samples. If the positional relationship between a sample and the fiber was always constant, a reproducible experimental system could be established. Lastly, the end of the guide channel would have the function of grasping materials from the fiber, which can be used to estimate mechanical properties.

### 2.2 MICROFLUIDIC DEVICE DESIGN

Modular microfluidic devices were fabricated using conventional soft-lithography techniques from polydimethylsiloxane (PDMS; SYLGARD 184, Dow Corning). The mold was designed with 2DCAD (AutoCAD 2015, Autodesk) and made from an Si-wafer with a diameter of 80 mm. The mold was used to form two separate channels with a height of 200  $\mu\text{m}$  (Fig. 1, (C)(D)). The channel of the middle layer was designed to lead the fiber trajectory and had a jagged end that was used to capture soft materials from the fiber (Fig. 1, (C)). One of the bottom layers was used as a

flow pathway to load negative pressure on the embryo (Fig. 1, (D)). The thickness of the top, middle, and bottom PDMS layers were 3 mm, 0.7 mm, and 0.7 mm respectively (Fig. 1, (B)). Each layer, including the glass slide (SLIDES, 25×75×1 mm, Globe Scientific) was adhered to each other by reforming the surfaces with O<sub>2</sub> plasma treatment at 60W for 30 seconds, and baking at 80°C for a few minutes while in contact with each other.

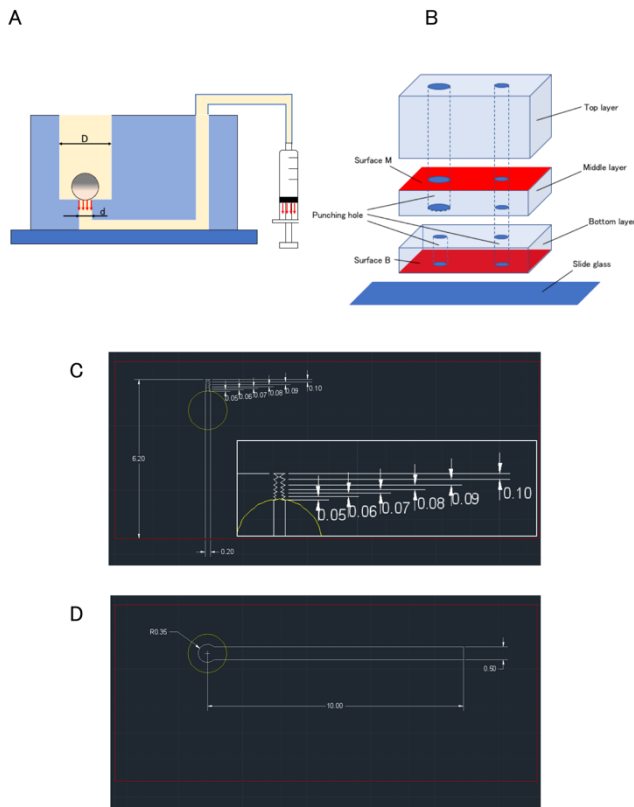


Fig. 1 Concept and design of new device. (A) Sketch of embryo held by negative pressure. (B) Positional relationship of layers. (C) 2D drawing of Middle layer surface (Surface M). (D) 2D drawing of Bottom layer surface (Surface B). Yellow circle indicates *Xenopus laevis* embryo.

### 3. RESULTS AND DISCUSSION

#### 3.1 MANUFACTURING THE DEVICE

It was confirmed that the surfaces were molded as designed (Fig. 2, (A)(B)). Adherence of all layers was also confirmed.

#### 3.2 GUIDING THE FIBER

We confirmed that a fiber with a diameter of 75  $\mu\text{m}$  could pass through the guide without causing water to leak (Fig. 3, (A)). Furthermore, the fiber tip was captured by the jagged end of the guide channel. Thus, any soft materials around the fiber could be released into the embryo if we could establish

a way to wrap it around the fiber. An alternative plan is that a water absorbing fiber would be inserted through the guide channel within a 100  $\mu\text{m}$  capillary tube. In that case, the guide channel would be helpful because it could grasp the fiber that is swollen with water.

#### 3.3 LOADING NEGATIVE PRESSURE

A PDMS cylinder, with both a diameter and height of 1.5 mm, was used as a phantom of *Xenopus laevis* embryo and placed in the large hole of the device. Cavitation due to negative pressure occurred in a combination of a large hole with a diameter of 3 mm and a suction hole with a diameter of 0.75 mm (Table 1, Fig. 3, (B)). In the other devices, complete cavitation did not occur because the suction hole was not entirely covered by the phantom. Furthermore, because the embryo is much softer than the phantom, the appropriate magnitude of pressure that can be exerted on the embryo to keep it in place without causing it to break must be determined.

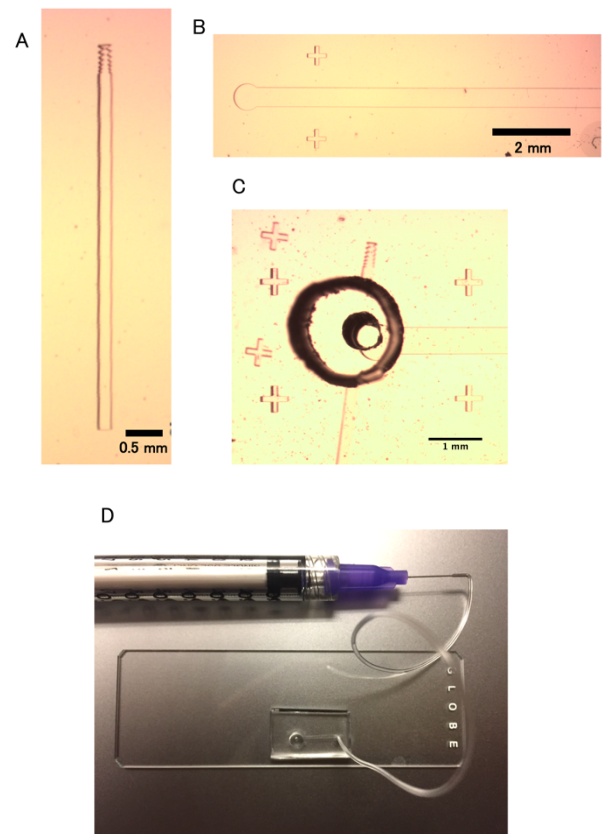


Fig. 2 Completed device. (A) Fiber guide channel on Surface M. (B) Flow path on Surface B. (C) Embryo holding part of the device. (D) Overhead view of completed device.

Table 1 Relationship between dimension of holes and rate of cavitation occurrence.

Device	D (mm)	d (mm)	Cavitation
1	2.0	0.75	0/5
2	2.0	1.0	2/5
3	3.0	0.75	5/5
4	3.0	1.0	3/5

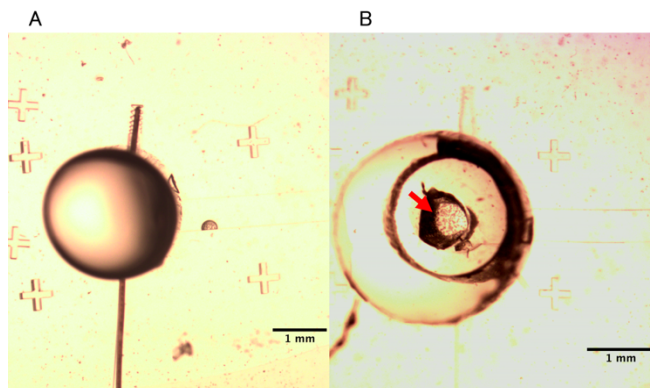


Fig. 3 Confirming functions of the device. (A) Guiding the fiber. (B) Loading negative pressure. Red arrow indicates cavitation.

#### 4. CONCLUSION

In this study, we manufactured a micro-device that can guide a fiber in order to pierce and deposit soft materials within an embryo. The device was also designed to hold a *Xenopus laevis* embryo with negative pressure. The ability of the device to load negative pressure was confirmed by successful cavitation of a phantom *Xenopus laevis* embryo. For future work, we will find the appropriate magnitude of pressure for real embryos.

#### ACKNOWLEDGEMENTS

I thank Meng Ting Chang for making the mold and teaching me soft-lithography techniques.

#### REFERENCES

- [1] Adams, D. S., Keller, R. & Koehl, M. a. R., Elongation, Straightening and Stiffening in the Embryo of *Xenopus-Laevis*, *Development*, 110, pp. 115-130 (1990).
- [2] Davidson, L. A., Embryo mechanics: balancing force production with elastic resistance during morphogenesis, *Curr Top Dev Biol*, 95, pp. 215-241, (2011).
- [3] Lecuit, T., Lenne, P. F. & Munro, E., Force generation, transmission, and integration during cell and tissue morphogenesis, *Annu Rev Cell Dev Biol*, 27, pp. 157-184, (2011).

- [4] Murakami, F., Ando, Y., Miyagi, A., Sugita, S., Ueno, N., Matsumoto, T., Measurement of surface topography and stiffness distribution on cross section of *Xenopus laevis* tailbud for estimation of mechanical environment in embryo, *Dev Growth Differ*, 59, pp. 434-443, (2017).
- [5] Wang, K., Salcic, Z., Yeh, J., Akagi, J., Zhu, F., Hall, C., Crosier, K. E., Crosier, P. S., Wlodkowic, D., Toward embedded laboratory automation for smart lab-on-a-chip embryo arrays, *Biosens Bio*, 48, pp. 188-196, (2013)
- [6] Xia, Y., Whitesides G. M., SOFT LITHOGRAPHY, *Rev Mater Sci*, 28, pp. 153-184, (1998)

# DEMONSTRATION OF DIGITAL IN-LINE HOLOGRAPHY FOR PRIMARY BREAKUP OF WATER COLUMN

Hiroki Fujiwara

Department of Aerospace Engineering, Graduate school of Engineering, Nagoya University  
Fujiwara.hiroki@h.mbox.nagoya-u.edu

Mirko Gamba

Department of Aerospace Engineering, University of Michigan  
mirkog@umich.edu

## ABSTRACT

The objective of this experimental study is to demonstrate the application of digital in-line holography to investigate primary breakup of water column. To conduct experiments, a water column generator was developed. It can generate continuous water column of 1.7 mm diameter [1]. A code was developed to conduct computational reconstruction of holography images. The code is based on the angular spectrum method, and it was successfully built to reconstruct holography images. To test the code, images of a wire grid and water column was taken. The reconstructed image has successfully captured the edge of an object at a recording distance.

## 1. INTRODUCTION

Mixing processes of fuel and air in air-breathing engine need to be fast and efficient to limit the size of the combustion chamber. When a liquid fuel is injected into the air flow, it undergoes the following mixing processes:

1) Primary breakup: the first process is the breakup of the liquid column into ligaments and drops. This breakup is due to liquid turbulence and aerodynamic forces.

2) Secondary breakup: following the primary breakup, the ligaments and drops breakup into smaller drops due to aerodynamic forces exerted by the air flow.

3) Evaporation and 4) mixing of

In this paper, we focus on primary breakup under conditions typical of supersonic combustion ramjet, where the flow inside a chamber is supersonic. Many studies have been conducted on primary breakup process using 2D techniques such as Schlieren techniques [2-3]. Figure 1 shows the sequence image of a water column interacted with Mach 1.4 shock wave, which was done in the lab previous to this work [1]. The image was taken by a high speed camera (Phantom v711) with Schlieren technique. The exposure is  $0.28\mu\text{s}$ , and the field of view is  $35.6\text{ mm} \times 8.9\text{ mm}$ . From

the image, we can see the water column breakup into droplets and showers, and the column itself is moved downstream after interacting with a shock. However, 2D imaging can only focus on small number of droplets created in the breakup, and difficult to measure important properties such as droplet sizes and velocities. Therefore, we utilize an imaging technique called digital holography [4] that can be utilized to obtain 3D information of the breakup process, and has been used for breakup process investigation [4-6]. In this work, digital holography was utilized for the experiment in same condition as shown in Figure 1. The objective of the work were to conduct the experiment, and a water column generator [1], and a holography reconstruction algorithm based on the angular spectrum method were developed.

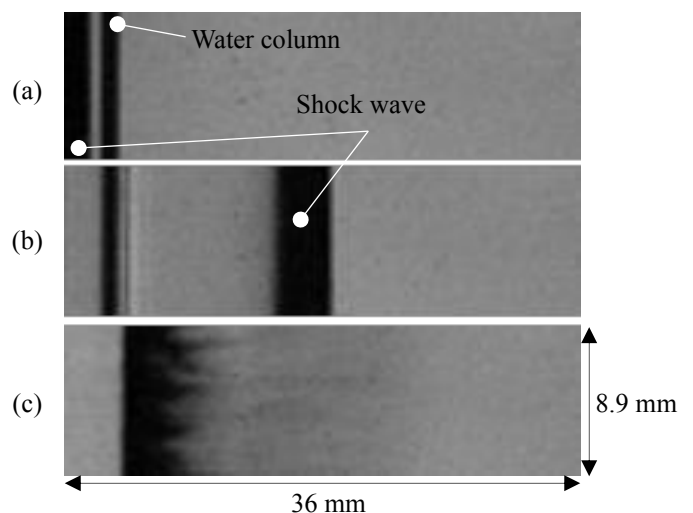


Fig. 1 Schlieren image of water column and shock interaction at (a)  $t = 0$ , (b)  $t = 39\ \mu\text{s}$  (c)  $t = 135\ \mu\text{s}$  [1].

## 2. HOLOGRAPHY

### 2.1 Background

Holography is capable of forming 3D image from a 2D recording because it contains both intensity and phase

information of the light diffracted from an object. Holography is the interference of two waves of coherent light:

1) The objective wave, which is diffracted by the object being recorded;

2) The reference wave, which represents the status of the object wave before it was affected by the object.

As the object wave interacts with the object, the phase of the light wave is altered. After that, when it interferes with the reference wave, an interference pattern (hologram) is formed that can be recorded on the recording medium. This interference pattern, which is the interference between the complex scattered field from the object and the reference, has information of both the phase and the magnitude of the object wave. When the original reference beam is shone onto the hologram, then a 3D image is reproduced having the same characteristics as the original object.

While the conventional analogue holography requires chemical processing for developing holography plate and physical re-illumination of the hologram with a reference light to get 3D real or virtual image, digital holography is a numerical procedure that simulates the diffraction of light from the re-illuminated hologram on a computer and numerically determines the images. In digital holography, the interference of light scattered from an object and a reference wave is recorded directly onto a CCD sensor, electronically recorded and stored. Reconstruction of the original object image is done by computation of the propagation of the light through the hologram and its subsequent diffraction.

There are several types of optical alignment in digital holography, and in this research, in-line holography is used. In the in-line holography, light source and the object is placed on an axis perpendicular to the sensor. A plane wave illuminates the observed objects, and a part of the wave is diffracted by the object while the remaining part passes through the setup without being diffracted. This part of the wave serves as a reference beam. Because of this simple setup, and also because it reduces requirements of the spatial resolution on the CCD sensor, this in-line holography is used in this work.

## 2.2 Digital Holography Algorithms

General principles and numerical reconstruction can be mathematically explained as following [4]. The complex amplitude of the object wave is described by

$$E_O(x, y) = a_O(x, y) \exp(i\phi(x, y)) \quad (1)$$

where real amplitude  $a_O$  and phase  $\phi_O$ .

$$E_R(x, y) = a_R(x, y) \exp(i\phi(x, y)) \quad (2)$$

is the complex amplitude of the reference wave with real amplitude  $a_R$  and phase  $\phi_R$ .

Both waves interfere at the surface of the recording medium. The intensity  $I$  is calculated by

$$\begin{aligned} I(x, y) &= |E_O(x, y) + E_R(x, y)|^2 \\ &= (E_O(x, y) + E_R(x, y))(E_O(x, y) + E_R(x, y))^* \\ &= E_O(x, y)E_R^*(x, y) + E_R(x, y)E_O^*(x, y) + \\ &\quad E_O(x, y)E_R^*(x, y) + E_R(x, y)E_O^*(x, y) \end{aligned} \quad (3)$$

The amplitude transmission  $h(x, y)$  of the developed photographic plate is proportional to  $I(x, y)$

$$h(x, y) = h_0 + \beta \tau I(x, y) \quad (4)$$

The constant  $\beta$  is the slope of the amplitude transmittance versus exposure characteristic of the light sensitive material. For photographic emulsions  $\beta$  is negative.  $\tau$  is the exposure time and  $h_0$  is the amplitude transmission of the unexposed plate.  $h(x, y)$  is named hologram function. In Digital Holography using CCD's as recording medium  $h_0$  can be neglected.

For hologram reconstruction the amplitude transmission has to be multiplied with the complex amplitude of the reconstruction (reference) wave:

$$\begin{aligned} E_R(x, y)h(x, y) &= \\ &[h_0 + \beta \tau (a_R^2 + a_O^2)]E_R(x, y) + \beta \tau a_R^2 E_O(x, y) \\ &+ \beta \tau E_R^2(x, y)E_O^2(x, y) \end{aligned} \quad (5)$$

The first term on the right side of this equation is the reference wave, multiplied by a factor. It represents the undiffracted wave passing the hologram (zero diffraction order). The second term is the reconstructed object wave, forming the virtual image. The real factor  $\beta \tau a_R^2$  only influences the brightness of the image. The third term generates a distorted real image of the object.

## 2.3 Reconstruction

The three-dimensional spatial distribution of small moving particles can be detected by scanning the reconstruction distance numerically. Since in numerical reconstruction it may be chosen freely, the field can be scanned by it and checking at which distances the particles are in focus.

There are several numerical reconstruction algorithms for digital holography reconstruction, such as Fresnel transformation, convolution approach, and angular spectrum method [4]. In this work, angular spectrum method was used because it doesn't have a limit on propagation distance, and it doesn't produce noises due to approximation of the traveling distances like other methods.

Process for reconstructing digital hologram is as follows; the hologram intensity in the CCD sensor is multiplied by the reference wave, and the resulting wave  $hE_R$  is numerically propagated to the virtual image plane. The complex amplitude distribution  $\Gamma(\xi, \eta)$  in any plane can be calculated from  $hE_R$  using the well-known Fresnel-Kirchhoff formulation of diffraction as:

$$\Gamma(\xi, \eta) = \frac{j}{\lambda} \iint hE_R \frac{\exp(-jk\rho)}{\rho} dx dy \quad (6)$$

with

$$\rho = \sqrt{(x - \xi)^2 + (y - \eta)^2 + d^2} \quad (7)$$

where it is the distance between a hologram and image plane,  $\lambda$  is the wavelength,  $k$  is the wave number  $2\pi/\lambda$  and  $\rho$  is

the distance from a point in the sensor to any point in the image plane. This integral can be regarded as a convolution of  $hE_R$  and

$$g = \frac{j}{\lambda} \frac{\exp(-jk\rho)}{\rho} \quad (8)$$

The Fourier transform of (8) can be calculated analytically, and is written as

$$G = \exp(jkd) \sqrt{1 - (\lambda f_x)^2 + (\lambda f_y)^2 + d^2} \quad (9)$$

where

$$f_x = \frac{\xi}{\lambda d}, f_y = \frac{\eta}{\lambda d} \quad (10)$$

Therefore, the complex amplitude distribution in the image plane can be numerically calculated using the Fourier transform  $F$  as

$$\Gamma(\xi, \eta) = F^{-1}[F(hE_R) \bullet F(g)] \quad (11)$$

To obtain reconstructed image, calculation of (6), (7) was done on MATLAB using Fast Fourier Transform (FFT), with the reconstruction code developed based on [7, p151-152], with some modifications.

### 3. EXPERIMENTAL CONFIGURATIONS

A schematic of the experimental setup used for the in-line digital holography is shown in Figure 2. A He-Ne laser ( $\lambda = 632.8$  nm, 2 mW power) was used as a light source. An objective lens with 4.5 mm focal length and a plano-convex lens with focal length of 200 mm was used to create a collimated beam of 42 mm. 15  $\mu$ m pinhole was placed after the objective lens to eliminate irregular interference structures. Neutral density filter was used to avoid the damage of CCD by an excess of energy. The pattern created by the interference between the water column (object) and the collimated (reference) beam directly illuminates the CCD sensor of a digital camera. The CCD array contains 1024  $\times$  1280 pixels, each of them with the size of 6.45  $\times$  6.45  $\mu$ m<sup>2</sup>. The area of the CCD sensor was 10.3  $\times$  8.3 mm<sup>2</sup>. Holographic image was taken by a CCD camera (Sensicam qe) with a resolution of 0.0062 mm/pix, exposure time of 0.2  $\mu$ s

The flow was generated in the Michigan Hypersonic Expansion Tube (MHEXT) [8] used in the shock tube mode.

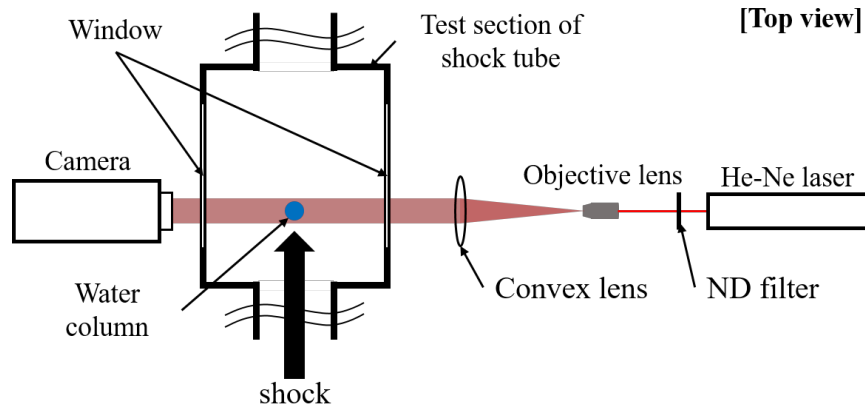


Fig. 2 Top View of an Experimental Setup

The test condition of the shock tube was; driver section 85 psi shop air; driven section: atmospheric pressure. The water column generator was mounted in the test section of the expansion tube, just downstream of the end of the shock tube.

Water tank was placed 860 mm above the column generator exit to run water column by static pressure. The diameter of water column was 1.15 mm. A solenoid valve was mounted and the time of water running was manually controlled by opening the valve right before running a shock.

### 4. RESULTS AND DISCUSSION

First, holography reconstruction was tested. Fig. 2 is the reconstruction of a grid with 0.127 mm diameter, placed 1 mm apart. Fig.3 shows the reconstruction of a water column. The distance from CCD sensor to the water column was 270 mm, and the reconstructed image was done at 260 mm. From both Fig. 1 and Fig. 2, it can be seen that the holography with diffraction fringes are reconstructed and sharper edges appear.

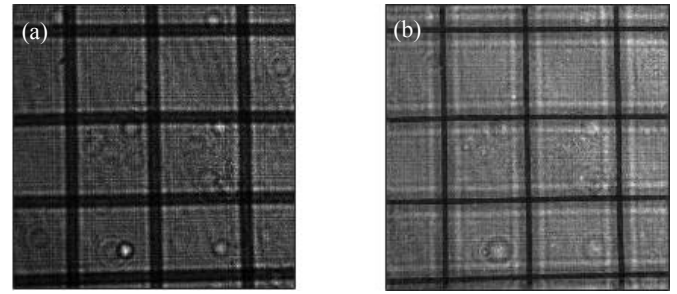
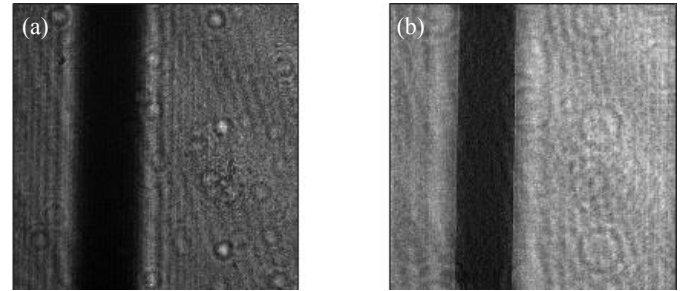
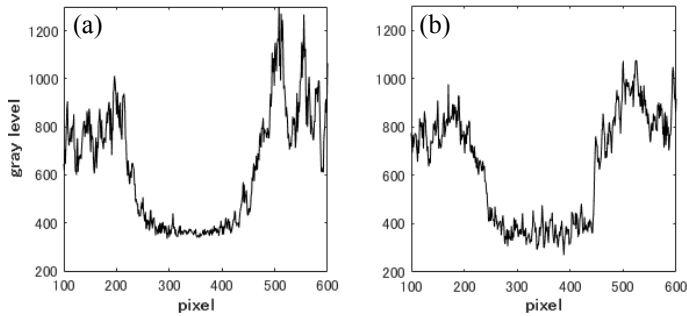


Fig. 3 (a) Hologram of a grid of 1 mm spacing (b) reconstructed image



**Fig. 4 (a) Hologram of water column (b) reconstructed image.**

From Figure 5, we see a sharper edge of the water column around 250 and 450 pixel on an intensity profile of the reconstructed image.



**Fig. 5 Intensity profile of a line through the center of the water column (a) holography and the (b) reconstructed image**

## 5. CONCLUSIONS

Reconstruction algorithm based on angular spectrum method was developed, and has been shown that it successfully reconstructs an image of an object.

## ACKNOWLEDGEMENTS

I would like to express my gratitude to my supervisor Professor Mirko Gamba for the supervision of my research through the JUACEP program. Weekly meeting helped me think what the best step to take next, and made my research vision clearer. I would like to thank all the lab members in Gas Dynamics Imaging Laboratory for helping me with my experiments. I would like to thank my supervisor at Nagoya University, Akira Iwakawa, for letting me take part in this program. I would like to contribute to the research at Nagoya University by further developing what I have learned through this program. I would also like to thank all the staff members who help me through this program.

Finally, this work was supported by Japan-US Advanced Collaborative Education Program (JUACEP).

## REFERENCES

- [1] C. Zoller, Investigation of shock induced primary breakup at high Mach numbers, Master thesis, Technical University of Munich
- [2] K. A. Sallam, Z. Dai, and G.M. Faeth, Drop Formation at the Surface of Plane Turbulent Liquid Jets in Still Gases, *Int. J. Multiphase Flow*, vol. 25, pp. 1161–1180, 1999.
- [3] K. A. Sallam, Z. Dai, and G. M. Faeth, Liquid Breakup at the Surface of Turbulent Round, Liquid Jets in Still Gases, *Int. J. Multiphase Flow*, vol. 28, pp. 427–449, 2002.
- [4] Schnars, U. and Jueptner, W., *Digital Holography: Digital Hologram Recording, Numerical Reconstruction, and Related Techniques*, Springer-Verlag, Berlin, 2005
- [5] K. A. Sallam, C. Aalburg, and G. M. Faeth, Breakup of Round Nonturbulent Liquid Jets in Gaseous Crossflow, *AIAA J.*, vol. 42, pp. 2529–2540, 2004.

- [6] Gao J, Guildenbecher DR, Reu PL, Kulkarni V, Sojka PE, Chen J (2013b) Quantitative, 3D diagnostics of multiphase drop fragmentation via digital in-line holography. *Opt Lett* 38(11):1893–1895
- [7] G. Nehmetallah, R. Aylo, and L. Williams, *Analog and Digital Holography With MATLAB* (SPIE, 2015).
- [8] Y.M., Abul-Huda, M. Gamba, Design and Characterization of the Michigan Hypersonic Expansion Tube Facility (MHEXT), 53rd AIAA Aerospace Sciences Meeting (2015) 1785-1797

# Thin alumina films via colloidal processing of flame made nanopowders

Makoto Takeuchi

Department of Micro Nano Mechanical Engineering, Graduate School of Engineering, Nagoya University  
takeuchi@ume.mech.nagoya-u.ac.jp

Monika Jansohn, Eongyu Yi, Richard Laine

Department of Materials Science and Engineering, Graduate School of Engineering, University of Michigan  
mjansohn@umich.edu, eonyi@umich.edu, talsdad@umich.edu

## ABSTRACT

Dense, very fine-grained  $\alpha$ -Al<sub>2</sub>O<sub>3</sub> ceramics have been investigated by many researchers for their superior hardness, wear resistance, strength, and/or optical properties. The objective of the work reported here is to fabricate transparent, very thin Al<sub>2</sub>O<sub>3</sub> films doped with small amounts of MgO using pressureless sintering. In this work, nanopowders synthesized by liquid-feed flame spray pyrolysis were used as the starting material to fabricate thin films. A dispersion of Al<sub>2</sub>O<sub>3</sub> (+ x wt. % MgO, x = 0.0, 0.50, 1.0, 2.0, 3.0 or 5.0) was made by powders, plasticizer, dispersant and solvent. After ball-milling for 48 h, suspensions were cast on Mylar and dried to obtain green films. Green films were uniaxially pressed and then sintered at selected temperatures. Optimization of properties of density, transparency, thickness and flexibility provided films 10  $\mu$ m thick. The microstructures of sintered films produced in all phases of the work were characterized by SEM and XRD.

## 1. INTRODUCTION

Very fine-grained structures with sub  $\sim$  $\mu$ m average grain sizes (AGSs) typically offer superior hardness, wear resistance, strength, and/or optical properties. This is true of most ceramics and especially important yet problematic for  $\alpha$ -Al<sub>2</sub>O<sub>3</sub>. In this instance densification of any transition-Al<sub>2</sub>O<sub>3</sub> (*t*-Al<sub>2</sub>O<sub>3</sub>) based green body must occur with transformation to  $\alpha$ -Al<sub>2</sub>O<sub>3</sub>. This transformation is often problematic as going from a tetragonal unit cell to a hexagonal unit cell leads to densification mismatches associated with the different grain axes. Furthermore, the *a* and *c* axes have different refractive indices that lead to extensive light scattering for average grain sizes (AGSs) greater than about 600 nm. Thus, numerous research groups have sought to resolve these issues over many years.<sup>1-4</sup>

If we simply choose to consider only cubic or tetragonal based crystal structures, then one can state that the optical and mechanical properties of polycrystalline ceramic materials depend highly on their AGSs and residual porosity. AGSs are closely related to mechanical properties typically following the Hall-Petch equation:

$$\sigma = \sigma_0 + k \cdot d^{-0.5} \quad (1)$$

where  $\sigma$  is the yield stress, *d* is the average grain diameter, and  $\sigma_0$  and *k* are empirical constants, strength or hardness

should increase as grain size decreases.<sup>5,6</sup> Moreover, light scattering occurs primarily at grain boundaries, pores and impurities, which decrease transparency. Therefore, various strategies have been employed to control the grain sizes and minimize residual porosity.

The literature reports that introduction of MgO into *t*-Al<sub>2</sub>O<sub>3</sub> powders leads to formation of MgO·Al<sub>2</sub>O<sub>3</sub> spinel at grain boundaries both during transformation of *t*-Al<sub>2</sub>O<sub>3</sub> to  $\alpha$ -Al<sub>2</sub>O<sub>3</sub> and during densification that impedes grain growth.<sup>7</sup> Thus, we anticipated that introduction of MgO to our  $\delta$ -Al<sub>2</sub>O<sub>3</sub> nanopowders (NPs) would serve the same purpose.

Our efforts here are built on recent successes in using NPs to fabricate a number of ceramic thin films for applications ranging from Li and Na solid state electrolytes to capacitors.<sup>8,9</sup> We herewith extend such efforts targeting fabrication of transparent, dense and flexible Al<sub>2</sub>O<sub>3</sub> thin films by tape-casting *t*-Al<sub>2</sub>O<sub>3</sub> NPs. We sintered Al<sub>2</sub>O<sub>3</sub> films doped with small amounts of MgO at several doping levels and under select sintering conditions, and evaluated the thin film properties including density, AGSs and porosity using XRD and SEM.

## 2. EXPERIMENTAL

### 2.1 Liquid-Feed Flame Spray Pyrolysis (LF-FSP)

MgO doped (0.0, 0.50, 1.0, 2.0, 3.0 and 5.0 wt. %)  $\delta$ -Al<sub>2</sub>O<sub>3</sub> NPs were prepared by liquid-feed flame spray pyrolysis (LF-FSP). As practiced at University of Michigan<sup>8-13</sup> the LF-FSP apparatus consists of a precursor reservoir, an ultrasonic atomizer, a combustion chamber, and electrostatic precipitators (ESPs). The precursors are dissolved in ethanol at selected molar ratios that provide an overall 3-5 wt. % ceramic yield. The precursor solution is pumped into an ultrasonic atomizer, aerosolized and combusted with methane/oxygen pilot torches on the spray head. Combustion at  $\geq 1500$  °C produces MgO doped  $\delta$ -Al<sub>2</sub>O<sub>3</sub> nanopowders that are collected down-stream in electrostatic precipitators operated at a DC potential of 10 kV.

The as-produced powders are then dispersed in EtOH (200 proof, Decon Labs) using an ultrasonic horn (Vibra cell VC-505, Sonics & Mater. Inc.) at 100 W for 10 min. The suspension is allowed settle for 5 h to remove larger particles. The supernatant is decanted and allowed to oven dry providing the starting  $\delta$ -Al<sub>2</sub>O<sub>3</sub> nanopowders.

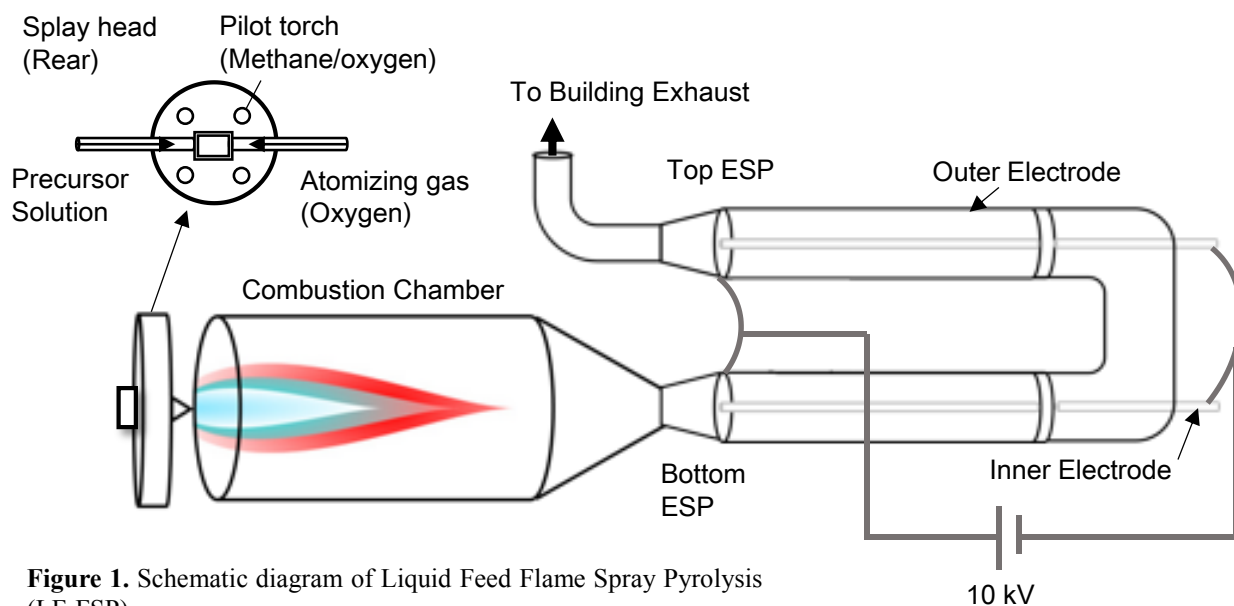


**Figure 1.** Schematic diagram of Liquid Feed Flame Spray Pyrolysis (LF-FSP)

## 2.2 Precursors synthesis

Magnesium propionate [ $\text{Mg}(\text{O}_2\text{CCH}_2\text{CH}_3)_2$ ] and alumatrane [ $\text{Al}(\text{OCH}_2\text{CH}_2)_3\text{N}$ ] were synthesized and mixed to produce NPs of  $\delta\text{-Al}_2\text{O}_3$  with 0.0, 0.50, 1.0, 3.0, and 5.0 wt. % of MgO on combustion.

Magnesium propionate [ $\text{Mg}(\text{O}_2\text{CCH}_2\text{CH}_3)_2$ ] was synthesized by reacting magnesium hydroxide with propionic acid in a 1 L round bottom flask equipped with a still head at  $140^\circ\text{C}$  in  $\text{N}_2$  atmosphere. Once a transparent liquid was obtained, heat was removed and the liquid cooled to ambient. Crystallized magnesium propionate was filtered off.

Alumatrane [ $\text{Al}(\text{OCH}_2\text{CH}_2)_3\text{N}$ ] was synthesized by reacting aluminum sec-butoxide [ $\text{Al}[\text{OCH}(\text{CH}_3)\text{CH}_2\text{CH}_3]_3$ , 97% [Alfa Aesar, Ward Hill, MA] with triethanolamine. [ $\text{N}(\text{CH}_2\text{CH}_2\text{OH})_3$ , 99 +% : Acros Organics, Morris Plains, NJ] in a 1 L round bottom flask equipped with a still head at room temperature in  $\text{N}_2$  atmosphere. Once a transparent liquid was obtained, heat was removed and the liquid cooled to room temperature. Residue was filtered off and alumatrane was obtained as a solution (ceramic yield 7.6 wt. %).

## 2.3 Film processing

The 0.0, 0.50, 1.0, 2.0, 3.0, and 5.0 wt. % MgO doped  $\delta\text{-Al}_2\text{O}_3$  powders, polyvinylbutyral, benzyl butyl phthalate, ethanol, and acetone at selected ratios were prepared in vials. Six types of suspensions were prepared, see

**Table 1.** The suspensions were ball-milled using a ball tumbler (Thumler's Tumbler Model B, Tru-Square Metal Products, Auburn, WA, United States) with 6.0 g of spherical  $\text{Al}_2\text{O}_3$  beads for at least 48 h. The suspensions were cast on Mylar film using a wire wound rod coater (1137, Sheen, Richmond Road, Kingston, United Kingdom). The cast thickness was adjusted to  $125\ \mu\text{m}$  in order to control the thickness of the films.

After solvent evaporated, one/two dry green films were uniaxially pressed between stainless steel dies at  $100^\circ\text{C}$  at 20 MPa for 5-30 min using a heated bench top laboratory manual

press (Model 3851-0, Carver, Inc., Wabash, IN, United States) to improve packing density.<sup>14</sup>

**Table 1.** Starting materials and composition of suspension of  $\text{Al}_2\text{O}_3$  (+ x wt. % MgO, x = 0.0, 0.50, 1.0, 2.0, 3.0 or 5.0)

Components	Roles	Mass (g)	Wt. %	Vol. %
x wt. % MgO doped $\delta\text{-Al}_2\text{O}_3$	Powder	1.00	24.9	36.5
Polyvinyl butyral	Binder	0.135	3.36	2.99
Benzyl butyl phthalate	Plasticizer	0.135	3.36	2.99
Ethanol	Solvent	1.38	34.1	42.6
Acetone	Solvent	1.37	34.1	42.6

## 2.4 Film sintering

Green films were placed between two  $\text{Al}_2\text{O}_3$  substrates and sintered to selected temperatures and times with a ramp rate of  $5^\circ\text{C}/\text{min}$  using a vacuum tube furnace (GSL-1600X, Richmond, CA, United States). The plates were used to prevent warping. One aspect of the efforts reported here used one-step sintering (Figure 2) at  $t_I=1500^\circ\text{C}$  for  $h_I=0$  h, 1 h, 3 h, and 5 h.

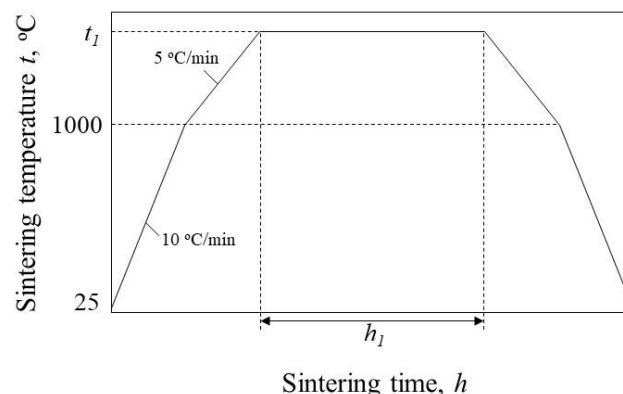


**Figure 2.** Sintering schedule for one-step sintering (below  $1000^\circ\text{C}$  heating rate was  $10^\circ\text{C}/\text{min}$ , above  $5^\circ\text{C}/\text{min}$ ).

## 2.6 Scanning Electron Microscopy (SEM) analysis

Sample morphologies were characterized by JSM-IT300 SEM (JEOL Ltd., Akishima, Tokyo, Japan). Since all the samples lacked of electrical conductivity, they were sputter coated with a gold/palladium film using a Technics Hummer VI sputtering system (Anatech Ltd., Alexandria, VA, United States) to avoid charging and to improve resolution.

## 2.5 X-Ray Diffraction (XRD) analysis

Measurements were carried out using a Rigaku Rotating Anode Goniometer (Rigaku Denki., LTD., Tokyo, Japan) at 40 kV and 100 mA with Cu K $\alpha$  radiation (1.541 Å). Scan range was between 10 and 70° 2 $\theta$ , using a scan rate at 5°/min with 0.02° intervals. The Jade program 2010 (Version 1.1.5 from Materials Data, Inc.) was used to determine the presence of crystallographic phases, wt. fraction, and to refine lattice constants. Peak positions and intensities were evaluated by comparison with ICDD files of  $\delta$ -Al<sub>2</sub>O<sub>3</sub>, Aluminum oxide (00-004-0877),  $\alpha$ -Al<sub>2</sub>O<sub>3</sub>, corundum (98-000-0174), and (MgAl<sub>2</sub>)O<sub>4</sub>, spinel (98-000-5499).

## 3. RESULTS AND DISCUSSION

### 3.1 Characterization of as-produced powders of 0.0, 0.50, 1.0, 2.0, 3.0 and 5.0 wt. % MgO doped $\delta$ -Al<sub>2</sub>O<sub>3</sub>

SEMs of 0.0, 0.50, 1.0, 2.0, 3.0, and 5.0 wt. % MgO doped  $\delta$ -Al<sub>2</sub>O<sub>3</sub> powder prepared by LF-FSP (Figure 3) show that the particles are spherical, Figure 3. The average particle sizes (APSs) were measured using the linear interception method, Figure 4. The majority of pure  $\delta$ -Al<sub>2</sub>O<sub>3</sub> powder particles had APSs of  $\approx$  35 nm. About 5 % of the powder showed some medium sized particles of about 80 nm and a small number of large particles up to 130 nm. Note that in many instances the larger particles are simply agglomerates of the finer powders.

With increasing MgO content, APSs decreased. 5.0 wt. % MgO doped  $\delta$ -Al<sub>2</sub>O<sub>3</sub> showed an APS of  $\approx$  30 nm with 50 nm medium and 90 nm large sized grains. MgO seems to prevent particle growth in LF-FSP powders. It is reported that as particles become smaller,  $T_m$  drops. NP sintering leads to the reduction in sintering temperatures and times when compared to micron sized powders.<sup>15</sup>

XRDs of as-produced powders are given in Figure 5. 0.0 wt. % MgO doped  $\delta$ -Al<sub>2</sub>O<sub>3</sub> exhibits a single phase which corresponds to  $\delta$ -Al<sub>2</sub>O<sub>3</sub>, and 0.50, 1.0, 2.0, 3.0 and 5.0 wt. % MgO doped  $\delta$ -Al<sub>2</sub>O<sub>3</sub> exhibit two phases  $\delta$ -Al<sub>2</sub>O<sub>3</sub> and spinel (MgAl<sub>2</sub>)O<sub>4</sub>.

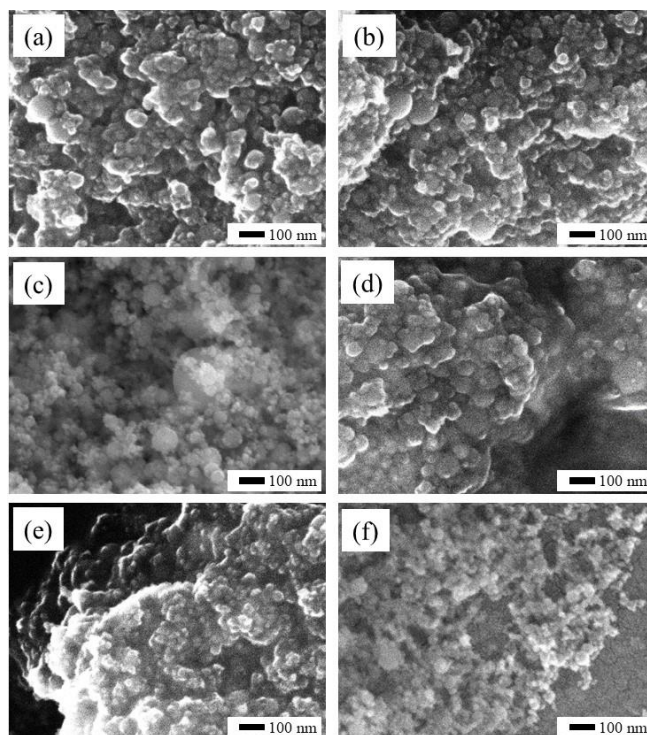


**Figure 3.** SEM images of (a) 0.0, (b) 0.50, (c) 1.0, (d) 2.0, (e) 3.0, and (f) 5.0 wt. % MgO doped  $\delta$ -Al<sub>2</sub>O<sub>3</sub> powders produced by LF-FSP (magnification: 100,000X).

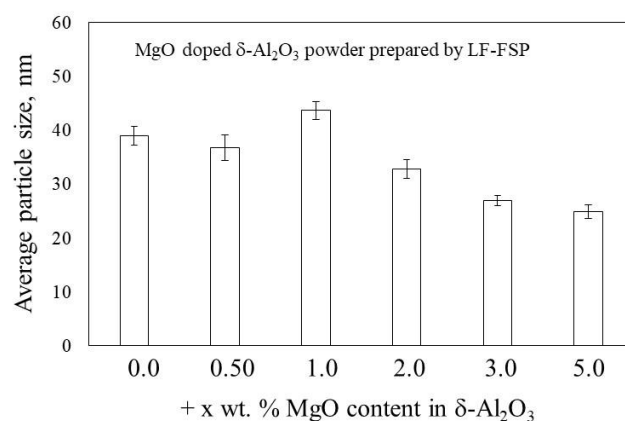


**Figure 4.** APSs of 0.0, 0.50, 1.0, 2.0, 3.0, and 5.0 wt. % MgO doped  $\delta$ -Al<sub>2</sub>O<sub>3</sub> powder prepared by LF-FSP

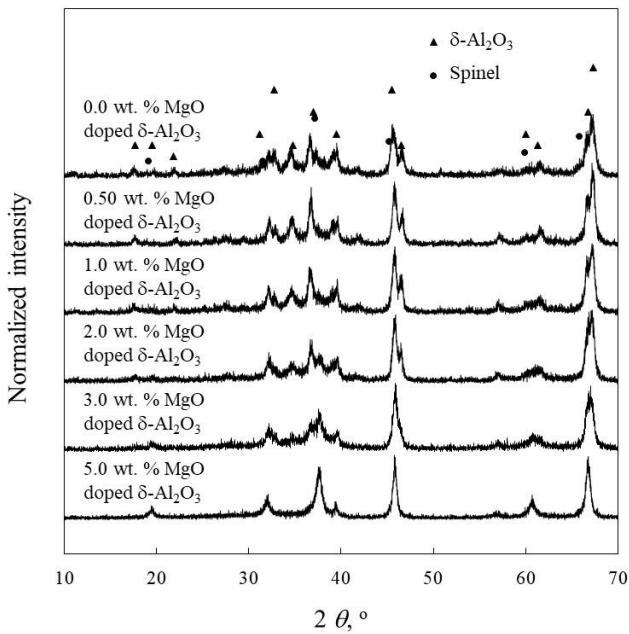


**Figure 5.** XRD patterns of 0.0, 0.50, 1.0, 2.0, 3.0, and 5.0 wt. % MgO doped  $\delta$ - $\text{Al}_2\text{O}_3$  powders produced by LF-FSP.

### 3.2 Characterization of 20 $\mu\text{m}$ films of 0.0, 0.50, 1.0, 2.0, 3.0 and 5.0 wt. % MgO doped $\text{Al}_2\text{O}_3$

The 0.0, 0.50, 1.0, 2.0, 3.0 and 5.0 wt. % MgO doped  $\text{Al}_2\text{O}_3$  films (0MA, 0.5MA, 1MA, 2MA, 3MA, and 5MA respectively) were sintered using a one-step process wherein the films are heated to a peak temperature of  $t_f=1500^\circ\text{C}$  for  $h_f = 0$  h, 1 h, 3 h, 5 h. Green films were placed between  $\alpha$ - $\text{Al}_2\text{O}_3$  substrates ( $D = 42$  mm, where films are 5 mm x 5 mm) and sintered using a vacuum tube furnace. Figure 6 presents a fracture surface of a representative sintered film, see Table 2. The greatest densification was seen in 2 and 3MA. Vertical shrinkages of 20-40 % of the pressed green film thickness are observed.

SEMs of 0, 0.5, 1, 2, 3, and 5MA thin films are presented in Figure 7 (1500  $^\circ\text{C}/0$  h), Figure 11 (1500  $^\circ\text{C}/1$  h), Figure 15 (1500  $^\circ\text{C}/3$  h), and Figure 19 (1500  $^\circ\text{C}/5$  h). 2 and 3MA [Figure 19 (d) and (e)] sintered at 1500  $^\circ\text{C}/5$  h exhibit the highest density. It seemed that 5MA exhibits the high density, but the film is very brittle, which indicates that the film has a low density.

AGSs of sintered films are presented in Figure 8, (1500  $^\circ\text{C}/0$  h) Figure 12 (1500  $^\circ\text{C}/1$  h), Figure 16 (1500  $^\circ\text{C}/3$  h) and Figure 20 (1500  $^\circ\text{C}/5$  h). Basically up to 1.0 wt. % MgO, AGS decreased and then increased with increasing MgO content.

XRDs of sintered films are shown in Figure 9 (1500  $^\circ\text{C}/0$  h), Figure 13 (1500  $^\circ\text{C}/1$  h), Figure 17 (1500  $^\circ\text{C}/3$  h), and Figure 21 (1500  $^\circ\text{C}/5$  h). 0MA exhibits a  $\alpha$ - $\text{Al}_2\text{O}_3$  single phase whereas 0.5, 1, 2, 3, and 5MA present two phases:  $\alpha$ - $\text{Al}_2\text{O}_3$ , and spinel ( $\text{MgAl}_2\text{O}_4$ ).

Optical images of sintered films are shown in Figure 10 (1500  $^\circ\text{C}/0$  h), Figure 14 (1500  $^\circ\text{C}/1$  h), Figure 18 (1500  $^\circ\text{C}/3$  h), Figure 22 (1500  $^\circ\text{C}/5$  h). Films with 2, 3j, and 5MA compositions exhibit the highest transparency [Figure 22 (d), (e), and (f)] sintered at 1500  $^\circ\text{C}/5$  h.

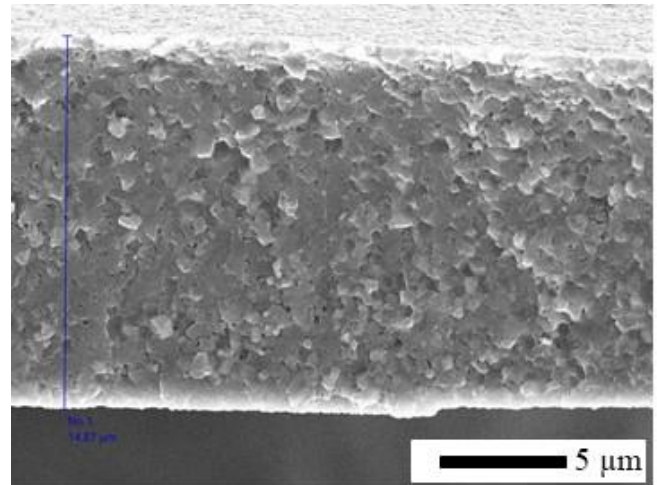


**Figure 6.** Typical fracture surface of sintered film.

**Table 2.** Thickness of 0MA, 0.5MA, 1MA, 2MA, 3MA, and 5MA 20  $\mu\text{m}$  films (one-step process).

Wt. % MgO in $\text{Al}_2\text{O}_3$	Cast green film	Uniaxially pressed green film	Film sintered at 1500 $^\circ\text{C}/0$ h	Film sintered at 1500 $^\circ\text{C}/1$ h	Film sintered at 1500 $^\circ\text{C}/3$ h	Film sintered at 1500 $^\circ\text{C}/5$ h
0.0	26 $\pm$ 2 $\mu\text{m}$	27 $\pm$ 2 $\mu\text{m}$	18 $\mu\text{m}$	11 $\mu\text{m}$	17 $\mu\text{m}$	14 $\mu\text{m}$
0.50	26 $\pm$ 2 $\mu\text{m}$	25 $\pm$ 2 $\mu\text{m}$	17 $\mu\text{m}$	17 $\mu\text{m}$	18 $\mu\text{m}$	18 $\mu\text{m}$
1.0	28 $\pm$ 2 $\mu\text{m}$	26 $\pm$ 2 $\mu\text{m}$	16 $\mu\text{m}$	19 $\mu\text{m}$	17 $\mu\text{m}$	21 $\mu\text{m}$
2.0	38 $\pm$ 2 $\mu\text{m}$	36 $\pm$ 2 $\mu\text{m}$	29 $\mu\text{m}$	25 $\mu\text{m}$	18 $\mu\text{m}$	20 $\mu\text{m}$
3.0	28 $\pm$ 2 $\mu\text{m}$	26 $\pm$ 2 $\mu\text{m}$	19 $\mu\text{m}$	15 $\mu\text{m}$	27 $\mu\text{m}$	17 $\mu\text{m}$
5.0	28 $\pm$ 2 $\mu\text{m}$	25 $\pm$ 2 $\mu\text{m}$	18 $\mu\text{m}$	20 $\mu\text{m}$	16 $\mu\text{m}$	22 $\mu\text{m}$

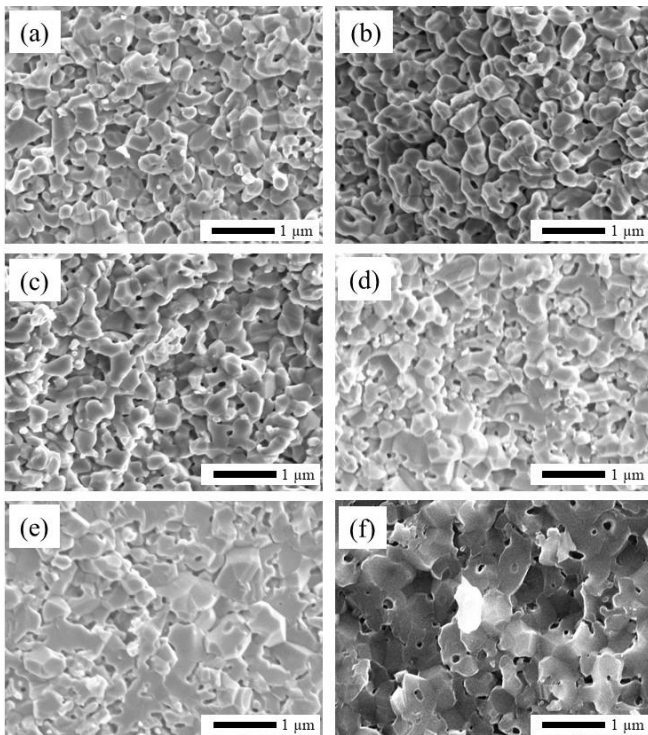


**Figure 7.** SEM fracture surface images of (a) 0, (b) 0.5, (c) 1, (d) 2, (e) 3, and (f) 5MA 20 μm films sintered at 1500 °C/0 h/O<sub>2</sub> (magnification: 25,000X).

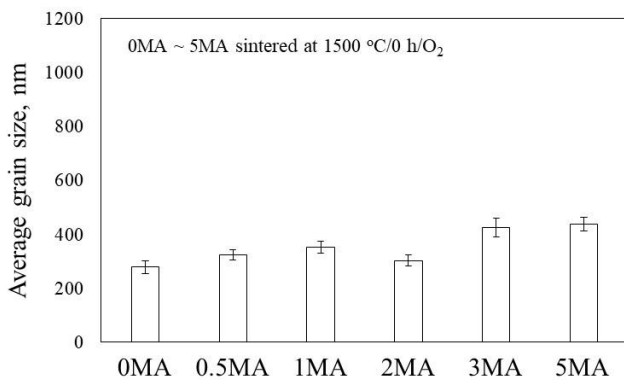


**Figure 8.** AGSs of 0, 0.5, 1, 2, 3, and 5MA 20 μm films sintered at 1500 °C/0 h/O<sub>2</sub>.

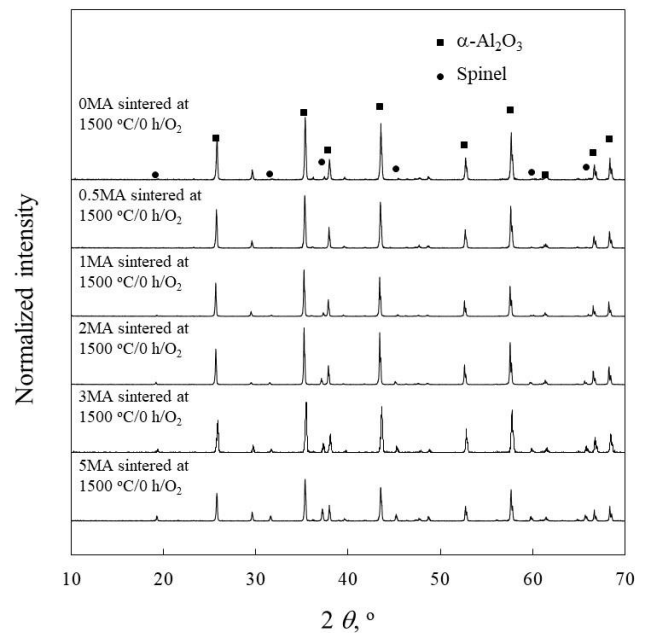


**Figure 9.** XRDs of 0, 0.5, 1, 2, 3, and 5MA 20 μm films sintered at 1500 °C/0 h/O<sub>2</sub>.

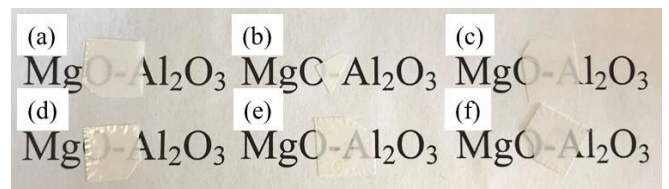


**Figure 10.** Optical images of (a) 0, (b) 0.5, (c) 1, (d) 2, (e) 3, and (f) 5MA 20 μm films sintered at 1500 °C/0 h/O<sub>2</sub>.

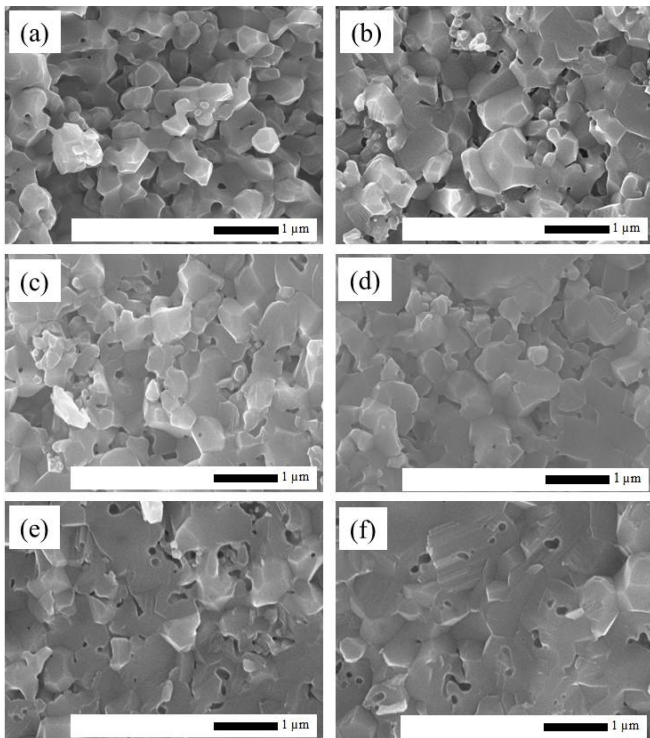


**Figure 11.** SEM fracture surface images of (a) 0, (b) 0.5, (c) 1, (d) 2, (e) 3, and (f) 5MA 20 μm films sintered at 1500 °C/1 h/O<sub>2</sub> (magnification: 25,000X).

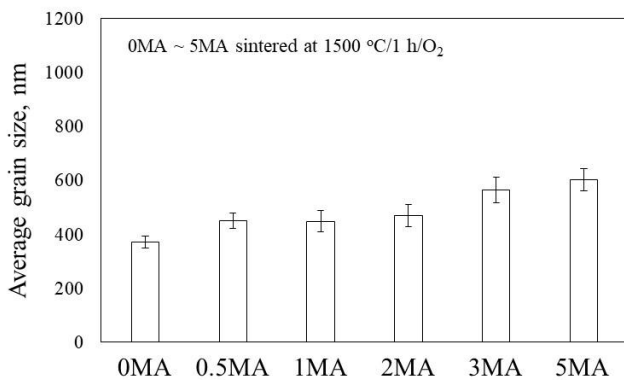


**Figure 12.** AGSs of 0, 0.5, 1, 2, 3, and 5MA 20 μm films sintered at 1500 °C/1 h/O<sub>2</sub>.

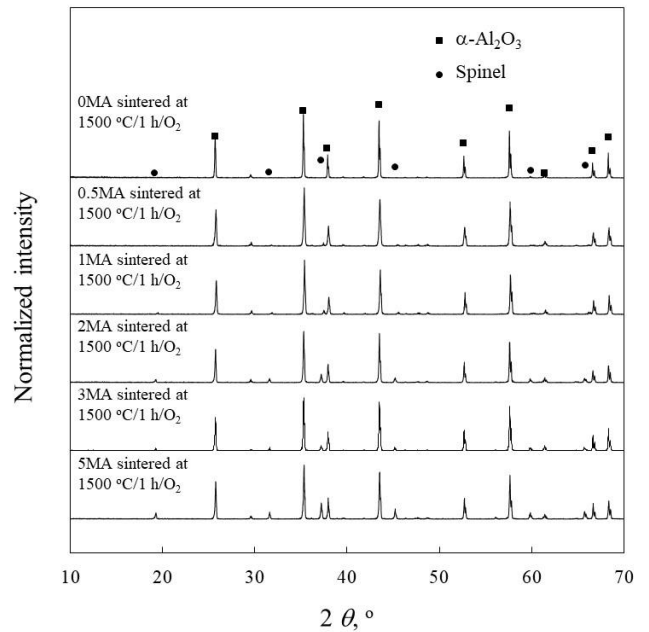


**Figure 13.** XRDs of 0, 0.5, 1, 2, 3, and 5MA 20 μm films sintered at 1500 °C/1 h/O<sub>2</sub>.

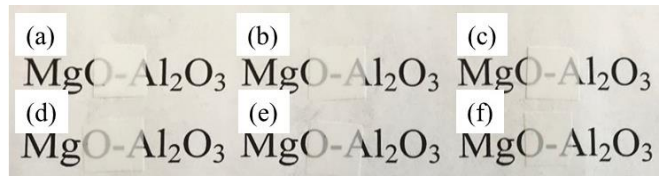


**Figure 14.** Optical images of (a) 0, (b) 0.5, (c) 1, (d) 2, (e) 3, and (f) 5MA 20 μm films sintered at 1500 °C/1 h/O<sub>2</sub>.

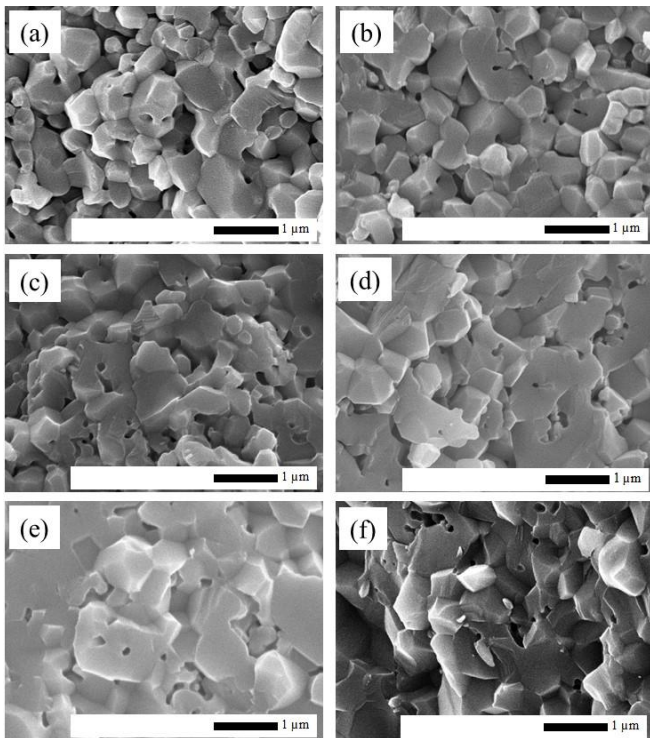


**Figure 15.** SEM fracture surface images of (a) 0, (b) 0.5, (c) 1, (d) 2, (e) 3, and (f) 5MA 20 μm films sintered at 1500 °C/3 h/O<sub>2</sub> (magnification: 25,000X).

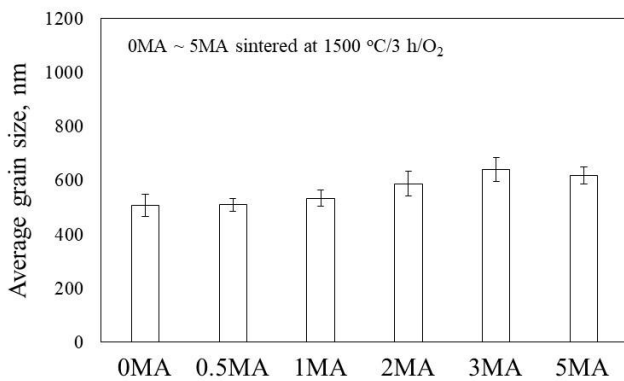


**Figure 16.** AGSs of 0, 0.5, 1, 2, 3, and 5MA 20 μm films sintered at 1500 °C/3 h/O<sub>2</sub>.

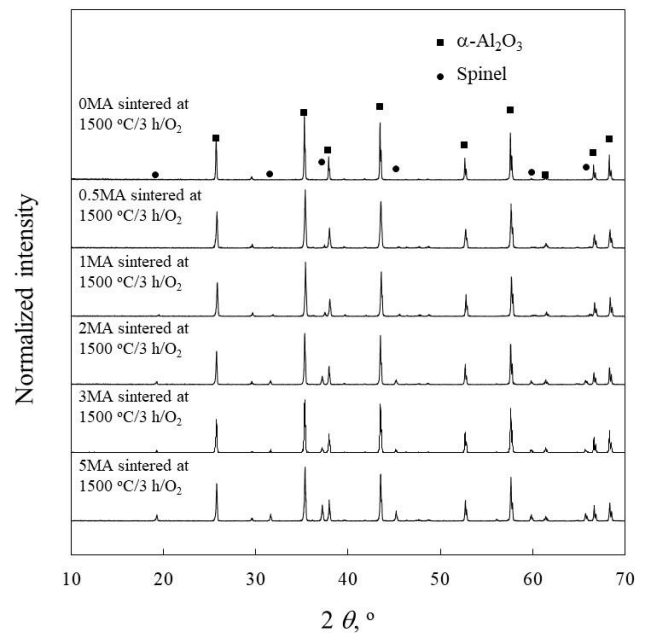


**Figure 17.** XRDs of 0, 0.5, 1, 2, 3, and 5MA 20 μm films sintered at 1500 °C/3 h/O<sub>2</sub>.

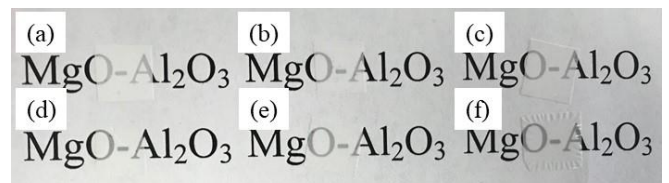


**Figure 18.** Optical images of (a) 0, (b) 0.5, (c) 1, (d) 2, (e) 3, and (f) 5MA 20 μm films sintered at 1500 °C/3 h/O<sub>2</sub>.

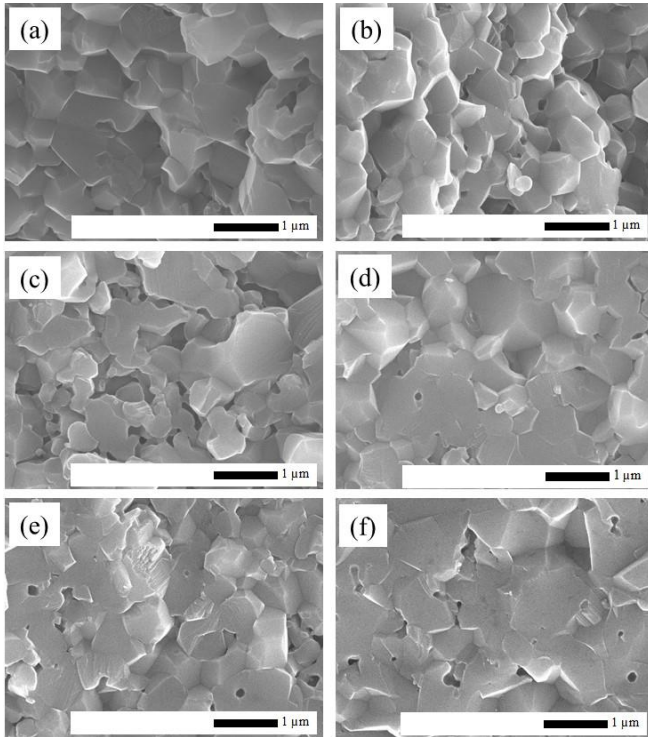


**Figure 19.** SEM fracture surface images of (a) 0, (b) 0.5, (c) 1, (d) 2, (e) 3, and (f) 5MA 20 μm films sintered at 1500 °C/5 h/O<sub>2</sub> (magnification: 25,000X).

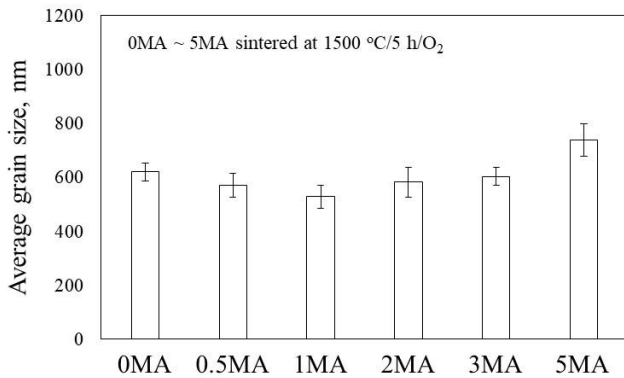


**Figure 20.** AGSs of 0, 0.5, 1, 2, 3, and 5MA 20 μm films sintered at 1500 °C/5 h/O<sub>2</sub>.

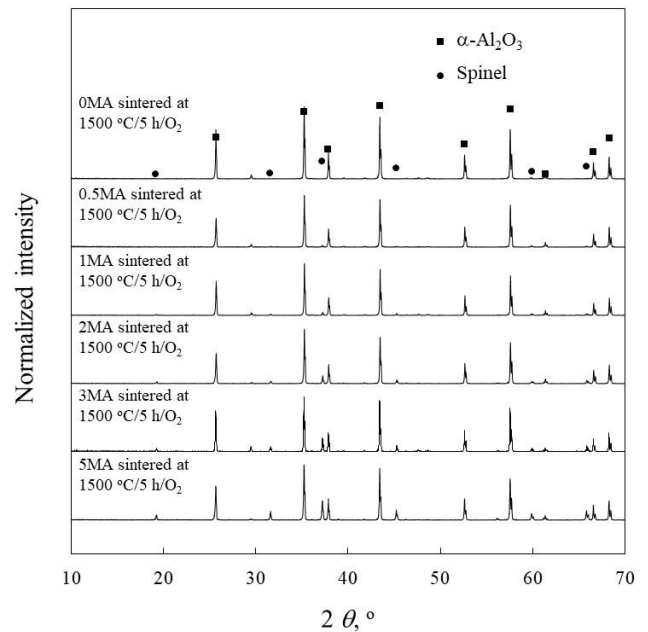


**Figure 21.** XRD patterns of 0, 0.5, 1, 2, 3, and 5MA 20 μm films sintered at 1500 °C/5 h/O<sub>2</sub>.

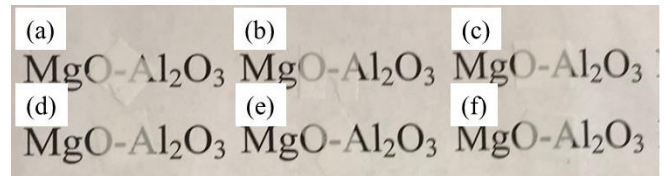


**Figure 22.** Optical images of (a) 0, (b) 0.5, (c) 1, (d) 2, (e) 3, and (f) 5MA 20 μm films sintered at 1500 °C/5 h/O<sub>2</sub>.

### 3.2 Characterization of 10 μm thin films of 0.0, 0.50, 1.0, and 2.0 wt. % MgO doped Al<sub>2</sub>O<sub>3</sub>

The 0.0, 0.50, 1.0, and 2.0 wt. % of MgO doped Al<sub>2</sub>O<sub>3</sub> films (0, 0.5, 1, and 2MA respectively) were sintered using a one-step process wherein the films were heated to  $t_f=1500$  °C for  $h_f = 5$  h. Green films were placed between  $\alpha$ -Al<sub>2</sub>O<sub>3</sub> substrates ( $D = 42$  mm, where films are 5 mm x 5 mm) and sintered using vacuum tube furnace. Fracture surfaces of sintered films (typically 10 μm thick) is shown in Figure 23. Film thicknesses are listed in Table 3. The greatest densification was seen in 1.0 and 2.0 wt. % MgO films. Vertical shrinkage ranged about 30-40 %.

SEMs of 0, 0.5, 1, and 2MA thin films are presented in Figure 24 (1500 °C/5 h). 1 and 2MA [Figure 24 (c) and (d)] exhibit the highest density.

The AGSs of sintered films are shown in Figure 25. Basically the AGSs increase with increasing MgO content. Compared to 20 μm films sintered at 1500 °C/5 h, Figure 19, AGSs are larger because films are heated relatively faster.

Figure 26 presents XRDs of sintered films. 0MA is a single phase  $\alpha$ -Al<sub>2</sub>O<sub>3</sub>, whereas 0.5, 1, and 2MA present two phases  $\alpha$ -Al<sub>2</sub>O<sub>3</sub>, and spinel (MgAl<sub>2</sub>)O<sub>4</sub>.

Optical images of sintered films are shown in Figure 27 (1500 °C/5 h). 1 and 2MA [Figure 27 (c) and (d)] exhibit the highest transparency.

The simple bend test for sintered films is shown in Figure 28 (1MA, 1500 °C/5 h), which exhibits the highest flexibility.

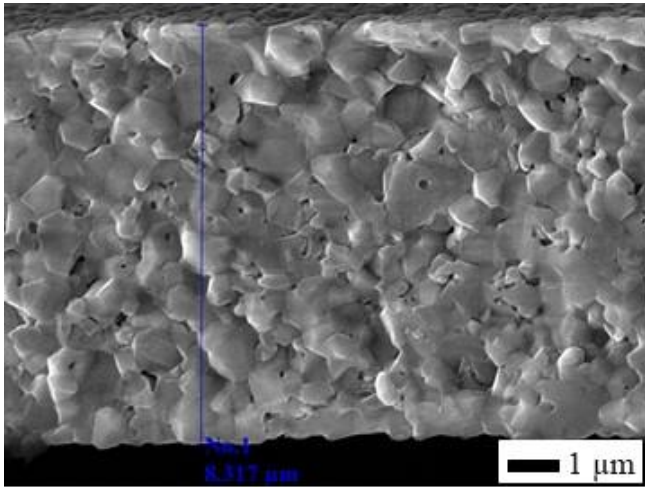


**Figure 23.** Typical transgranular fracture surface of sintered film.

**Table 3.** Thickness of 0, 0.5, 1, and 2MA 10 μm films (one-step process).

Wt. % MgO in Al <sub>2</sub> O <sub>3</sub>	Cast green film	Uniaxially pressed green film	Film sintered at 1500 °C/5 h
0.0	13 μm	11 μm	8.7 μm
0.50	13 μm	12 μm	9.2 μm
1.0	14 μm	13 μm	8.3 μm
2.0	17 μm	16 μm	11 μm

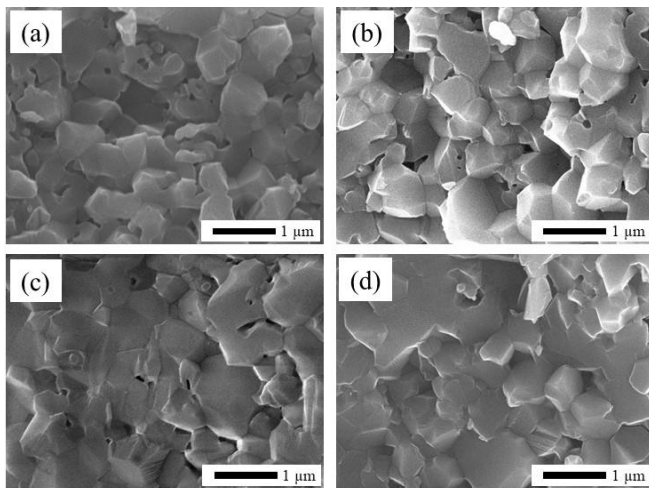


**Figure 24.** SEM fracture surface images of (a) 0, (b) 0.5, (c) 1, and (d) 2MA 10 μm films sintered at 1500 °C/5 h/O<sub>2</sub> (magnification: 25,000X).

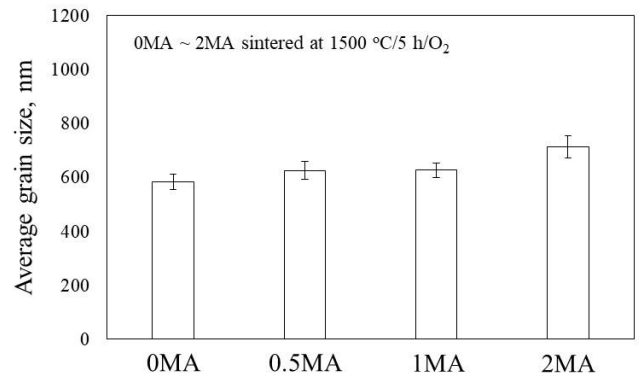


**Figure 25.** AGSs of 0, 0.5, 1, and 2MA 10 μm films sintered at 1500 °C/5 h/O<sub>2</sub>.

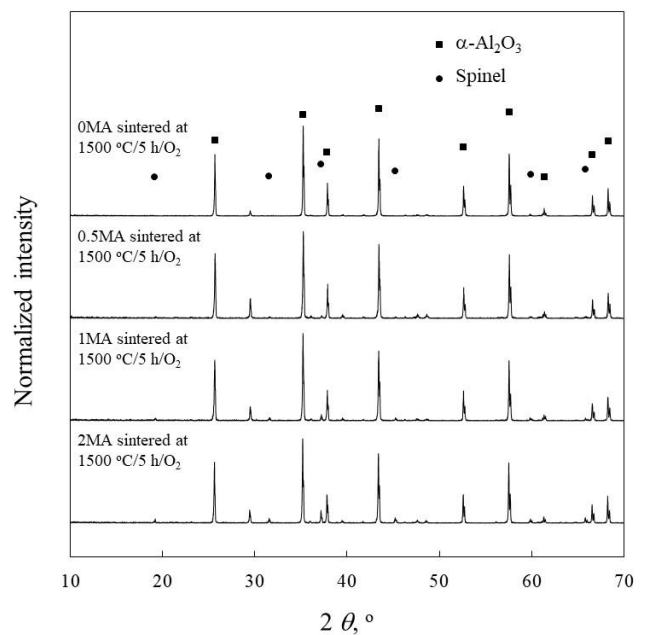


**Figure 26.** XRDs of 0, 0.5, 1, and 2MA 10 μm films sintered at 1500 °C/5 h/O<sub>2</sub>.

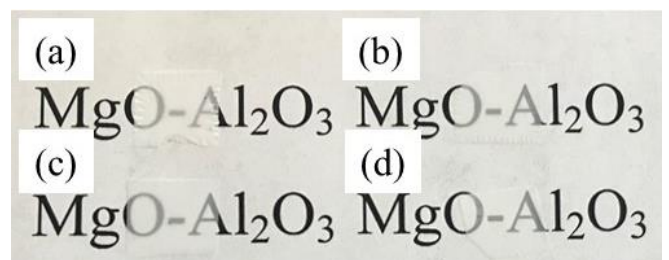


**Figure 27.** The images of (a) 0, (b) 0.5, (c) 1, and (d) 2MA 10 μm films sintered at 1500 °C/5 h/O<sub>2</sub>.

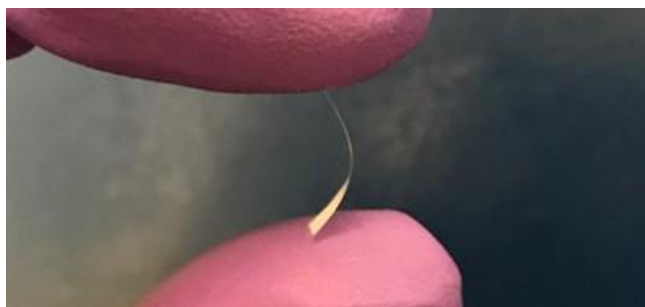


**Figure 28.** The bend tests for IMA 10  $\mu\text{m}$  films sintered at 1500  $^{\circ}\text{C}/5\text{ h}/\text{O}_2$ .

#### 4. CONCLUSIONS

Rapid optimization of phases and stoichiometry in mixed metal oxide NPs is desirable for a number of applications, which can be achieved by controlling precursor compositions used for LF-FSP. Here, we demonstrate the use of LF-FSP to produce MgO doped  $\delta\text{-Al}_2\text{O}_3$  and the fabrication of transparent, dense, flexible and thin (typically 10  $\mu\text{m}$ )  $\text{Al}_2\text{O}_3$  films by tape-casting  $t\text{-Al}_2\text{O}_3$  NPs.

APSs were observed to decrease with increasing MgO content. XRD confirmed that 0.0 wt. % MgO doped  $\delta\text{-Al}_2\text{O}_3$  NP exhibited a single phase which corresponds to  $\delta\text{-Al}_2\text{O}_3$ , and 0.50, 1.0, 2.0, 3.0 and 5.0 wt. % MgO doped  $\delta\text{-Al}_2\text{O}_3$  NPs present two phases  $\delta\text{-Al}_2\text{O}_3$  and spinel ( $\text{MgAl}_2\text{O}_4$ ).

AGSs were observed to decrease with small MgO content, and increase with high MgO content. XRD confirmed that OMA exhibited a single phase which corresponds to  $\alpha\text{-Al}_2\text{O}_3$ , whereas 0.5, 1, 2, 3, and 5MA present two phases which correspond to  $\alpha\text{-Al}_2\text{O}_3$ , and spinel ( $\text{MgAl}_2\text{O}_4$ ).  $\text{Al}_2\text{O}_3$  films doped with small amounts of MgO (1.0 and 2.0 wt. %) exhibited transparency, high density and flexibility after sintered at 1500  $^{\circ}\text{C}$  for 5 h.

#### ACKNOWLEDGEMENTS

Firstly, I would like to express my sincere gratitude to my advisor Prof. Richard M. Laine for his continuous support, patience, motivation, and immense knowledge. His guidance helped me throughout my research and writing of this report.

I would also like to show my gratitude to Dr. Monika Jansohn who cooperatively worked with me. Without her precious support it would not have been possible to conduct this research.

My sincere thanks also goes to Dr. Eongyu Yi, and Dr. Yoshiyuki Abe, and Dr. Eleni Temeche who gave access to the laboratory and research facilities gave me great advice.

Moreover, I would also like to thank my lab-mates for the fun and support.

Lastly, this work was fully supported by Japan-US Advanced Collaborative Education Program. I have to express my deep appreciation to everyone involved in this program.

#### REFERENCES

- [1] Yang, Y., Wu, Y., Tape-casted transparent alumina ceramic wafers, *J. Mater. Res.*, 29, pp. 2312-2317 (2014).
- [2] Krell, A., Blank, P., Ma, H., Hutzler, T., Nebelung, M., Processing of High-Density Submicrometer  $\text{Al}_2\text{O}_3$  for New Applications, *J. Amer. Ceram. Soc.*, 86, pp. 546-553 (2003).
- [3] Krell, A., Bales, A., Grain Size-Dependent Hardness of Transparent Magnesium Aluminate Spinel, *Int. J. Appl. Ceram. Technol.*, 8, pp. 1108-1114 (2011).
- [4] Vozdecky, P., Roosen, A., Knieke, C., Peukert, W., Direct Tape Casting of Nanosized  $\text{Al}_2\text{O}_3$  Slurries Derived from Autogenous Nanomilling, *J. Amer. Ceram. Soc.*, 93, pp. 1313-1319 (2010).
- [5] Nieh, T. G., Wadsworth, J., Hall-Petch relation in nanocrystalline solids, *Scripta Metallurgica et Materialia*, 25, pp. 955-958 (1991).
- [6] Chokshi, A. H., Rosen, A., Karch, Gleiter, H., On the validity of the Hall-Petch relationship in nanocrystalline materials, *Scripta Metallurgica*, 23, pp. 1679-1684 (1989).
- [7] Bowen, P., Carry, C., Luxembourg, D., Hofmann, H., Colloidal processing and sintering of nanosized transition aluminas, *Powder Technol.*, 157, pp. 100-107 (2005).
- [8] Yi, E., Furgal, J., Azurdia, J., Laine, R. M., Roll Your Own Nano-Nanocomposite Capacitors, *J. Mater. Chem. A*, 2, pp. 3766-3775 (2014).
- [9] Yi, E., Wang, W., Kieffer, J., Laine, R. M., Flame made nanoparticles permit processing of dense, flexible,  $\text{Li}^+$  conducting ceramic electrolyte thin films of cubic- $\text{Li}_7\text{La}_3\text{Zr}_2\text{O}_{12}$  (c-LLZO), *J. Mater. Chem. A*, 4, pp. 12947-12954 (2016).
- [10] Yi, E., Wang, W., Mohanty, S., Kieffer, J., Tamaki, R., Laine, R. M., Materials that can replace liquid electrolytes in Li batteries: Superionic conductivities in  $\text{Li}_{1.7}\text{Al}_{0.3}\text{Ti}_{1.7}\text{Si}_{0.4}\text{P}_{2.6}\text{O}_{12}$ . Processing combustion synthesized nanopowders to free standing thin films, *J. Power Sources*, 269, pp. 577-588 (2014).
- [11] Taylor, N. J., Laine, R. M., Extrusion of YAG Tubes Shows that Bottom-up Processing is Not Always Optimal, *Adv. Funct. Mater*, 24, pp. 1125-1132 (2014).
- [12] Hinklin, T., Toury, B., Gervais, C., Babonneau, F., Gislason, J. J., Morton, R. W., Laine, R. M., Liquid-Feed Flame Spray Pyrolysis of Metalloorganic and Inorganic Alumina Sources in the Production of Nanoalumina Powders, *Chem. Mater*, 16, pp. 21-30 (2004).
- [13] Kim, M., Laine, R. M., Pressureless Sintering t-zirconia@ $\delta\text{-Al}_2\text{O}_3$  (54 mol %) Core-Shell Nanopowders at 1120 $^{\circ}\text{C}$  Provides Dense t-Zirconia-Toughened  $\alpha\text{-Al}_2\text{O}_3$  Nanocomposites, *J. Am. Ceram. Soc.*, 93, pp. 709-715 (2010).
- [14] Azar, M., Palmero, P., Lombardi, M., Garnier, V., Motanaro, L., Fantozzi, G., Chevalier, J., Effect of initial particle packing on the sintering of nanostructured transition alumina, *J. Europ. Ceram. Soc.*, 28, pp. 1121-1128 (2008).
- [15] Sun, J., Simon, S. L., The melting behavior of aluminum nanoparticles, *Thermochimica Acta*, 463, pp. 32-40 (2007).

# ANALYSIS OF ASSEMBLY LINE WITH LEARNING EFFECTS

Taro Mizutani

Department of Mechanical Engineering, Graduate School of Engineering, Nagoya University  
mizutani@me1.mae.nagoya-u.ac.jp

Prof.Freiheit, Prof.Hu

Department of Mechanical Engineering, College of Engineering, University of Michigan  
[tfreihei@umich.edu](mailto:tfreihei@umich.edu), [jackuhu@umich.edu](mailto:jackuhu@umich.edu)

## ABSTRACT

An optimal design of an assembly line can save much production time by reducing idle time for workstations. In an assembly line, the production workers or machines repeat tasks that are same or similar. Since they get used to tasks assigned to them, the time to accomplish tasks is shortened by learning. This learning can increase idle time for workers, leading waste of time and money. The purpose of this paper is to introduce time learning effects to assembly line tasks, then find an optimal solution for cycle time. In addition, some assembly lines also have to deal with multiple product types having different task time and idle time. We consider about the effect of learning effects for tasks in sequencing product types and compare the idle time with/without learning effects.

## 1. INTRODUCTION

Assigning tasks to stations in assembly line is a one of the key issue in designing production system, mostly for medium to long term production planning. There are many factors leading to waste of money or time in production line<sup>1</sup>. It is economic approach by reducing time waste since rebuilding machines or rearranging the workers cost much time and money. Also, if the assembly line is arranged efficiently and optimally, then idle time can be eliminated.

An assembly line is a set of workstations where component parts are assembled and to produce a finished product. In assembly line, whole tasks from first task to last one to be completed, are divided into work elements such as putting a screen into iPhone frame or attaching a window to a car. A set of those work elements and their workers are assigned to a workstation. Workstations are connected continuously in a line. Products enter each workstation with a set of tasks already completed at the previous workstations. Upon completion of the assigned tasks, the product move to the next workstation and new product is obtained from the previous workstation. It is desired that all workstations be simultaneously busy with tasks, having equal time assigned to each station (i.e., having not idle time).

In assembling a product, we have to follow an assembly order since product parts must be put together properly, otherwise a mismatch of parts or an incomplete product will happen. We will review some examples of representing the relation of parts or the order of sequencing<sup>2,3</sup>. One method is to represent the order relationship is a liaison graph which helps us to see overall relation between the parts in a product. Figure.1 is an example of liaison graph for the powertrain of an automobile. In this graph, the nodes represent parts and the lines between the nodes represent the relation between the parts. These relationships represent the physical connection between the product components. For assembly, a precedence graph (Figure.2) is made according to liaison graph. This graph represents the constraints for the assembling order; it's useful to identify which components can be assembled at each stage.

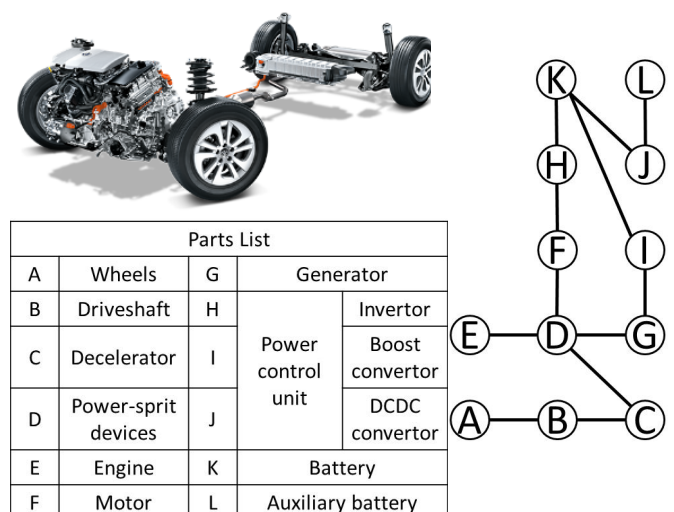


Fig.1 liaison graph

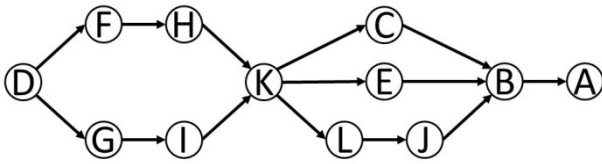


Fig.2 precedence graph

The most important objective in an assembly line is to minimize the assembly cost, which is composed of labor cost and idle time cost. Since labor cost is connected to task times and task times can generally be assumed to be fixed, we simply need to concentrate on reducing idle time. Idle time is generated when the task time at the workstations are different, since there is waiting time at workstations that are already done with its tasks and would be considered a waste while other workstations are still working. Hence we need to set task time as same as possible at each workstation. Some example of the many papers considering the waste of cost or time by taking account for fields, demands, preference, or generation are given in the references<sup>3,4,5</sup>.

In an assembly line, the production workers or machines repeat tasks that are the same or similar. Since they get used to doing the tasks assigned to them, the time to accomplish tasks would become shortened. This effect of reducing time by repeating tasks is called learning effect. If we consider the learning effect, the time to complete a task at each workstation is changing as time passes, and therefore the idle time could also change. Ignoring the learning effect can lead to large waste of time. We can also focus on not only idle time but also on equipment cost, smoothness of the line, or the number of stations in the line<sup>6,7</sup>. Consideration about forgetting has also been examined in some papers<sup>8,9</sup>. In this paper, we only focus on idle time that indirectly affects these factors.

In this paper we consider both assigning tasks to a workstation and scheduling the sequence for multiple product types. Then we introduce learning effects to the assembly line, specifically in assigning tasks and sequencing multiple product types. We consider the effect of learning effects to assembly line and compare the idle time with/without learning effects.

## 2. METHOD

### 2.1 ASSIGNING TASKS TO WORKSTATIONS

First we will examine the order of tasks and also to which station a set of tasks should be assigned in designing an assembly line. We define a production stage  $k$  as the stage wherein a product unit  $m$  is processed at workstation  $n$  (Table.1). We assign one or some tasks to each workstation.

Table.2 (a) and (b) show examples when we assign the tasks differently without learning effects. Let the time for tasks 1, 2 and 3 be 10, 8 and 15 minutes, respectively. In Table. 2(a), tasks 1 and 2 are assigned to station 1 and task 3 is assigned to station 2. Alternatively, task 1 is assigned to station 1 and tasks 2 and 3 are assigned to station 2, as shown in Table.2(b). Tasks are done to each product unit repeatedly, so the total task time in the same station doesn't change (when learning effects are not included). Idle time is calculated as:

$$IDLE = \sum_{n \in N} \sum_{k \in K} (M_k - t_{n,k}) \quad (1.1)$$

where  $N$  and  $K$  is the total number of workstations and stages, respectively.  $M_k$  is the time at the workstation that have maximum time (the bottleneck time) in production stage  $k$ , and  $t_{n,k}$  is the time at workstation  $n$  in production stage  $k$ . Parameter  $t_{n,k} = 0$  if  $n$  is inactive in stage  $k$ . Idle time of this example is calculated as  $18 + (18 - 15) + (18 - 15) + 15 = 39$  minutes in Table.2(a), and  $10 + (23 - 10) + (23 - 10) + 23 = 59$  minutes in Table.2(b). Comparing these examples, idle time will be different if the way the tasks are distributed to workstations is changed. While there are only 3 tasks, 2 workstations, and 5 production stages here, in practice we have to deal with much bigger assembly lines, where the difference between idle time can be dramatically large with/without taking into account an efficient way to assign tasks to assembly line stations.

Table.1 production stage

		Production stage $k$				
		1	2	3	4	5
Workstation $n$	1	Unit 1	Unit 2	Unit 3		
	2		Unit 1	Unit 2	Unit 3	
	3			Unit 1	Unit 2	Unit 3

**Table.2** time for each station and units

without learning effects

(a) upper

Station1	Unit 1	Unit 2	Unit 3	
Task number 1,2	18	18	18	
Station2		Unit 1	Unit 2	Unit 3
Task number 3		15	15	15

(b) lower

Station1	Unit 1	Unit 2	Unit 3	
Task number 1	10	10	10	
Station2		Unit 1	Unit 2	Unit 3
Task number 2,3		23	23	23

Assuming that we have to deal with  $I$  tasks, then the total possible solution of order will be  $I$  factorial. As the number of tasks increase, it takes much time to calculate an exact solution. Therefore heuristics such as COMSOAL (Arcus [1966]) are used to solve task assignment problems that have a large number of possible solutions. Tasks are chosen randomly among the set of feasible tasks, and it is repeated until all tasks are selected. Tasks are selected in order to meet the cycle time at a workstation and a new workstation is opened when needed.

Let  $NIP(i)$  the number of immediate predecessors for each task  $i$ ,  $D$  the idle time at each trial, and  $WIP(i)$  indicates for which other tasks  $i$  is an immediate predecessor.  $TK$  indicates for  $I$  tasks and  $t_i$  indicates for the time of specific task  $i$ . Now we have a total of  $I$  tasks and a cycle time is  $C$ . At the start all tasks that are not assigned belong to group A. Next, feasible tasks among A (that don't have a constraint of predecessors) are assigned to group B. Then, only tasks that don't exceed the remaining cycle time at the current workstation are assigned to group F. Last, we select one random task  $i$  and assign it to the station, and then the selected task  $i$  is removed from groups A, B and F. Constraints related to task  $i$  are removed. We repeat this process until all tasks belonging to group A are assigned to a station. The procedure for generating  $X$  trial solutions is then as follows:

Procedure<sup>10</sup>

1. Set  $x = 0$ ,  $UB = \infty$ ,  $c = C$ .
2. Set  $x = x + 1$ ,  $A = TK$ ,  $NIPW(i) = NIP(i)$ .
3. For all  $i \in A$ , if  $NIPW(i) = 0$ , add  $i$  to B.
4. For all  $i \in B$ , if  $t_i \leq c$ , add  $i$  to F.
5. If F empty, go to 6; otherwise 7.
6.  $D = D + c$ ,  $c = C$ . Go to 3.
7. Set  $l = \text{card}\{F\}$ . Randomly generate  $RN \in U(0,1)$ .  
Let  $i^* = [l * RN]$ th task from F.  
Remove  $i^*$  from A, B and F.  $c = c - t_{i^*}$ .  
For all  $i \in WIP(i^*)$ ,  $NIPW(i) = NIPW(i) - 1$ .

If A empty, go to 8; otherwise 3.

8.  $D = D + c$ . If  $D \leq UB$ ,  $UB = D$ , and record it.  
If  $x = X$ , stop; otherwise go to 2.

## 2.2 TIME LEARNING EFFECTS

The production workers learn how to do the tasks as they repeat them. Hence we need to consider their rate of change in task time as the repeat the tasks. Table.3 shows an example considering the learning effects on task time. The time for each task changes as the workers repeat tasks. Since the maximum time (the bottleneck time) at each production stage may change, idle time at each production stage can also change, leading to difficulty in obtaining an optimal task assignment. In this example, idle time is  $18 + (15 - 13) + (10 - 9) + 7 = 28$  minutes. Idle time will be different if the assigned task at each workstation is changed.

The learning effect can be modelled as<sup>11</sup>;

$$t_{i,j} = t_i(j)^{-a_i} \quad (2.1)$$

where  $t_{i,j}$  is the time for  $j$ th production unit on the  $i$ th task and  $t_i$  is the time for 1st production unit on the  $i$ th task.  $a_i$  is the learning coefficient for  $i$ th task.

**Table.3** time for each station and units

with learning effects

Station1	Unit 1	Unit 2	Unit 3	
Task number 1,2	18	13	10	
Station2		Unit 1	Unit 2	Unit 3
Task number 3		15	9	7

We can get a task assignment for each station using COMSOAL program. Table.4 shows an example of the result of assigning 5 tasks. We will adopt learning effects to all these task assignment orders. First we calculate the total time at each workstation. We introduce learning effects to each task and list the time at every workstation and production stage such as Table.1. Then we can calculate the idle time at each trial by using equation (1.1).

**Table.4** result of sequencing order

		Number of trial $x$			
		1	2	3	...
Workstation $n$	1	1,2	1,2,3	2,1	...
	2	3,4	4	3,4	...
	3	5	5	5	...

## 2.3 SCHEDULING MULTIPLE PRODUCT TYPES

In practice, many facilities have to deal with multiple product types simultaneously on a single production line. If we produce only one product type on the line at a time, then other product types will be delayed in the fulfillment of their demand. Each product type may have a different time to produce, as well as a different demand. One desirable way to solve this problem is to sequence the different product types such that the deviation of each product types from the demand is minimized<sup>12,13</sup>.

Assume that we have  $P$  product types and  $Q_p$  items for each product. We set  $r$  as the number of items that are produced each cycle and  $N_p = Q_p / r$ . We want to schedule the production rate for each product type to be smooth and the idle time is as short as possible. When considering scheduling multiple product types, the bottleneck station is the key to do it since the cycle time for each product type is defined by the time at the bottleneck station. The variable for cycle time for scheduling multiple product types is defined as  $C_n$ . Generally we set  $C_n$  by calculating the average time of the product types at each bottleneck station. However, since we will take into account leaning effects, for example, we will use the average time for a sequence of tasks, as for example the task time for parts  $i = 1\sim 10$  and  $i = 11\sim 20$  are different. Hence we have to recalculate  $C_n$  every cycle such as<sup>10</sup>:

$$C_n = \sum_{i \in S_n} \sum_{p \in P} t_{i,p} \times \frac{Q_p}{\sum_{p \in P} Q_p} \quad (2.2)$$

where  $S_n$  is the set of tasks assigned to the (bottleneck) workstation  $n$ , and  $t_{i,p}$  is the time of tasks  $i$  of product type  $p$ . We introduce a function to select the  $l^{\text{th}}$  set of product for each cycle to be entered to the line.

$$\min \max_{1 \leq l \leq L} \sum_{p=1}^l \left| \sum_{i \in S_n} t_{i,p(n)} - lC_n \right| \quad (2.3)$$

Constrained as below<sup>10</sup>.

$$\sum_{l=1}^L X_{pl} = N_p \quad p = 1, \dots, P \quad (2.4)$$

$$\frac{lN_p}{L} - s_1 \leq \sum_{h=1}^l X_{ph} \leq \frac{lN_p}{L} + s_1$$

$$l = 1, \dots, L \quad p = 1, \dots, P \quad (2.5)$$

$$\sum_{h=1}^l \sum_{p=1}^P \sum_{i \in S_n} t_{i,p} X_{ph} \leq (l + s_2)C_n$$

$$l = 1, \dots, L \quad n = 1, \dots, N \quad (2.6)$$

where  $L = \sum_{p=1}^P N_p$ , and  $X_{pl}$  is 1 if product type  $p$  is selected in the  $l^{\text{th}}$ , otherwise 0. Equation (2.4) ensures that all

product items are assigned. Equation (2.5) restricts the production ratio of each product type to be within  $s_1$  of its average rate and (2.6) restricts the over utilization of each product types at all times. We set  $s_1 = s_2 = 0.9$ .

When scheduling multiple product types, we decide  $L$  firstly, where  $L$  is the number of cycle for scheduling multiple product types.  $N_p / L$  is the progress of the schedule for each product types that is increasing as the cycle proceeds. Cycle time  $C_n$  is calculated by equation (2.2) and AA indicate the number of times to be selected for each product types. Only product type that is satisfied equation (2.5), (2.6) and (2.7) are assigned to group BB. Deviations of time for each product types from average cycle time,  $d_p$ , are calculated and minimum is assigned to group FF in this cycle time. If there are more than one feasible candidate product type in a cycle, the one that is later of schedule is selected. Every time after assigning product type in each cycle, we recalculate  $C_n$ , deviations and progress of schedule by using the time for  $1 + r * (l - 1)^{\text{th}}$  to  $r * l^{\text{th}}$  tasks and repeat it until all items are assigned. The deviations in the  $l^{\text{th}}$  cycle are calculated as idle time,  $IDLE2$ . The procedure for scheduling  $P$  product types is as follows:

Procedure<sup>10</sup>

1. Set  $l = 0$ .
2. Set  $l = l + 1$ . Calculate  $C_n$ .
3. For all  $p$ , if the product type is satisfied with equation (2.5), (2.6) and (2.7), add  $p$  to BB.
4. For all  $p \in BB$ , if  $d_p$  is minimum among BB, add  $p$  to FF.
5. If D has only one candidate, let this  $p^*$  and go to 7; otherwise 6.
6. For all  $p \in FF$ , latest delay of schedule is selected as  $p^*$ .
7. Remove  $p^*$  from AA, BB and FF.  $IDLE2 = IDLE2 + d_{p^*}$ . If  $l = L$ , stop; otherwise go to 2.

## 2.4 SOLUTION COMPARISONS WITH CHANGING PARAMETER

Using above method, we can calculate the idle time generated from different assignment of tasks to workstations due to differences among the task times for different product types at each workstation, and the deviation of time generated in scheduling multiple product types on one product line due to difference among the time of bottleneck station for each product type. We combine the above methods to find an optimal solution. The procedure is as follows;

Procedure

1. Sequence tasks to workstations. We get X (trials) orders of sequencing tasks.
2. Apply learning effects. We apply learning effects to the solutions, and calculate idle time of each solution.
3. Pick most optimal solution. We pick one task assignment solution that provides minimum idle time.

4. **Repeat.** We repeat procedure 1 to 3 with P different product types until all product types are done.
5. **Apply solutions to each product type.** Having one best solution for every product types, then applying each solution to all product type.
6. **Schedule multiple product types.** We determine one schedule for each solution and calculate the deviation of time for that solution.
7. **Change parameter and repeat.** We change a parameter such as cycle time  $C$ , learning coefficient  $a_i$ , or the number of repeat products produced at one cycle in the schedule, then repeat step 1 to 6.

### 3. RESULT AND DISCUSION

#### 3.1 EFFECT OF LEARNING EFFECTS TO TASK TIME ON WORKSTATIONS

Assume that we have 4 product types A, B, C and D, and each product type has 12 tasks. Even if the product type is different, the products have the same tasks to complete, but the times for each task are different because of using different parts or tool. Each product type has a demand of 50, 50, 100, 100 items, respectively. The ship date requires we set a cycle time of 70 minutes, and we have a learning coefficient of 0.3. We used toy car problem in reference and relationship between parts and of precedence is same as well\*. Table.5 shows the task time for each task and product type. Figure.2 shows the change in task time of tasks for product type 1 with learning effects.

**Table.5** time of each task and product type

		Product type			
		A	B	C	D
Task No.	1	20	23	19	17
	2	6	5	5	8
	3	5	4	8	4
	4	21	23	17	24
	5	8	10	11	5
	6	35	33	30	38
	7	15	13	18	12
	8	10	17	7	6
	9	15	18	18	19
	10	5	9	3	7
	11	46	41	48	43
	12	16	13	12	19

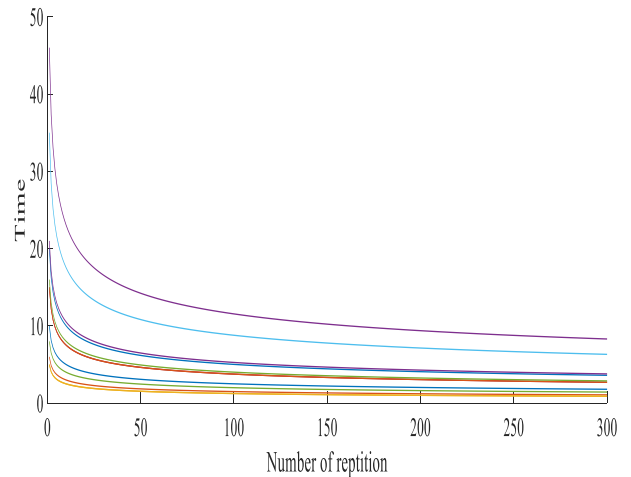


**Figure.2** time of tasks for product type 1 with learning effect

Table.6 shows the difference of the idle time in sequencing tasks to workstations with and without learning effects. In this example, we consider only one product type and the number of items corresponded to it. Idle times with learning effects are shorter than those without learning effects because task times shorten as task is repeated. The effect is more significant when producing more items. The total time of all tasks for products A and B are 202 and 209, but the idle times without learning effects are much different. We can understand this by considering that the difference of time among workstations is bigger in producing product A than B. Hence the effect produces more efficiency for product A.

**Table.6** difference time of idle time with/without learning effects

		Product type			
		A	B	C	D
Learning effect	without	674	480	1808	924
	with	354	379	578	380

#### 3.2 EFFECT OF LEARNING EFFECTS TO SCHEDULE MULTIPLE PRODUCT TYPES

Consider the four task assignment solutions obtained from each product type. We will use these four solutions to calculate the idle time in scheduling multiple product types, as the line may require structural change if the tasks were

assigned to different stations depending on what product type is on the line. Hence we apply the four solutions to all product types and compare those idle time. Table.7 shows the deviations of time from average cycle time. The deviation is large because the average cycle time for multiple product types is flexible when considering learning effects. Every solution changes when we schedule one product type due to the change of time by learning effects.

**Table.7** deviations of time from average cycle time

	Solution for each product type			
	1	2	3	4
Deviation	364	321	375	446

### 3.3 CHANGING PARAMETERS

#### 3.3.1 CYCLE TIME

We will change cycle time from 65 to 75 minutes in order to find the optimal cycle time. If we can find a solution the provides minimum idle time at a cycle time that is shorter than the original target of 70, we should pick this cycle time to save time and money. We will pick the solution that provides both minimum idle time and deviation.

The result is shown in Figures.3 and 4. The numbers in the graph indicate the best solution number at that cycle time. Usually we set the cycle time first depending on the demand of the product, however, there are frequently restrictions about assembly sequences, especially in assembly lines. We get an optimal cycle time after the analysis, so whether the original cycle time is greater or shorter is identified after this analysis. In this example, the optimal cycle time is 69 because idle time is the same as cycle time 70, and 69 is shorter than 70. Figure.3 shows that minimum idle time is mostly decreasing up to 70, and increasing after 70. The reason why idle time at cycle times less than 66 increases is that more workstations are required. Idle time is increasing after cycle time is 70 because we permit some product types to be over cycle time only when solutions are adopted. Hence at those cycle times some product types might be over cycle time. Otherwise the deviations are not so different from Figure.4. This is because sequence of the schedule is analyzed by using the time of bottleneck station, which is not directly connected to the cycle time. This suggests that the largest time of bottleneck station is same at cycle times 65 to 71.

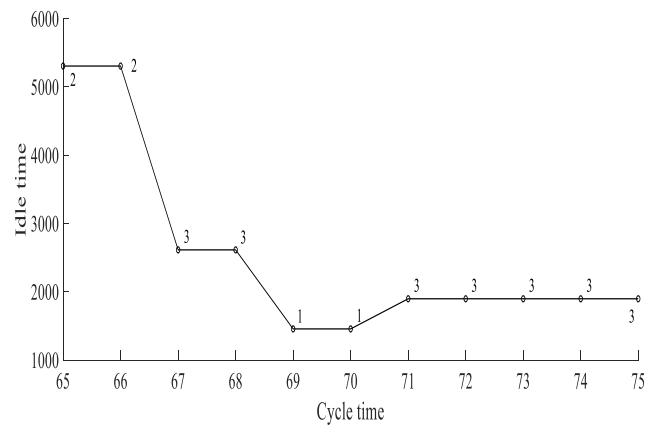


**Figure.3** minimum idle time at each cycle time

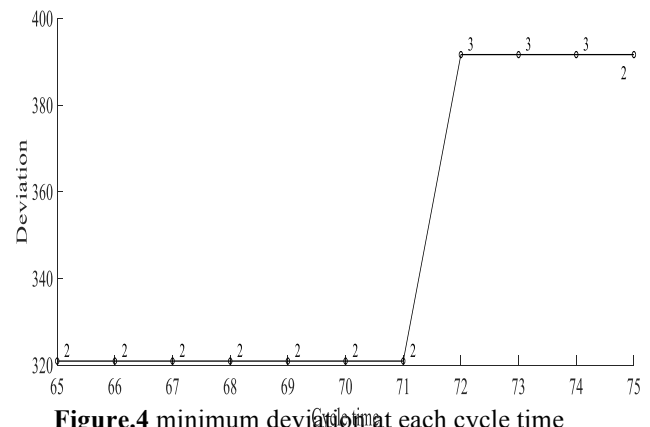


**Figure.4** minimum deviation at each cycle time

#### 3.3.2 LEARNING COEFFICIENT

We originally set the learning coefficient to be 0.3. The learning coefficient might change depending on the product, the worker, or the environment. In this section we analysis the effect of changing the learning coefficient. Figure.5 and 6 show minimum idle time and deviation at each cycle time with changing learning coefficient. We can see that mostly same solution is adopted at each cycle time less than 70, even if learning coefficients are different. However, at cycle times over 70, the solution adopted is different depending on the learning coefficient. This is related to the number of workstations.

Since total task time for product 3 is shortest among other product types in this example, the number of workstations that is needed for all tasks for product type 3 is assigned can be smallest. It leads other product types to be over cycle time. When cycle time is increasing, other product types can also have same number of workstation with product type 3. Time is generally decreased and the asymptotic number is bigger with a small learning coefficient than with a large learning coefficient. This might affect the results in Figure.5. In Figure.6, deviation is increased as the learning coefficient is increased. This is because the schedule sequence is analyzed by using the time

of the bottleneck station, which is not directly connected to cycle time. If the bottleneck station time is small, then the deviation is also small. In this graph the tendency is almost same.

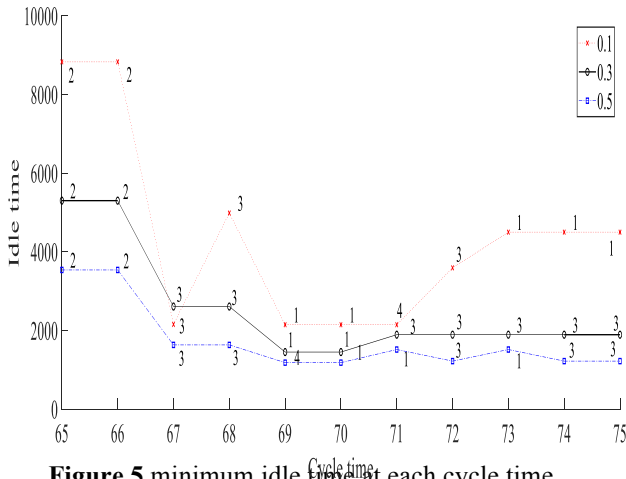


**Figure.5** minimum idle time at each cycle time with changing learning coefficient

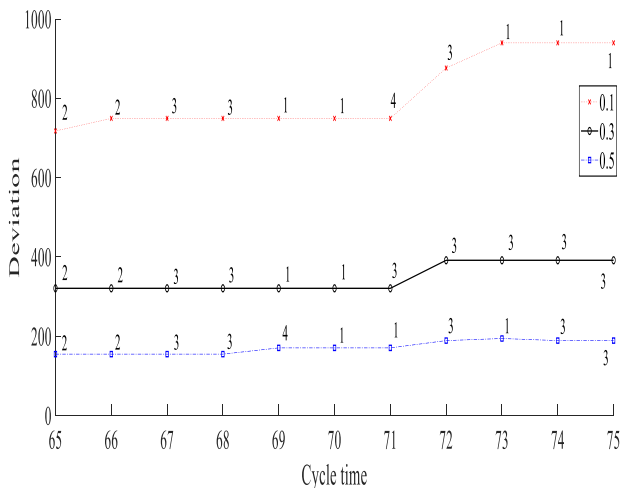


**Figure.6** minimum deviation at each cycle time with changing learning coefficient

#### 4. CONCLUSION

We introduce learning effects to assembly line especially in assigning tasks to workstation and scheduling the order of multiple product types. We can get more efficient sequence by considering these effects. We also consider deviation that is connected to delay from demand that can be connected to idle time. We can find more optimal solution by connecting these two methods. Idle time is really affected by many elements such as cycle time, number of products and so on. We should also consider how other factors affect to idle time.

#### ACKNOWLEDGEMENTS

I would like to express my deepest gratitude to my supervisor, Professor Jack Hu, Professor Theodor Freiheit, Professor Mihaela Banu. I could know many things in this field, develop the skill of MATLAB and also learn about how to research even though I was not familiar with this field. You gave me a great opportunity and I have more interest in this research.

I also would like to thank all laboratory members for being kind to me and teaching me many things such as good information for living or advice.

#### REFERENCES

- [1] Sainath Gopinath, Theodor I. Freiheit, A waste relationship model and center point tracking metric for lean manufacturing system, *IIE Transactions* 44, pp. 136-154 (2012).
- [2] Heng Kuang, S. Jack Hu, Yoram Koren, Concurrent Design of Assembly Plans and Supply Chain Configurations Using AND/OR graphs and Dynamic Programming, *Journal of Manufacturing Science and Engineering* Vol.138, 051011.1-9(2016).
- [3] S. J. Hu, J. Ko, L. Weyand, H. Assembly system design and operations for product variety. , *CIRP Annals* 60, pp. 715-733(2011)
- [4] Nils Boysen, Malte Flidner, Armin Scholl, Assembly line balancing: Which model to use when?, *Production Economics* Vol1, pp.509-528 (2008).
- [5] April Bryan, S. Jack Hu, Yoram Koren, Assembly System Reconfiguration Planning, *Journal of Manufacturing Science and Engineering* Vol.135, 041005.1-13(2013).
- [6] M. Duran Toksari, Selcuk K. Isleyen, Ertan Guner, Omer Faruk Baykoc, Assembly line balancing problem with deterioration tasks and learning effect, *Expert Systems with Applications* Vol37, pp.1223-1228 (2010).
- [7] Nima Hamta, S. M. T. Fatemi Ghomi, F. Jolai, M. Akbarpour Shirazi, A hybrid PSO algorithm for a multi-objective assembly line balancing problem with flexible operation times, sequence-dependent setup times and learning effect, *Production Economics* 141, pp.99-111 (2013).
- [8] Scott M. Shafer, David A. nembhard, Mustafa V Uzumeri, The Effects of Worker Learning, Forgetting, and Heterogeneity on Assembly Line Productivity, *Management Science* Vol.47, pp.1639-1653 (2001).
- [9] John K. Mccreery, Lee J. Krajewski, Improving performance using workforce flexibility in an assembly environment with learning and forgetting effects, *Production Research*, pp.2031-2058 (2010).
- [10] Ronald G. Askin, Charles R. Standridge, *Modeling And Analysis Of Manufacturing Systems*, John Wiley & Sons, INC., pp. 31-59(1993).
- [11] Amiya K. Chakravarty., *Line Balancing With Task Learning Effects*, *IIE Transactions*, pp. 186-193 (1988).
- [12] Nick T. Thomopoulos, *Line Balancing-Sequencing for Mixed-Model Assembly*, *Management Science* Vol4, pp.B59-B75 (2009).
- [13] Joseph Bukchin, Ezey M. Dar-El, Jacob Rubinvitz, *Mixed model assembly line design in a make-to-order*

environment, Computers & industrial Engineering  
Vol41, pp.405-421 (1967).

# **FORCES: THE QUANTITATIVE VALUES OF SHARPENED AND BLUNT MICROWIRE FOR IN-VIVO BRAIN INSERTION**

Makoto Terada

Department of Micro-nano Mechanical Science and Engineering, Graduate School of Engineering, Nagoya University

terada@ume.mech.nagoya-u.ac.jp

Supervisor: Prof. Albert Shih

Department of Mechanical Engineering and Biomedical Engineering, Graduate School of Engineering, University of Michigan

shiha@umich.edu

## **ABSTRACT**

The brain implantation holds great promise to restore motor and sensory functions for patients suffering from neurological disorders. The most challenging task for researchers during the brain implantation is to manually insert the microwires into target region. In this research, we make the PVC phantom with mineral oil to mimic brain tissue. Moreover, we conducted insertion test for PVC and in vivo rat brain. We evaluate the effect of mineral oil in PVC and effect of sharpening wire.

# **Undisclosed**

# Ab Initio Molecular Dynamics Simulation about Dielectric Properties of Boron-doped Diamond-Like Carbon

Tatsuya Okamoto

Department of Micro/Nano Mechanical Science of Engineering, Graduate School of Engineering, Nagoya University  
[okamoto@ume.mech.nagoya-ac.jp](mailto:okamoto@ume.mech.nagoya-ac.jp)

Supervisor: L. Jay Guo  
[guo@umich.edu](mailto:guo@umich.edu)

## ABSTRACT

B-DLC coating is known as high permittivity DLC compared to a-C:H and show lower friction. Ab-initio molecular dynamics was carried out to study the structure and dielectric properties of B-DLC coatings as a function of B concentrations (0–10.93 at.%). RDF result show that the structure made by AIMD was amorphous structure. 1st peak in B-DLC coatings deviated from the position of the 0 at.% boron concentration B-DLC coatings, was shifted, it implied that the bond structure playing an important role in the dielectric properties of the coating. However, there were huge differences between experimental result and AIMD simulation result, so it is necessary to change the program to get more proper results.

## 1. INTRODUCTION

Depletion of energy sources is a concern in recent years, which depends on petroleum and natural gas as energy source. It is reported that 16.5% of the energy input to automobiles is friction loss.<sup>[1]</sup> In order to increase energy efficiently, it is important to reduce friction loss in mechanical sliding parts. Diamond-Like Carbon (DLC) coating has been widely accepted as materials for reducing friction. DLC coating is a thin film with carbon atom as framework. Its physical properties and frictional characteristics are changed depending on the bonding state of the carbon atom and the contained elements. Several investigations about low friction mechanism of DLC coating under lubricant condition have already been reported. In particular, Boron doped DLC (B-DLC) coating was showed low friction coefficient ( $\mu < 0.01$ ) under poly alpha olefin (PAO) oil. However, the low friction mechanism of B-DLC was not fully examined.<sup>[2]-[4]</sup> It is necessary to clarify the low friction mechanism of B-DLC coating in order to apply for sliding parts of car engine.

In my previous work, in order to clarify the low friction mechanism of B-DLC coating, reflectance spectroscopy was used to in-situ observe the friction area under mixed lubrication which the change in lubricant condition appears clearly.<sup>[5]</sup> To clarify the low friction mechanism under the mixed lubrication, it was necessary to verify the effects of the decrement of load carrying ratio of boundary lubrication area under mixed lubrication, or the decrement of friction coefficient of boundary lubrication. To verify the former effect, surface roughness was measured, and for the latter, thickness and polarizability of transformed layer was

measured. We focused on polarizability of transformed layer because the polarizability was related to van der Waals force which control physical adsorption of oil molecular. Polarizability  $\alpha$  of B-DLC was given as Eq. (1).<sup>[6]</sup>  $M$  is atomic weight,  $\rho$  is density,  $N_A$  is Avogadro number,  $n$  is refractive index,  $k$  is extinction coefficient.

$$\alpha = \frac{3M}{4\pi\rho N_A} \frac{n^2 - k^2 - 1}{n^2 - k^2 + 2} \quad (1)$$

Transformed layer, which top surface structure of B-DLC was changed, was observed in accordance with increasing the sliding cycles. Polarizability of transformed layer was measured by using in-situ reflectance spectroscopy. In accordance with decrement of friction coefficient of boundary lubricant area, transformed layer with high polarizability was increased. It suggested that increment of transformed layer with high polarizability effected on low friction. In other words, it suggested that polarizability of the materials increased, then van der Waals force between transformed layer and PAO4 oil increased. By increasing of van del Waals force, oil molecule adsorbed on top surface layer, then friction coefficient decreased.

Next, another my previous work was conducted to make sure that materials with high polarizability really show low friction. Materials with several permittivity was prepared, B-DLC, HT-DLC (Hydrogenated amorphous carbon), three types of CN<sub>x</sub> (Carbon Nitride), TiO<sub>2</sub> and BaTiO<sub>3</sub>. Permittivity  $\epsilon$  is a parameter representing the magnitude of the polarization. Fig.1 shows that permittivity of as-deposited for various materials, friction coefficient decreased with increase in permittivity of as-deposited materials. However, the wear property of TiO<sub>2</sub> and BaTiO<sub>3</sub> was not good because only the initial cycles of TiO<sub>2</sub> and BaTiO<sub>3</sub> shows low friction but after middles cycles shows higher friction than DLC coatings. From this result, it suggested that as-deposited DLC coatings with high permittivity shows low friction. But in this case, several materials were used not only B-DLC coating. And only this study cannot make sure what kind of structure of B-DLC show high permittivity, means low friction. Now it is necessary to verify the structure of B-DLC coating with high permittivity to establish design guidelines to apply for car engines

In this paper, ab initio molecular dynamics (AIMD) simulation based on density functional theory (DFT) was carried out to study the structure and dielectric properties of B-DLC coatings. The Boron concentration ratio was changed from 0 to 10.93 at.%. Radial distribution function

(RDF) was evaluated to reveal the effect of boron concentration on structure, and dielectric function was calculated to reveal the effect of boron concentration on permittivity.

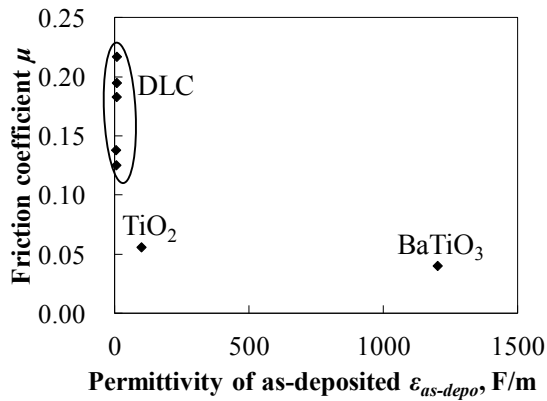


Fig.1 Permittivity of as-deposited materials and friction coefficient

## 2. METHOD OF CALCULATION

### 2.1 MODELING METHOD

Deterministic modeling method frequently used in the material science field is AIMD, tight binding molecular dynamics (TBMD) and classical molecular dynamics (CMD).<sup>[7]-[20]</sup> These methods elucidate the physical properties or phenomena of materials from the micro level by appropriate modeling. However, modeling of molecular simulation has two problems, spatial scale problem and temporal scale problem can be handled. Fig.2 shows schematic illustration of spatial and temporal scales achievable by various simulation approaches. AIMD method is ultimate method to know the physical properties because AIMD is carried out the calculation in the view of ground state of electrons. However, AIMD simulation can only follow the phenomenon on the time scale of few picoseconds and about 100 atoms. The time performance of AIMD simulation is not good. That is, selection of a method corresponding to the spatial and temporal scale of the phenomenon to be considered becomes extremely important.

DLC coating has amorphous structure. Modeling methods of amorphous structure is completely different from crystal structure because it is necessary to simulate the process imitating the generation process in the experiments. One of the methods for creating general amorphous structure is Melt-Quench method, which is the method cooling rapidly from the liquid state structure to solid state structure. After Melt-Quench method, stable amorphous structure is obtained by structural optimization. However, if whole calculation were carried out by AIMD simulation, it takes a lot of times to get the data. In this paper, the following steps were used to produce amorphous structure with less computation time performance.

1. Create initial structure by Melt-Quench method using CMD calculation
2. Structural optimization of initial structure obtained by first principle calculation

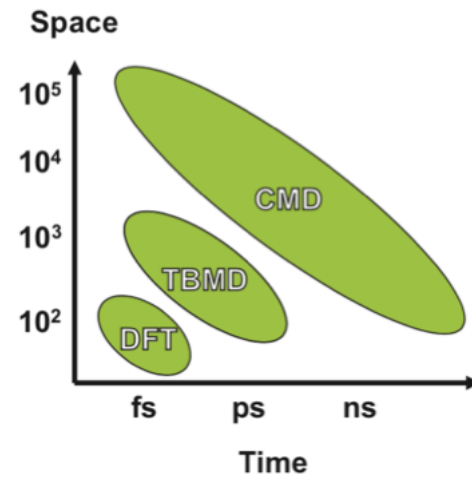


Fig.2 Schematic illustration of spatial and temporal scales achievable by various simulation approaches.

### 2.2 GENERATION OF AMORPHOUS STRUCTURES

#### 2.2.1 MELT-QUENCH METHOD BY CMD CALCULATION

The Lammmps was used for CMD calculation to generate amorphous structure of B-DLC coatings. CMD calculations were performed under NVT ensemble<sup>[21]</sup>, using CMD time interval of 1.0 fs, and BNC tersoff potential was used for atomic interaction potential. The periodic boundary conditions were imposed on the supercell. In this work, the initial configuration contained 64 atoms in a simple cubic supercell,  $8 \times 8 \times 8 \text{ \AA}$ , with constant volume throughout the simulation. To obtained B-doped amorphous structures, the systems were firstly equilibrated at 5000 K for 8 ps to become completely liquid and eliminate their correlation to the initial configurations. This temperature 5000 K is higher than the experimental melting point of diamond. Then the temperature was cooling down to 1 K linearly corresponding to a cooling rate of  $1.5 \times 10^{16} \text{ K/s}$ . And then the resulting quenched solid state was maintained at 1 K. We analyzed MD structures averaged over final 4.0 ps at 1 K and used them as initial structure of B-DLC coatings.

#### 2.2.2 STRUCTURAL OPTIMIZATION BY AIMD CALCULATION

The quantum espresso based on DFT within the local density approximation (LDA) was used for AIMD calculation to optimize initial structure estimated by CMD calculation.<sup>[21]-[23]</sup> And our AIMD calculation was a Methfessel-Paxton smearing factor of 0.01 eV. One-electron Kohn-Sham equations were solved self-consistently by using the norm-conserving pseudopotential method. AIMD was performed using conjugated gradient method, in which a self-consistent field was created using an energy convergence

threshold of  $10^{-6}$  Ry, and atomic relaxation was repeated until the forces acting on the atoms were below  $10^{-3}$  Ry/Bohr, the density of mass was kept during the optimization, electronic structure and atomic force calculations were made by using a cut-off energy of 50 Ry for Kohn-Sham wave functions and k-point sampling at the gamma point in the Brillouin zone.

Four samples were obtained at density (2.49 g/cm<sup>3</sup>) with various concentrations (0, 1.56, 4.69 and 10.94 at.%, corresponding to 0, 1, 3, and 5 B atoms in 64 atom systems, respectively). The energy-optimized structures were used as model structures of B-DLC coating, and the dielectric constants of the model structures were calculated by ab initio methods.

### 3. RESULT AND DISCUSSION

#### 3.1 RADIAL DISTRIBUTION FUNCTION

Fig.3, 4, 5, 6 shows the final morphologies for B-DLC coating with the Boron concentrations of 0, 1.56, 4.69 and 10.94 at.%. Red spheres represent the carbon atoms while green ones are B atoms. All the films are amorphous as will be described later by RDF.

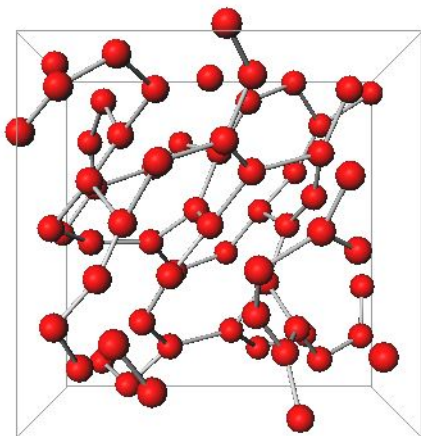


Fig.3 Atomic structure of pure DLC coating with B concentrations of 0 at.%

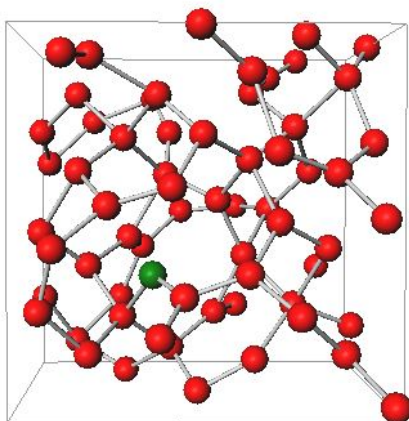


Fig.4 Atomic structure of B-DLC coating with B concentrations of 1.56 at.%

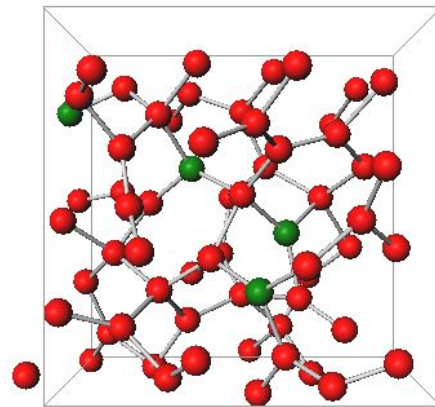


Fig.5 Atomic structure of B-DLC coating with B concentrations of 4.69 at.%

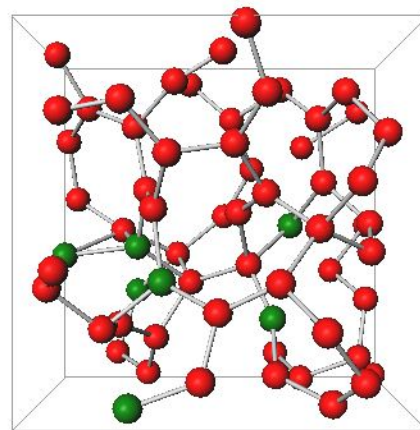


Fig.6 Atomic structure of B-DLC coating with B concentrations of 10.94 at.%

Fig. 7, 8, 9,10 shows the RDF spectra of B-DLC coating with different B concentrations, all bonding states, only C-C bonding, only B-C bonding and only B-B bonding, respectively. In the long-distance region of over 0.30 nm, all bonding states, only C-C bonding, only B-C bonding and only B-B bonding RDFs have no distinct peak and the values are approximately 1.0. This indicates the absence of the long-range structural order in B-DLC coatings. There is a distinct peak around 0.145 nm, corresponding to the nearest neighboring C-C interatomic distance. The RDF results indicate that the models have short-range structural orders though they have no long-range structural order, having the structural feature of an amorphous state. 1st and 2nd nearest peak positions of crystalline diamond is 0.154 nm and 0.252 nm. In general, the 1st peak is related with the atomic bond lengths, and the 2nd peak has correlation with both the bond angles and bond lengths. However, after the additions of B into DLC films, the positions of the 1st and 2nd nearest peaks in B-DLC coatings deviated from the position of the 0 at.% boron concentration B-DLC coatings. It demonstrates the atomic bond structure playing an important role in the dielectric properties of the coating.

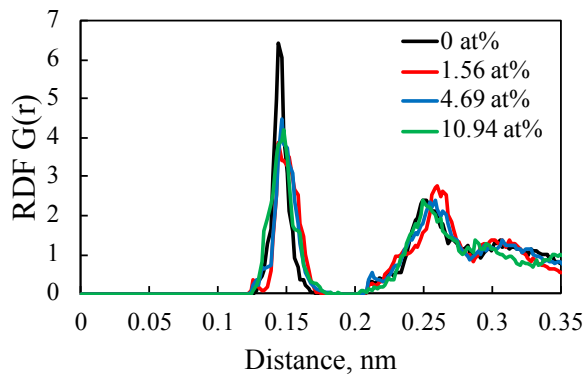


Fig.7 RDF spectra (Total) of B-DLC coatings with different B concentrations, 0, 1.56, 4.69, 10.94 at.%

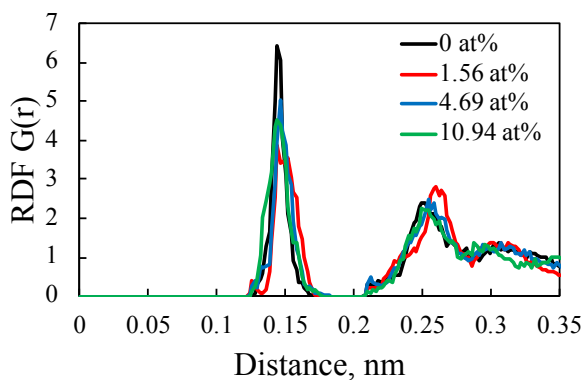


Fig.8 RDF spectra (C-C bond) of B-DLC coatings with different B concentrations, 0, 1.56, 4.69, 10.94 at.%

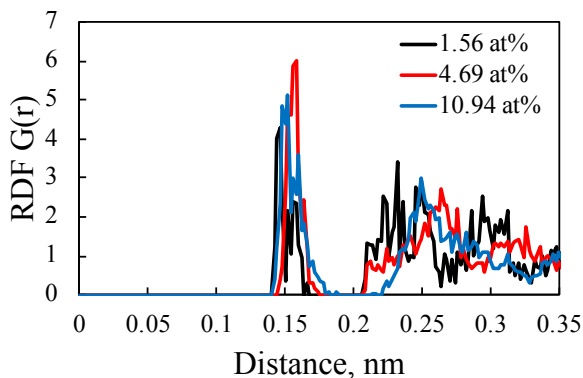


Fig.9 RDF spectra (B-C bond) of B-DLC coatings with different B concentrations, 0, 1.56, 4.69, 10.94 at.%

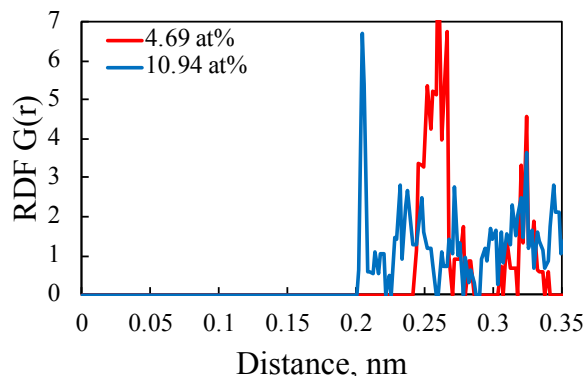


Fig.10 RDF spectra (B-B bond) of B-DLC coatings with different B concentrations, 0, 1.56, 4.69, 10.94 at.%

### 3.2 DIELECTRIC PROPERTIES

In order to evaluate the effect of doping B into DLC coating on permittivity, the dielectric function was calculated. The dielectric function represents the interaction of the materials when the electric fields are applied and is a complex quantity given as Eq. (2).

$$\varepsilon = Re(\varepsilon) - iIm(\varepsilon) \quad (2)$$

In general, the real part of the dielectric function ( $Re(\varepsilon)$ ) represents the amount of energy stored in the material from the external electric field. The imaginary part ( $Im(\varepsilon)$ ) of the dielectric constant is called the loss coefficient and is an index of the energy consumption of the material with respect to the external electric field.

Fig.11 shows that dielectric function of real part of B-DLC coatings with different B concentrations, 0, 1.56, 4.69, 10.94 at.%. Fig.12 shows that dielectric function of imaginary part of B-DLC coatings. By using those results, permittivity  $\varepsilon$  of B-DLC coatings at wavelength 589 nm was calculated.

Fig.13 shows that permittivity (wavelength at 589 nm) of experimental results (B-DLC, a-C:H) and AIMD calculation results (B-DLC coatings with different B concentrations, 0, 1.56, 4.69, 10.94 at.%). Experimental results of B-DLC coatings and a-C:H (Hydrogenated amorphous carbon) was measured by Ellipsometer, and simply calculated as  $\varepsilon = n^2 - k^2$ . Permittivity of experimental a-C:H and B-DLC coatings is 3.49, 4.54 F/m respectively. Experimental results said that B-DLC coatings have higher permittivity than a-C:H coatings, friction coefficient of B-DLC coatings was lower than friction coefficient of a-C:H coatings. However, permittivity calculated by AIMD simulation of B-DLC coating with the Boron concentrations of 0, 1.56, 4.69 and 10.94 at.% was 18.90, 13.66, 13.63 and 13.10 F/m, respectively. The magnitude relationship between B-DLC and a-C:H coating was different, and there was also a big difference in the magnitude of the value.

Different calculation methods of permittivity were considered as the cause of the difference between the experimental value and the simulation value of the dielectric constant in the simulation. Because experimental permittivity was calculated simply as  $\varepsilon = n^2 - k^2$ , while AIMD simulation permittivity was calculated in the exact way as using dielectric function. In order to compare the experimental result and simulation results, it is necessary to measure the permittivity of DLC coatings by using Dielectricmeter etc.

In only considered about AIMD simulation results, permittivity of 0 at.% B-DLC coatings was taken the highest value. This was a result different from the experimental value, B-DLC coating has a higher permittivity than a-C:H in experimental. The reason why this time 0 at.% B-DLC coating was taken higher value of permittivity was that molecular model was not considered the existence of Hydrogen and Oxygen at this simulation.

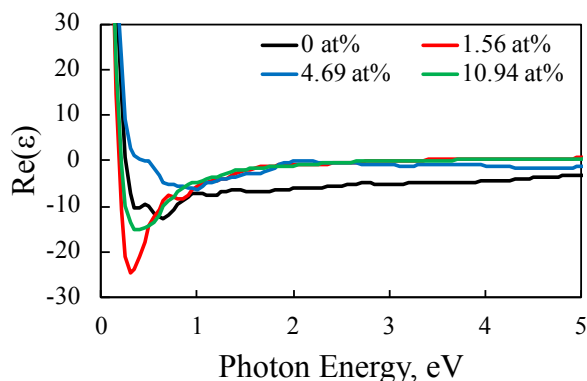


Fig. 11 Dielectric function of real part of B-DLC coatings with different B concentrations, 0, 1.56, 4.69, 10.94 at.%

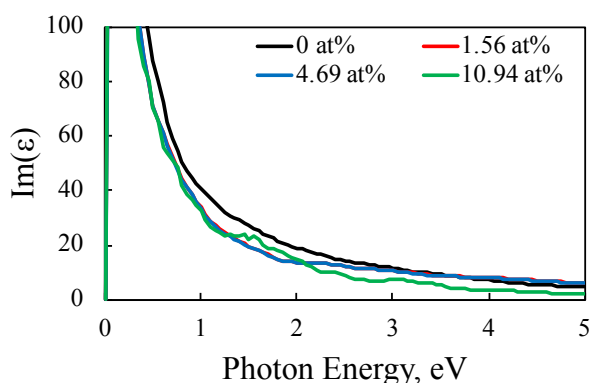


Fig.12 Dielectric function of imaginary part of B-DLC coatings with different B concentrations, 0, 1.56, 4.69, 10.94 at.%

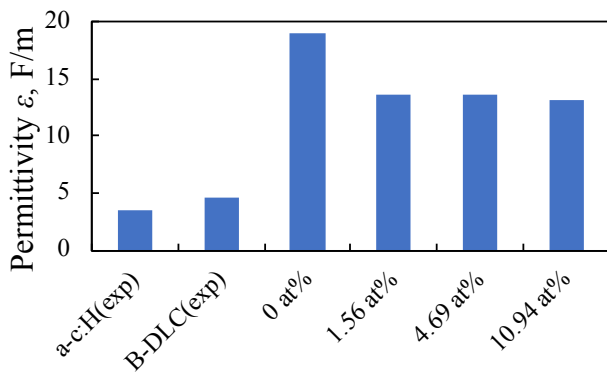


Fig.13 Permittivity (wavelength at 589 nm) of experimental results (B-DLC, a-C:H) and AIMD calculation results (B-DLC coatings with different B concentrations, 0, 1.56, 4.69, 10.94 at.%.)

#### 4. CONCLUSION

AIMD simulation was carried out to study the structure and dielectric properties of B-DLC coatings. The Boron concentration ratio was changed from 0 to 10.93 at.%. RDF result show that the structure made by AIMD was amorphous structure. 1st peak in B-DLC coatings deviated from the position of the 0 at.% boron concentration B-DLC coatings, was shifted, it implied that the bond structure playing an important role in the

dielectric properties of the coating. However, there were huge differences between experimental result and AIMD simulation result, so it is necessary to change the program to get more proper results.

#### ACKNOWLEDGEMENTS

I would like to express my sincere gratitude to my supervisor, Professor L. Jay Guo for providing me this precious experience. I would like to thank Chengang Ji and all of laboratory's members for supporting me and giving advice. This study was also supported by Japan-US Advanced Collaborative Education Program.

#### REFERENCES

- [1] K. Holmberg, Global energy consumption due to friction in passenger cars, *Tribology International*, 47 (2011), 221-234.
- [2] Y. J. zou, X. W. zhang, Y. L. Li, B. wang, H. Yan, Bonding character of the boron-doped C60 films prepared by radio frequency plasma assisted vapor deposition, *Journal of Materials Science* 37 (2002), 1043-1047
- [3] H. Morri, M. Thoyama, M. Okuyama, T. Ohmori, Low Friction Property of Boron Doped DLC under Engine Oil, *Tribology Online*, Vol. 12, No. 3 (2017), 135-140.
- [4] N. Orlovskaya, M. Lugovy, *Boron Rich Solids*, Springer (2009)
- [5] H. Nishimiura, N. Umehara, H. Kousaka, M. Murashima, Clarification of effect of transformed layer and oil film on low friction coefficient of CNx coating in PAO oil lubrication by in-situ observation of friction area with reflectance spectroscopy, *Tribology International*, 113 (2017) pp. 383–388
- [6] Jacob N. Israelachvili, *Intermolecular and Surface Forces*, Academic Press
- [7] D. Mark, J. Hutter, *Ab Initio Molecular Dynamics: Basic Theory and Advanced Methods*, Cambridge University Press
- [8] G. Zilibotti, M. C. Righi, Ab Initio Calculation of the Adhesion and Ideal Shear Strength of Planar Diamond Interfaces with Different Atomic Structure and Hydrogen Coverage, *Langmuir* 27 (2011), 6862-6867
- [9] X. Li, P. Ke, A. Wang, Ab initio molecular dynamics simulation on stress reduction mechanism of Ti-doped diamond-like carbon films, *Thin Solid Films* 584 (2015), 204-207
- [10] M. M. M. Bilek, D. R. McKenzie, D. G. McCulloch, C. M. Goringe, Ab initio simulation of structure in amorphous hydrogenated carbon, *Physical Review B* Vol. 62, No. 5, (2000), 3071-3077
- [11] F. Legrain, K. Kotsis, S. Manzhos, Amorphous carbon a promising material for sodium ion battery anodes: a first principles study, *J. Phys. Chem. C*, 119, 24, (2015), 13496-13501
- [12] M. Boero, A. Oshiyama, Car-Parrinello Molecular Dynamics Method, (2011), Springer
- [13] H. Momida, T. Hamada, Y. Takagi, T. Yamamoto, T. Uda, T. Ohno, Dielectric constants of amorphous hafnium

- aluminates: First-principles study, *Physical Review B* 75, 195105 (2007) 1-10
- [14] A. Calzolaril, M. B. Nardelli, Dielectric properties and Raman spectra of ZnO from a first principles finite-differences/finite-fields approach, *Scientific Reports* 3, Article number: 2999 (2013) doi:10.1038/srep02999
- [15] K. Li, Y. Yan, H. Wang, Q. Zhan, Y. Sh. Mohammed, H. Jin, Ferromagnetism in phosphorus-doped ZnO: First-principles calculation, *Physics Letters A* 374, (2010), 628–631
- [16] A. M. Ito, A. Takayama, S. Saito, H. Nakamura, Formation and Classification of Amorphous Carbon by Molecular Dynamics Simulation, *Japanese Journal of Applied Physics*, Vol. 52, No. 1S, (2013)
- [17] N. A. Marks, D. R. McKenzie, B. A. Pailthorpe, Microscopic Structure of Tetrahedral Amorphous Carbon, Vol. 76, No. 5, *Physical Review Letters*, (1996), 768-771
- [18] S. Uhlmann, Th. Frauenheim, Molecular-Dynamics Study of the Fundamental Processes Involved in Subplantation of Diamond like Carbon, Vol. 81, No. 3 *Physical Review Letters*, (1998), 641-644
- [19] X. Li, P. Ke, A. Wang, Stress reduction of Cu-doped diamond-like carbon films from ab initio calculations, *AIP Advances* 5, 017111 (2015)
- [20] H. Momida, T. Hamada, Y. Takagi, Theoretical study on dielectric response of amorphous alumina, *Physical Review B* 73, 054108 (2006)
- [21] E. Hernandez, Metric-tensor flexible-cell algorithm for isothermal-isobaric molecular dynamics simulations, *J. Chem. Phys.* Vol. 115, 10282 (2001)
- [22] P. Hohenberg, W. Kohn, Inhomogeneous Electron Gas, *Phys. Rev.* 136, B864 (1964)
- [23] J. P. Perdew, Y. Wang, Accurate and simple analytic representation of the electron-gas correlation energy, *Phys. Rev. B* 45, 13244, (1992)

# **Failure Detection and Control of Distributed Electric Propulsion Aircraft Engines**

Yudai Suzuki

Graduate School of Engineering, Nagoya University  
suzuki.yuudai@h.mbox.nagoya-u.ac.jp

William Dunham, Ilya Kolmanovsky and Anouck Girard  
Department of Aerospace Engineering, University of Michigan  
wdunham@umich.edu, ilya@umich.edu, anouck@umich.edu

## **Abstract**

An estimation and control scheme for a Distributed Electric Propulsion (DEP) aircraft with an engine failure is presented. Concepts for DEP aircraft have built in redundancy in engine operation that can be used to compensate for thrust loss which comes from engine failures. The motivating example is a DEP aircraft in cruise flight with thrust provided by the two motors on the wingtips where one fails. The motor failure is detected using a Kalman filter based method and cruise flight is recovered from the failure mode using a linear MPC for thrust allocation over the other engines. Simulations are performed on a full nonlinear model of a UAV.

**Undisclosed**

## **Developing Immersive Virtual Realities for Human Upper Limb Motor Recovery after Stroke**

**Yusuke Fukui**

Mechanical Systems Engineering, Nagoya University

**Supervisor: Jacob Rosen**

Professor, Mechanical and Aerospace Engineering, UCLA

### **Abstract**

Stroke is the leading cause of disability in the United States, which causes paralysis for patients. Although manually assisted stroke rehabilitation therapy has been used for decades, the therapeutic treatment needs intensive, repetitive and of long duration rehabilitation. Therefore previous studies have emphasized the benefits of immersive virtual realities (VR) for stroke rehabilitation therapy. The aim of this study is to hypothesize VR environment adequate for the stroke rehabilitation. Some requirements were identified for a VR rehabilitation, in suppressing the dominant instincts of embryonic posture and incorporating reaching, grasping and hitting oncoming ball activities in both static and dynamic environments. Consequently, 15 different VR activities were developed and programmed in Microsoft's VS 2017 with Unity, assuming subjects use Oculus Rift for VR headset and Kinect for windows v2 to detect body movement. These activities were classified as diagnosis, therapeutic and combined type to provide efficient rehabilitation to both patients and therapists.

# **Undisclosed**

## **Shelf-Life Testing of Bioink-Containing Pharmaceutical Tablets for 3D Pharming**

Fuga Matsubara

Department of Micro-Nano Mechanical Science and Engineering, Nagoya University  
matsubara.fuga@i.mbox.nagoya-u.ac.jp

Supervisor: Benjamin M. Wu, DDS, PhD

Bioengineering, University of California, Los Angeles  
benwu@ucla.edu

### **ABSTRACT**

Pharmaceutical dosages are defined by the amount of active pharmaceutical ingredient (API). This “one size fit all approach” fails due to physiological and genetic diversity of patients. Therefore the novel strategy to manufacture personalized medicine is required. 3D Pharming, direct printing of pharmaceutical tablet is attractive way to solve this problem, since it can rapidly produce medicines and design multiple drug combination. Inkjet 3D printer is intended way. So, we made ink which is suitable for inkjet printing and biocompatible for human body. Such ink is called bioink. In this study, we engineered bioink with ropinirole HCL, well known drug for Parkinson’s disease, as the API. And we conducted shelf- life testing to know if it is possible to store bioink-containing tablets for enough long term in practical use. As results, good shelf life was confirmed. Additionally, we examined the impact of humidity and hydrogel dehydration to drug degradation.

# **Undisclosed**

# ARTIFICIAL BACTERIAL TRAIL INFLUENCE SURFACE MOVEMENT

Kai Iio

Department of Biomolecular Engineering, Graduate School of Engineering, Nagoya University  
iio.kai@a.mbox.nagoya-u.ac.jp

Supervisor: Gerard C. L. Wong

Department of Bioengineering, University of California Los Angeles  
gclwong@seas.ucla.edu

## ABSTRACT

Bacterial biofilms are structured multicellular communities involved in a broad range of infections. The first step of biofilm organization is the transition from individual surface-attached bacteria into microcolonies. Recent work has shown that *P. aeruginosa* deposits a “trail” of exopolysaccharide (EPS) as it moves on a surface. EPS can influence the surface motility of subsequent cells that encounter these trails. Here, we hypothesize that bacteria follow artificial “EPS”. We observed bacterial movement on the surface with artificial “EPS”. As we expected, bacteria tend to follow artificial “EPS” as well as naturally secreted EPS. These results can be expanded to in-depth studies of EPS characteristics.

# Undisclosed



## <3> Research Presentations

- For 2017 Short-term course ...44  
Presented at the Matsumoto Lab. Research Meeting  
on September 29, 2017



- For 2017 Medium-term course ...45  
The 21<sup>st</sup> JUACEP Workshop on February 27, 2018



## Final report

Research period: 2017/08/08 – 2017/09/22

**Yoshiyuki Tange**  
 Department of Mechanical Systems Engineering,  
 Graduate School of Engineering, Nagoya University

Supervisor: Prof. Katsuo Kurabayashi  
 Department of Mechanical Engineering; Electrical  
 Engineering and Computer Science, University of Michigan

1

## Introduction

Identifying what mechanisms realize morphogenetic movement has been one of the most difficult questions in developmental biology.

Recent studies have suggested that mechanical properties play significant roles.

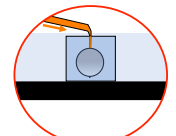
We are constructing a new method, *Micro-Piercing*, which estimates the stress direction inside of an embryo.

Deformation of the piercing hole

Differences of compression and expansion

Force direction

Cell migration



2

## New device

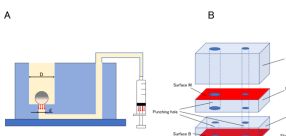
In *Micro-Piercing* methods, we have

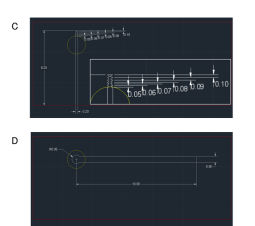
- embedded the sample in agarose gel.
- manipulated the fiber under the micros

↓

The new device could;

- hold the sample by negative pressure.
- guide the route of the fiber to consisten
- pierce the same position of the embryo.



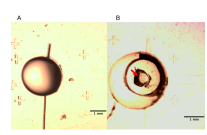


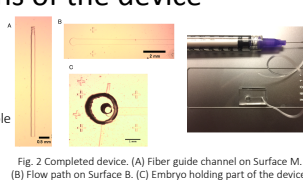
3

## Confirming functions of the device

We confirmed that;

- a fiber with a diameter of 75  $\mu\text{m}$  could pass through the guide.
- cavitation due to negative pressure occurred in a combination of a large hole with a diameter of 3 mm and a suction hole with a diameter of 0.75 mm.





Device	D (mm)	d (mm)	Cavitation
1	2.0	0.75	0/5
2	2.0	1.0	2/5
3	3.0	0.75	5/5
4	3.0	1.0	3/5

4

## Conclusion

In this study, we manufactured a micro-device that can guide a fiber in order to pierce and deposit soft materials within an embryo.

The device was also designed to hold a *Xenopus laevis* embryo with negative pressure.

The ability of the device to load negative pressure was confirmed by successful cavitation of a phantom *Xenopus laevis* embryo.

### Future works

We will find the appropriate magnitude of pressure for real embryos.

5

# The 21<sup>st</sup> JUACEP Workshop



*Research presentations by the 2017 medium-term course students of JUACEP at Univ. Michigan/UCLA*

**Date... 9:10-11:50, Tuesday, February 27, 2018**

**Venue... IB 013**

## Timetable

Time	Name (Affiliation at NU)	Presentation title	Advisor at US
<b>9:10</b>	Opening address		
<b>9:15</b>	<b>Tatsuya Okamoto</b> (Prof. N. Umehara Micro-Nano Mechanical Science and Engineering)	Ab initio molecular dynamics simulation about dielectric properties of boron-doped diamond-like carbon <b>(P.46)</b>	Prof. Jay Guo Electrical Engineering and Computer Science, U. Mich.
<b>9:30</b>	<b>Makoto Takeuchi</b> (Prof. N. Umehara Micro-Nano Mechanical Science and Engineering)	Thin alumina films via colloidal processing of flame made nanopowders <b>(P.49)</b>	Prof. Richar Laine Materials Science and Engineering, U. Mich.
<b>9:45</b>	<b>Makoto Terada</b> (Prof. N. Umehara Micro-Nano Mechanical Science and Engineering)	Forces: the quantitative values of sharpened and blunt microwire for in-vivo brain insertion <b>(Undisclosed)</b>	Prof. Albert Shih Mechanical Engineering, U. Mich.
<b>10:00</b>	<b>Yudai Suzuki</b> (Assoc. Prof. D. Tsubakino Aerospace Engineering)	Failure detection and control of distributed electrical propulsion aircraft engines <b>(Undisclosed)</b>	Prof. Anouck Girard Aerospace Engineering, U. Mich.
<b>10:15</b>	<b>Hiroki Fujiwara</b> (Assoc. Prof. A. Iwakawa Aerospace Engineering)	Demonstration of digital in-line holography for primary breakup of water column <b>(P.52)</b>	Prof. Mirko Gamba Aerospace Engineering, U. Mich.
<b>10:30</b>	Break		
<b>10:40</b>	<b>Kai Iio</b> (Prof. K. Hori Biomolecular Engineering)	Artificial bacteria trails influence surface movement <b>(Undisclosed)</b>	Prof. Gerard Wong Bioengineering, UCLA
<b>10:55</b>	<b>Taro Mizutani</b> (Prof. E. Shamoto Aerospace Engineering)	Analysis of assembly line with learning effects <b>(P.55)</b>	Prof. Jack Hu Mechanical Engineering, U. Mich.
<b>11:10</b>	<b>Yusuke Fukui</b> (Prof. Y. Yamada Mechanical Systems Engineering)	Developing immersive virtual realities for human upper limb motor recovery after stroke <b>(Undisclosed)</b>	Prof. Jacob Rosen Mechanical and Aerospace Engineering, UCLA
<b>11:25</b>	<b>Fuga Matsubara</b> (Prof. Y. Ju Micro-Nano Mechanical Science and Engineering)	Shelf-life testing of biink-containing pharmaceutical tablets for 3D pharming <b>(Undisclosed)</b>	Prof. Benjamin Wu Bioengineering, UCLA
<b>11:40</b> <b>11:50</b>	Completion Ceremony Adjournment		

*\*10 minutes presentation + 4 minutes Q&A for each*

Inquiry... JUACEP Office 052-789-2799



**Ab Initio Molecular Dynamics Simulation about Dielectric Properties of Boron-doped Diamond-Like Carbon**

Nagoya University  
Dept. Micro/Nano Mechanical Science and Engineering  
M1 **Tatsuya Okamoto**

University of Michigan  
Dept. Electrical Engineering and Computer Science  
Prof. L. Jay Guo

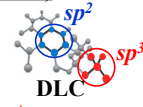
**Background- DLC**

Among the energy input to automobile cars, **friction loss is 16.5%**  
→ Reduce the friction loss is required for energy saving



**DLC (Diamond-Like Carbon)**

- High hardness
  - Low friction coefficient
  - High wear resistance
  - Chemical stability
- Applied to the car sliding part

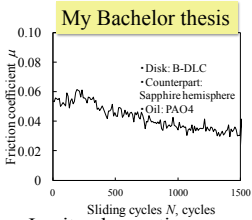


Frictional properties and physical properties of DLC coating change, depending on the bonding state and the contained element

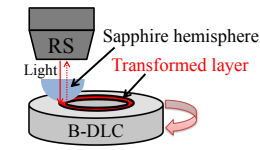
**Previous result 1**

**B-DLC (Boron doped DLC)**

-low friction in oil lubricant, but mechanism was not clear



Reflectance Spectroscopy(RS)  
-measure the optical constant(n, k)

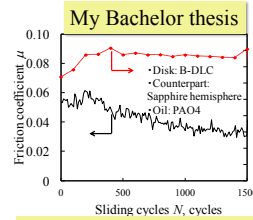


In-situ observation was conducted by using Reflectance Spectroscopy to clarify the low friction mechanism

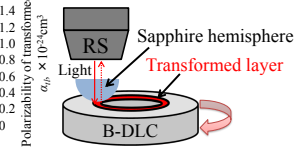
**Previous result 1**

**B-DLC (Boron doped DLC)**

-low friction in oil lubricant, but mechanism was not clear



Reflectance Spectroscopy(RS)  
-measure the optical constant(n, k)

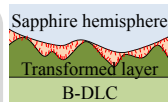


Increment of transformed layer with high polarizability effected on low friction

**Previous result 1**

**Low friction mechanism of B-DLC**

- Increment of polarizability  $\alpha$
- High Van der Waals force  $F_v$
- Adsorption of oil molecular on Transformed layer
- Relaxation of solid contact
- Low friction



Van der Waals force  $F_v$

$$F_v = \frac{9\alpha_1\alpha_2}{(4\pi\epsilon_0)^2 r^7} \frac{I_1 I_2}{I_1 + I_2}$$

**Design guideline for low friction material**

Deposit the materials with high polarizability

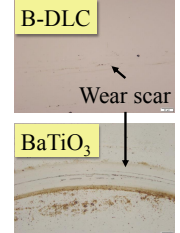
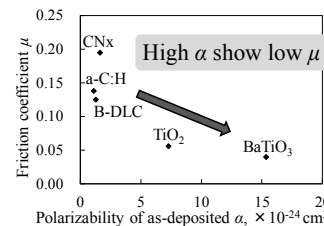
$\alpha$ : Polarizability  
 $\epsilon_0$ : permittivity  
 $r$ : molecular distance  
 $I$ : First ionization energy

**Problem of this design guideline**

- It is unclear whether the other materials with high  $\alpha$  show low friction
- It is unclear relationship between structure and polarizability

**Previous result 2**

Materials with high polarizability  $\alpha$  really show low friction  $\mu$ ?



BaTiO<sub>3</sub> violently wore compared to B-DLC

- It is necessary to increase the polarizability of B-DLC expected to be applied to actual automobile sliding part

## Purpose

### Previous Result

High polarizability material show low friction

### Purpose

What kind of B-DLC structure show high polarizability?

It is necessary to verify the structure of B-DLC film with high polarizability to establish design guideline to make further more low friction DLC



What is the optimal value with high polarizability ?

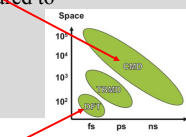
### In this paper

Ab initio Molecular Dynamics was carried out to study the structure and polarizability of B-DLC

## Modeling Methods

### Classical Molecular Dynamics(CMD) simulation

- the accuracy is not so high compared to AIMD simulation
- the governing equation is newton's equation  $F=ma$
- short computation time



### Ab initio Molecular Dynamics(AIMD) simulation

- the most accurate way to determine the stable structure and physical properties
- the governing equation is schrodinger's equation
- long computation time

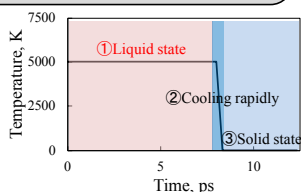
## Modeling Methods

### Modeling step : Imitating the deposition methods

1. Classical Molecular Dynamics(CMD) simulation  
-create initial structure by Melt-Quench method
2. Ab initio Molecular Dynamics(AIMD) simulation  
-structural optimization of initial structure

### ①Liquid state

Equilibrated at 5000 K to become completely liquid and eliminate their correlation to the initial configurations



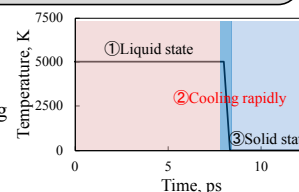
## Modeling Methods

### Modeling step : Imitating the deposition methods

1. Classical Molecular Dynamics(CMD) simulation  
-create initial structure by Melt-Quench method
2. Ab initio Molecular Dynamics(AIMD) simulation  
-structural optimization of initial structure

### ②Cooling rapidly

Temperature was cooling down to 1 K linearly corresponding to a cooling rate of  $1.5 \times 10^{16}$  K/s.



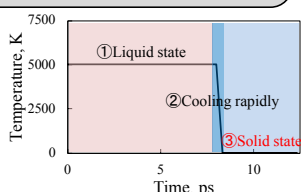
## Modeling Methods

### Modeling step : Imitating the deposition methods

1. Classical Molecular Dynamics(CMD) simulation  
-create initial structure by Melt-Quench method
2. Ab initio Molecular Dynamics(AIMD) simulation  
-structural optimization of initial structure

### ③Solid State

Quenched solid state was maintained at 1 K for 4 ps and used them as initial structure of B-DLC

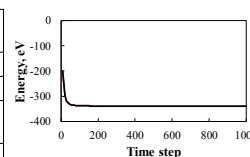


## Modeling Methods

### Modeling step : Imitating the deposition methods

1. Classical Molecular Dynamics(CMD) simulation  
-create initial structure by Melt-Quench method
2. Ab initio Molecular Dynamics(AIMD) simulation  
-structural optimization of initial structure

Exchange correlation number	LDA: local density approximation
Pseudopotential	Norm-conserving
Basis function	Plane Waves
Energy convergence threshold	$10^{-6}$ Ry
Solid information	Periodic

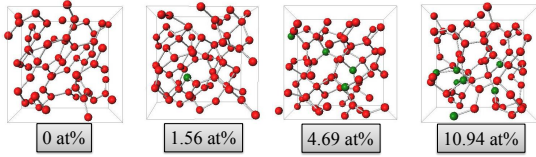


Simulation result



B-DLC model

● Carbon atom ● Boron atom



4 sample were obtained at density (2.49 g/cm<sup>3</sup>) with various concentration

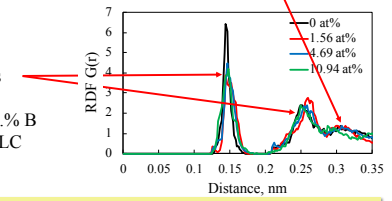
Verify whether this simulation structure is amorphous structure

Radial Distribution function(RDF)



1<sup>st</sup> peak: atomic bond lengths  
2<sup>nd</sup> peak: bond lengths and angles  
③ No distinct peak over long distance region(3.0 nm)

① Short range structural order  
② 1<sup>st</sup> and 2<sup>nd</sup> peaks deviated from the position of the 0 at.% B concentration B-DLC



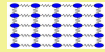
①, ③ ⇒ amorphous structure  
② ⇒ atomic bond structure playing an important role in dielectric properties of coating

Dielectric function



Lorenz model

Define a solid as assembly of electric dipoles  
Electronic dipoles are positive and negative charges connected by springs, assuming bound charges in atoms are simple harmonic motion at the natural frequency

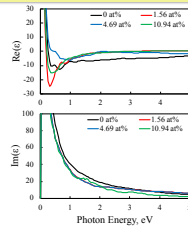


1. Dielectric function

$$Re(\epsilon) = 1 + \frac{Nq^2}{\epsilon_0 m V} \frac{\omega_0^2 - \omega^2}{(\omega_0^2 - \omega^2)^2 + \gamma^2 \omega^2}$$

$$Im(\epsilon) = 1 + \frac{Nq^2}{\epsilon_0 m V} \frac{\gamma \omega}{(\omega_0^2 - \omega^2)^2 + \gamma^2 \omega^2}$$

N: number of atoms  
q: point electric charge  
 $\omega_0$ : natural frequency  
m: atomic weight  
V: Volume  $\gamma$ : energy loss

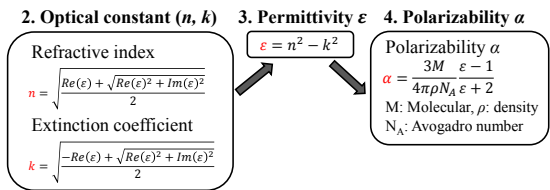


Calculate polarizability



Computation step of calculating the polarizability

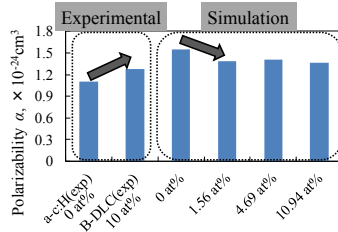
1. Dielectric function  $Re(\epsilon), Im(\epsilon)$
2. Optical constant (n, k)
3. Permittivity  $\epsilon$
4. Polarizability  $\alpha$



Polarizability of B-DLC



To find the optimal structure which have high polarizability



Different result and tendency between experimental and simulation

future Need to consider the model including H and O atom

Conclusion & Future plan



Purpose

Ab initio Molecular Dynamics was carried out to study the structure and polarizability of B-DLC

Conclusion

- B-DLC amorphous structure was obtained by ab initio molecular dynamics
- RDF result imply the bond structure playing important role in the dielectric properties

Future plan

- consider the model including H and O atoms

# Thin alumina films via colloidal processing of flame made nanopowders

Department of Micro-Nano Mechanical Engineering and Science  
 Graduate School of Engineering  
 Nagoya University  
 M1 Makoto Takeuchi  
 Materials Science and Engineering  
 University of Michigan  
 Prof. Richard M Laine



## 1.Introduction



Ceramics based on Nanopowders (NPs)

- Fine grain size
  - Dense structure
- ⇒
- Mechanical strength
  - Optical properties

Sodium vapor lamp

- Transparent alumina ceramics are used in for their optical properties



1

## 1.Introduction



Transparent alumina by HIP

Transparent alumina has been fabricated by hot isostatic pressing<sup>1</sup>

Transparent thin alumina

Transparent thin alumina has been fabricated by several deposition methods

Need in fabricating transparent alumina thin films without any special methods to achieve low cost and time-effectiveness

[1] Krell, A. et al, Processing of High-Density Submicrometer Al<sub>2</sub>O<sub>3</sub> for New Applications, J. Amer. Ceram. Soc., 86, 4, pp. 546-553 (2003).

2

## 2.Purpose



To achieve a transparent thin alumina film... Smaller grain size is very important



Introduction of small amount of MgO into Al<sub>2</sub>O<sub>3</sub> powders leads to formation of MgO·Al<sub>2</sub>O<sub>3</sub> spinel at grain boundaries that impedes grain growth<sup>2</sup>

Purpose

Develop and optimize processing parameters for making dense, flexible and transparent free standing films of α-Al<sub>2</sub>O<sub>3</sub> with MgO content by tape-casting method

[2] Bowen, P. et al., Colloidal processing and sintering of nanosized transition aluminas, Powder Technol., 157, pp. 100-107 (2005).

3

## 3.Experimental



Flow

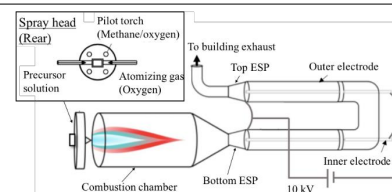
- Synthesize NPs (LF-FSP)
- ↓
- Make suspension (liquid-state sample)
- ↓
- Fabricate films
- ↓
- Sinter films at 1500 °C
- ↓
- Analyze thin films (SEM and XRD)

4

## 3.Experimental



Liquid feed flame spray pyrolysis (LF-FSP)<sup>3,4</sup>



- Alcohol solvents of low cost precursors
- Aerosolized w/O<sub>2</sub>
- Combustion ≥ 1500 °C

[3] Laine et al U.S. patent 5,958,361, Sept. 28, 1999.  
 [4] Sutorik et al U.S. patent 7,220,398 May 22, 2007.

5

### 3.Experimental

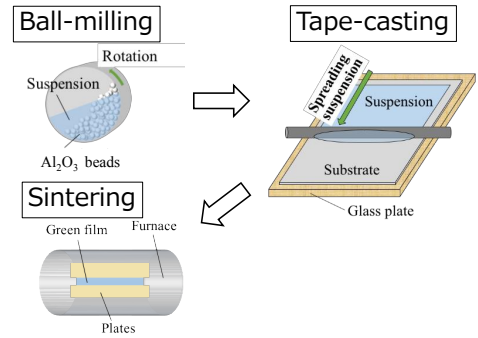


#### Composition of suspension

- Powder** (0.0, 0.50, 1.0 and 2.0 wt.% MgO doped  $\text{Al}_2\text{O}_3$ )  
Give the properties
- Plasticizer** (Benzyl butyl phthalate)  
Softens suspension and make uniform thickness
- Binder** (Polyvinyl butyral)  
Binds particles and prevents crack when drying
- Solvent** (Acetone and ethanol)  
Solves ingredients

6

### 3.Experimental

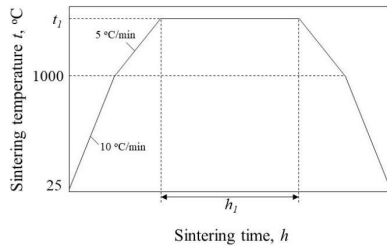


7

### 3.Experimental



#### One-step sintering



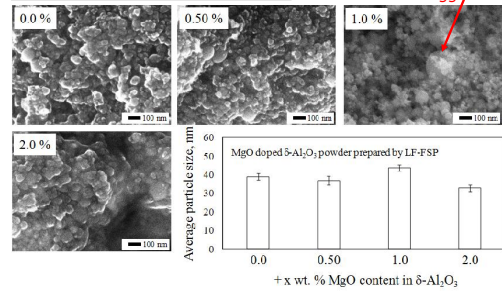
Sintering temperature  $t=1500\text{ }^\circ\text{C}$   
Sintering time  $h=0, 1, 5\text{ h}$  in  $\text{O}_2$

8

### 4.Results & Discussion



#### SEMs of nanopowders



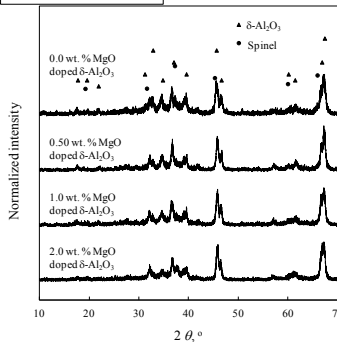
APS decreased with increasing MgO content

9

### 4.Results & Discussion



#### XRDs of NPs



Peaks showed 2 phases of  $\delta\text{-Al}_2\text{O}_3$  and spinel with the dope of MgO

Spinel impeded grain growth<sup>2</sup>

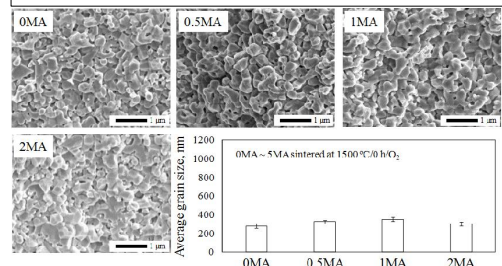
[2] Bowen, P. et al., Colloidal processing and sintering of nanosized transition aluminas, Powder Technol., 157, pp. 100-107 (2005).

10

### 4.Results & Discussion



#### SEMs of films sintered at 1500 °C for 0 h

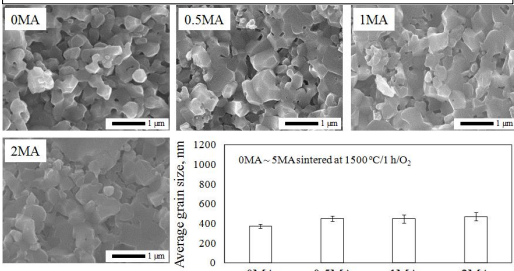


Structure did not show densification  
Additional sintering was needed

11

### 4.Results & Discussion

SEMs of films sintered at 1500 °C for 1 h

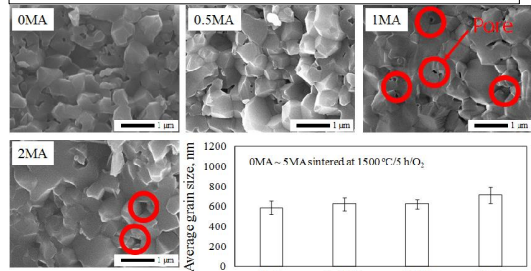


Higher MgO dopant induced more densification and grain growth as well

12

### 4.Results & Discussion

SEMs of films sintered at 1500 °C for 5 h

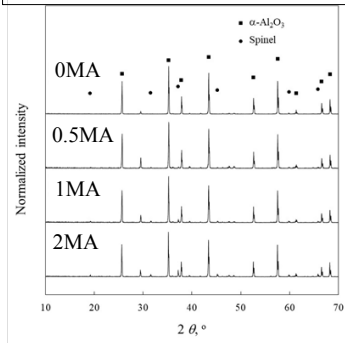


Higher MgO dopant induced full densification at 1MA & 2MA and grain growth as well

13

### 4.Results & Discussion

XRDs of films sintered at 1500 °C for 5 h



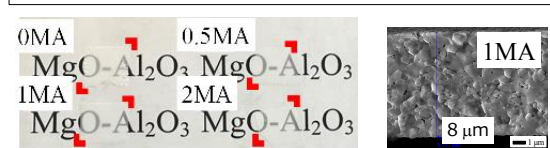
Peaks showed 2 phases of  $\alpha$ - $\text{Al}_2\text{O}_3$  and spinel with the dope of MgO

Spinel worked as a sintering aid

14

### 4.Results & Discussion

Images of films sintered at 1500 °C for 5 h



The films were not fully transparent because of pores in the structure

Sintering thin films in a vacuum because pores might be kept open by gas trapped inside



15

## 5.Conclusion

**Purpose**  
Develop and optimize processing parameters for making dense, flexible and transparent free standing films of  $\alpha$ - $\text{Al}_2\text{O}_3$  with MgO content

- It is possible to sinter 8  $\mu\text{m}$  thick films with average grain sizes of 600 nm producing robust films.

16



**NAGOYA**  
UNIVERSITY



**UNIVERSITY OF**  
**MICHIGAN**

## Demonstration of Digital In-Line Holography for Primary Breakup of Water Column

Hiroki Fujiwara  
Nagoya University Graduate school of Engineering, Aerospace Engineering  
2018/02/27  
21<sup>st</sup> JUACEP Workshop

1

### Table of contents

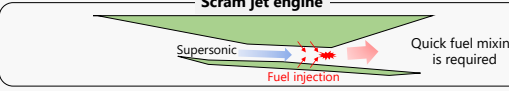
Contents	Slide pages
Background	3-5
About Holography	6-10
Experiment facility	11
Results	12-13

2

### Background

- To understand fuel mixing process in supersonic engine

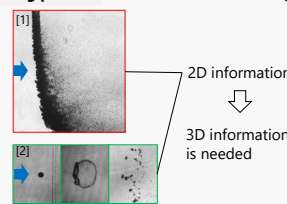
**Scram jet engine**



#### Mixing process

**1) Primary breakup**  
Injected liquid jet break up into droplets

**2) Secondary breakup**  
Each droplets breaks up into particles



[1] Z. Dai et al, International Journal of Multiphase Flow, 27(2):217-236, 2001., [2] KA Sallam et al, AIAA Journal, 42(12):2529-2540, 2004.

3

### Background | Previous study

- Shock-water column interaction at Mach 1.4 [1]

↓ Water column



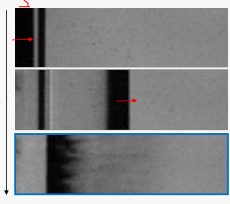
Resolution: 128 x 32  
Exposure: 0.29 μs  
Frame rate: 680,000fps

[1] C. Zoller, Investigation of shock induced primary breakup at high Mach numbers

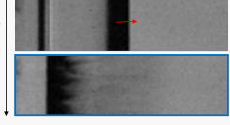
4

### Background | Previous study

shock



time



**Research Objective**  
Use 3D imaging technique holography to understand 3D phenomenon of primary breakup process

5

### Difference of photography and holography

**Photography**  
Record an intensity of light

$Intensity = Amplitude^2$

Three dimensional information is lost



Two dimensional image

**Holography**  
Record the interference fringe of waves

Include intensity and phase information

Three dimensional information can be reconstructed



Three dimensional image

6

### Principle of holography : 1. Recording

1. Recording  
Record the **interference** of objective wave and reference wave

2. Reconstruction

Analogue Illuminate hologram with reference wave	Digital Calculate propagation numerically
---	--

Coherent wave  
→ Creates clear fringe

Sensor: **Record hologram**

### Principle of holography : 2. Reconstruction

1. Recording  
Record the **interference** of objective wave and reference wave

After experiment

2. Reconstruction

Analogue Illuminate hologram with reference wave	Digital Calculate propagation numerically
---	--

Virtual image can be observed

### Principle of holography : 2. Reconstruction

1. Recording  
Record the **interference** of objective wave and reference wave

After experiment

2. Reconstruction

Analogue Illuminate hologram with reference wave	Digital Calculate propagation numerically
---	--

Reconstructed image

Digital hologram image

### Experiment setup

**In-line holography**  
Two waves from same angle

**Off-line holography**  
Two waves from different angle

Used In-line holography for better resolution

**Setup (Top View)**

Window, Test section of shock tube, [Top view], Camera, Water column, shock, Objective lens, He-Ne laser, Convex lens, ND filter

### Experimental apparatus | Shock tube

Driver section 586 kPa	Buffer section 310 kPa	Driven section 101 kPa	Window
---------------------------	---------------------------	---------------------------	--------

Before rupture

Diaphragm x 2

After rupture

shock

Shock tube

Water column generator

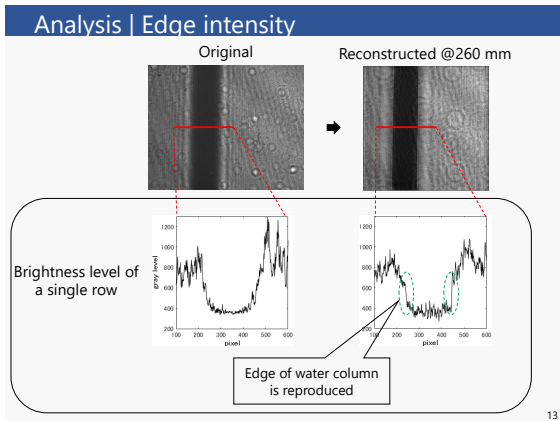
### Water column w/o shock

Original

Reconstructed @ 260 mm

Width on image [mm]	1.25
Actual width [mm]	1.12
Error [%]	11.8

Can be used for droplet investigation



- ### Conclusion
- Reconstruction algorithm was developed
  - Holography image was successfully reconstructed
  - Clear holography image of shock-water interaction was not taken
- 14

# Analyzing for assembly line with learning effect

Taro Mizutani , Nagoya Institute of Technology  
University student of university of Michigan  
2/27/2018

US supervisors; Theo Freiheit, Mihaela Banu and S.Jack Hu

## Back ground

2/8

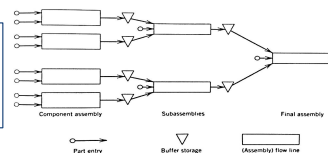
### Assembly line

This line is designed to assemble component parts and perform any related operations necessary to produce a finished product

Assembly cost is composed of **labor cost** while performing tasks plus **idle time cost**

$$\text{Idle time } : D = \frac{K \cdot C - \sum_{i=1}^M t_i}{K \cdot C}$$

$K$ : the number of stations required by the solution  
 $C$ : required time units  
 $t_i$ : the time to perform task  $i$



## Objective

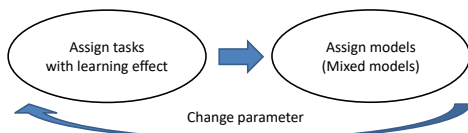
4/8

### Mixed models

Scheduling multiple product types simultaneously on a single assembly line

### Objective

Consider the effect of learning effects to assembly line and compare the idle time with/without learning effect



## Back ground

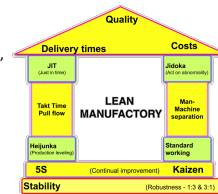
1/8

### Lean manufacturing

Systematic method for waste minimization within a manufacturing system  
... assembling, processing, scheduling .etc

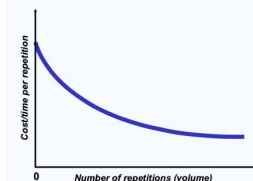
### Main strategy

- JIT(Just In Time)  
Generate and transport necessary items, when necessary, as much as need
- Act on automatically  
Build the machine that can judge good or bad about line



## Learning effect

3/8



### Learning effect

$$t_{ij} = t_j(i)^{-a_j}$$

$t_{ij}$ : processing time of the  $i$ th unit on the  $j$ th task  
 $t_j$ : processing time of the 1st unit on the  $j$ th task  
 $a_j$ : learning coefficient for the  $j$ th task

### Time for task decrease as person or machine learn

Station1	Unit 1	Unit 2	Unit 3	Unit 4
Tasks 1&2	35	23	19	16
Station2	Unit 1	Unit 2	Unit 3	Unit 4
Tasks 3&4	40	31	27	25

Total idle time = 35+(40-23)+(31-19)+(27-16)+25=100>75

Station1	Unit 1	Unit 2	Unit 3	Unit 4
Tasks 1,2&3	45	28	23	20
Station2	Unit 1	Unit 2	Unit 3	Unit 4
Tasks 4	30	26	23	21

Total idle time = 45+(30-28)+(26-23)+(23-20)+21=74<111

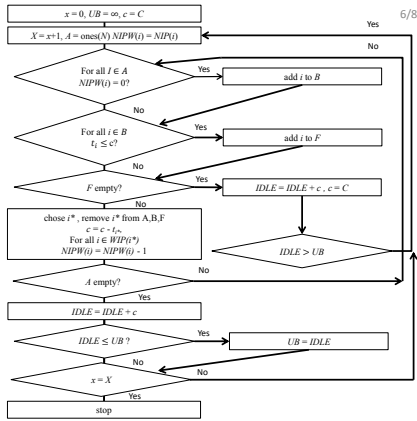
## Analysis method

5/8

### Procedure

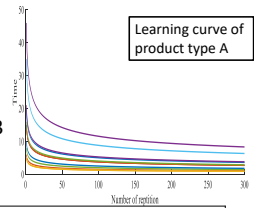
1. Sequence tasks to workstations
2. Apply learning effects
3. Pick most optimal solution
4. Repeat step 1 to 3
5. Apply solutions to each product type
6. Schedule multiple product types
7. Change parameter and repeat step 1 to 6

		Product type			
		A	B	C	D
Task No.	1	20	23	19	17
	2	6	5	5	8
	3	5	4	8	4
	4	21	23	17	24
	5	8	10	11	5
	6	35	33	30	38
	7	15	13	18	12
	8	10	17	7	6
	9	15	18	18	19
	10	5	9	3	7
	11	46	41	48	43
	12	16	13	12	19



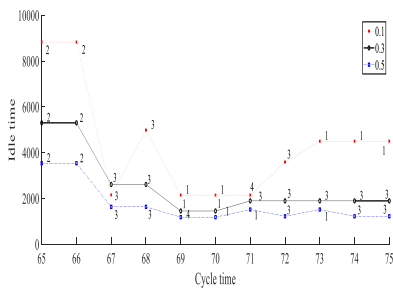
Result –effect of learning effects-

- Conditions
- 4 product types A,B,C,D
  - 12 tasks for each types
  - 50,50,100,100 demands
  - $a_j$  (learning coefficient) is 0.3
  - Cycle time is 70



		Product type			
		A (50 items)	B (50)	C (100)	D (100)
learning effect	without	674	480	1808	924
	with	354	379	578	380

Result –changing parameter-



Idle time is decreasing as  $a_j$  (learning coefficient) is increasing

<4> Findings through JUACEP	
● Students' reviews	...58
● Questionnaires (in Japanese)	...68

## Findings through JUACEP

**Name:** Yoshiyuki Tange

**Affiliation at home country:** Department of Mechanical System Engineering,

Graduate School of Engineering, Nagoya University

**Participated program:** Short course 2017

**Research theme:** Design of micro-device to implement in *Micro-Piercing Method*

**Advisor at the visiting university:** Prof. Katsuo Kurabayashi

**Affiliation at visiting university:** Mechanical Engineering, Univ. of Michigan



My stay in Ann Arbor was for two months, but I had a lot of experiences through JUACEP program. I lived in the house with one family and a UM student. The daughter chatted with me in English every day. It helped me to build up my English speaking and hearing ability. The mother sometimes asked me how to cook Japanese dishes. I showed her cooking “Nikuzyaga” and told her that it is said a woman who can cook “Nikuzyaga” can be married in Japan. The other day, she told me that it is said the middle child is often cared by nobody in U.S. I think there are a lot of cultures you cannot know without actually staying and talking. I was worried about living in an unknown person’s house before staying but I had good opportunity to communicate with people having different cultures.

The lab members were also friendly and kindness. A Ph.D. student always advised me about my research. It was surprised for me that Ph.D. students are diligently proceeding two or three projects and all projects were innovative. I would like to follow their attitudes for researching and working in Japan.

Ann Arbor is beautiful and safety city. You can do kayaking, running and cycling in the city. A lab member took me Huron River and we enjoyed kayaking. It was first time but I felt great nature. There were many runners and running shops in Ann Arbor, so I bought new running shoes and did running around my house every day.



## Findings through JUACEP

**Name:** Hiroki Fujiwara

**Affiliation at home country:** Aerospace Engineering, Nagoya University

**Participated program:** Medium course: August 2017-January 2018

**Research theme:** Demonstration of Digital In-Line Holography for Primary breakup of Water Column

**Advisor at the visiting university:** Prof. Mirko Gamba

**Affiliation at visiting university:** Department of Aerospace Engineering, University of Michigan



### Academic life and findings

Research through **JUACEP** has offered me a chance to broaden my scientific knowledge, and understand some differences in research culture. My research topic in Michigan was to investigate similar phenomenon that I have worked in Nagoya, by different technique. This required me a whole new set of knowledges, and for the first several weeks, I had hard time learning new concepts in English from textbooks and I felt like I wasn't making any progress. When I started doing experiments, however, I realized having fundamental knowledge is crucial when deciding experiment plans. Furthermore, I learned many lessons from professor and Ph.D. students, such as to have clear understanding and confidence of every steps of experiments, know what results I expect to get before experiments, and so on. Every lessons I learned here is meaningful and would definitely change the way I tackle challenges on my research in the future.

Having worked and talked with many Ph.D. students in the U.S., I realized that although research is always tough, they are satisfied with their decision of pursuing Ph.D. and they were fully committing to research. From what I have learned, this is because American society has systems of utilizing their talent in the real world. I also realized that many companies come to the university to hire students, and students were always asked to think about the impact of their research to the society. What I also learned is that master programs in the U.S. are more focused on the course work, and students don't have chance to do research. Being able to do research as a master student in the U.S. was thanks to this **JUACEP** program, and I also thought that I should take advantage of being able to do research in Japan as a master student.



### Daily life and findings

**JUACEP** wasn't just all about research, but was a great opportunity to experience American culture and having fun with new friends. I celebrated Thanks Giving Day, Christmas with delicious food, went to football game and surprised by their school pride, traveled around the U.S., and more. I even enjoyed having lunch with lab mates every day, and shared many ideas and thoughts. What I liked most about American life was the diversity of people and their ideas. In Japan, I felt the pressure of having to have similar ideas with other people. In the U.S., however, people shared the idea that it is natural to have different ideas with others, and made conversation to understand more about others' ideas. After understanding this, I learned the importance of expressing my own idea, in my own words. People were kind enough to understand my point even with my poor English.



## Findings through JUACEP

**Name:** Makoto Takeuchi

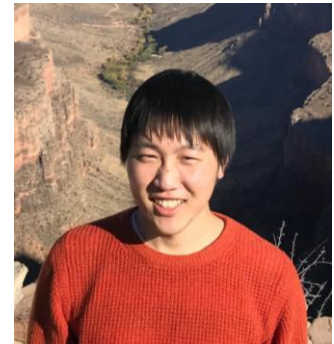
**Affiliation at home country:** Micro-Nano Mechanical Science and Engineering, Nagoya University

**Participated program:** Medium course 2017

**Research theme:** Thin alumina films via colloidal processing of flame made nanopowders

**Advisor at the visiting university:** Prof. Richard M Laine

**Affiliation at visiting university:** Materials Science and Engineering, University of Michigan



Firstly, I would like to express my gratitude to Prof. Richard M. Laine and everyone involved in this program for providing me with such a precious opportunity. It has been the best thing I've ever done in my life, and I'll never forget what I have learned through the life in the US.

Studying at the University of Michigan has taught me how to survive & thrive in any new environment.

Having done a couple months' preparation, I arrived at Ann Arbor, Michigan in August, 2017, thinking how good of a time I would have for the next 6 months.

However, the life in the US, at first, was not as easy as I had expected it to be. Since my research field was originally in mechanical engineering, I went through hard times involving myself in a completely new field. In addition, I had to overcome the language barrier (even ordering foods at fast food restaurant used to be challenging for me). However, thanks to my professor, lab-mates, friends outside of school, etc. (can't list all of them), I managed to get involved in the research life and/or the life in the US somehow.

Along with the research at the University of Michigan, I've enjoyed my life there. I can't even remember everything that has happened, such as traveling around several cities in the US (Los Angeles, Grand Canyon, Miami, D.C. etc.), watching football games (in the US, football is the most popular sport), which was really exciting, or just hanging out with friends. I especially liked visiting Los Angeles during thanksgiving break. It looked completely different from Ann Arbor in terms of race, culture, etc., which again made me realized that I had been living in my own little world.

Through my 6 month of experience in the US, what I learned the most is that in any situation, it is to take action and to have everyone involved rather than to hesitate alone.

Thanks for the great experience of a lifetime!



## Greatest experience to change my mind

**Name:** Taro Mizutani

**Affiliation at home country:** Mechanical Engineering, NU

**Participated program:** Medium course 201/8/8 ~2018/1/29

**Research theme:** Analysis of assembly line with learning effects

**Advisor at the visiting university:** Prof. Theodor, Prof. Hu

**Affiliation at visiting university:** Mechanical Engineering, U of M



It was my first visit abroad, so I didn't know everything about US before this program. As soon as I arrived in the US, I was surprised by using extremely expensive taxis. I was also surprised by the high prices of food and drinks in restaurants, and I was very worried about whether I could survive here on my own. According to those I knew, I couldn't totally understand the English people were speaking, and my English was hard for foreigners to catch. But for people like me, Ann Arbor is a good place to visit or live because there are many kind people here. For instance, almost everyone answered me kindly when I asked something, or they kept their doors open for the next person. I was always helped by someone kind, and thereby I could finish this program.

Talking about research, I could decide my research topic after discussing with my professor. The professor was thinking about my future work at a company and what you want to know thoroughly, and found a very suitable topic for me. Since the topic is very interesting for me, I could research eagerly, and my feeling was fulfilled with motivation to develop this topic. I could meet with the professor every week and have one-on-one discussions for a long time. It helped me to improve and develop my research. The difference in the way to research in Japan and the US is, for me, that I could do as I want to do in the US. It might be because I am an exchange student, though. Since the U of M is one of the good universities in the world, students and laboratory members were smart and helped me a lot of times.

Besides research, there are many opportunities to meet new people I don't know here. I went to many events and could make international friends. I rarely have a chance to talk with foreigners, so it was very stimulating for me and could know different ways to think for many things. Though there is almost no place to visit in Ann Arbor, most of the people living here are students. It helps us to get to know each other easily, and we would be best friends.

Lastly, I would say it was the greatest experience for me in my life. If I have a chance to experience something like this program, I will apply it positively.



## Findings through JUACEP

**Name:** Makoto Terada

Micro Nano Mechanical and Science Engineering, Nagoya University

**Participated program:** Medium course 2017

**Research theme:**

**Advisor at the visiting university:** Prof. Albert Shih

**Affiliation:** Mechanical Engineering, University of Michigan



I spent 6 months in University of Michigan. Firstly, I mention my research environment. I belong to the group of Prof. Albert Shih lab. They focus on biomechanical and they manufacture tissue mimicking material by 3D printer. At first, it was hard for me to catch up with other people in my laboratory because I had never studied that field. But, professor and members in my lab are so kind. Because they supported my research and I discuss my research with them, I could advance my research. Moreover, they sometimes took me dinner and playing. It was very good time to know their backgrounds and make friendship. Especially, Kai who is my mentor took me various places like Costco and casino in Detroit. All of these are good experiences for me. They would be leaders of industry, so I want to work with them as a coworker in the future.

Secondly, I would like to share my daily life. It was first time to live in US, so everything is new for me like sharing room, food, shopping and so on. In US, we need to pay money by credit or debit card. I realized convenience and risk of cards because my card was skimmed. So if you want to live in US, you should make some credit cards and be careful to save your cards.

Sometimes, I tripped to many places in US like Boston, Las Vegas and Niagara Falls. Especially, Red Rock Canyon, it's close to Las Vegas, was the best place to visit because the view of driving course was beautiful, we could go there 30 min from Las Vegas and it was very cheap. Actually, it's not so famous in Japan, but if you have time, I recommend you to visit there.

Finally, I really appreciate Japan-US Advanced Collaborative Education Program (JUACEP) for giving me such a great time.



## Findings through JUACEP

**Name:** Tatsuya Okamoto

**Affiliation at home country (Dept & Univ):**

Dept. of Micro/Nano Mechanical Science of Engineering, Nagoya Univ.

**Participated program:** Medium course (Aug. 2017 – Jan. 2018)

**Research theme:** Ab Initio Molecular Dynamics Simulation about Dielectric Properties of Boron-doped Diamond-Like Carbon

**Advisor at the visiting university:** Prof. L. Jay Guo

**Affiliation at visiting university:**

Electrical Engineering and Computer Science, University of Michigan



### Research in University of Michigan

I'd like to mention about my research at University of Michigan. The field of research in Prof. Guo group was completely different from what I did at Nagoya University. Before coming to the US, I thought my project theme in university of Michigan would be provided from Prof. Guo. However, the policy of Prof. Guo group was needed to prepare my theme by myself. First of all, I tried to make my new including both fields, Nagoya University and University of Michigan. It was of course first time to create my theme by myself, I read paper a lot, and finally, I can propose my theme to my Prof. Guo and he gave me an acceptance of my new theme. Then I started to my theme. I did research based on what I proposed for about four months. However, because of the theme I create was lack of detailed consideration, so I got in the situation to need to change theme. So I changed my theme to new one based on ab initio molecular dynamics simulation. I think big difference about research between Japan and US is the process of thinking. This research experience changed the view of thinking for the research.

### Life in University of Michigan

I stayed the house with three roommates for six months. The lifestyle was full of freedom, can do everything we want to do. Before coming to the US I thought I want to start something new for me, so I started Marathon. And I joined the running group which found on Facebook. I run the Detroit marathon. I also joined soccer team because my roommate invited me to his soccer team. I practiced soccer every weekend to entry the tournament. Our team won the first prize finally.



## Findings through JUACEP

**Name:** Yudai Suzuki

**Affiliation at home country (Dept & Univ):** Aerospace Engineering,  
Nagoya University

**Participated program:** Medium course 2017

**Research theme:** Failure Detection and Control of Distributed Electric  
Propulsion Aircraft Engines

**Advisor at the visiting university:** Prof. Anouck Girard

**Affiliation at visiting university (Dept & Univ):** Aerospace Engineering,  
University of Michigan



The life in Ann Arbor was the most amazing 6 months that I have ever had in my life. Here, I would like to introduce three things that made my life amazing and meaningful.

The first thing is the experience in my lab. Fortunately, thanks to great help of the JUACEP staff, I could get a chance to stay in a lab whose research area is very close to my interest and my research in Nagoya. The research experience was fulfilling. Compared to the lab life in Japan, I could devote more energy to only my own research because there are not any other tasks than doing my own research in the lab. Additionally, my mentor PhD student understood my poor English well and gave me helpful and insightful advices about my research direction every week. As a result, I was able to get research results simultaneously while pursuing my interest. This fulfilling time of research gave me a chance to think about what I want to do in my career. Now I want to continue working on my specialization field as an engineer. This experience helped me to have more concrete ideas about my career.

Many friends I met in the United States made my life too. At the beginning when I came to Ann Arbor, I had to do many things by myself to settle down to the new environment. It was a difficult time. However, I could enjoy this time a lot with helps of friends who I met here and are from Nagoya. I truly realized that we can't live without any helps of others because the friends in Ann Arbor made a difference in this situation. As far as I know, many friends have such warm hearts that gave me helps without expecting anything in return. In Japan, when someone does something helpful, I think we usually feel like that we owe them for what they have done for us so we have to do something in return, and vice versa. I suppose American people that I met here have less feelings like this, so they helped us a lot without expecting anything in return. Making many friends who are Christians was also a unique experience. Because there are very few people who have strong views on any religions in Japan, it was a unique and meaningful experience for me. They are rich in the spirit of giving helps to neighbors without expecting anything in return and accepting other's shortcomings or brokenness. I respect this aspect of them so much, and it was also a good chance to reflect on myself.

The third thing is all the experiences in the United States. I visited many places: Houston, Detroit, Niagara Falls, Grand Canyon, Las Vegas, Washington D.C, and Boston... It was fun and expanded my knowledge and vision. It was a privilege to work as a volunteer in Houston for Hurricane damage. I also enjoyed the nature in the Grand Canyon area the most. I spent New Year holidays with a lot of international students from all over the world in D.C. It was a memorable experience. Harsh winter in Michigan was also enjoyable.

At last, I would like to say the biggest thank you to my mentor, Will. He is such a great engineer that helped me a lot. Without his help, I couldn't spend such a fulfilling time in the lab. I highly recommend this program to those who are interested in studying abroad or broadening their visions through the lives in foreign countries no matter what their English levels are. Helpful and nice people would give you a lot of helps if you are open-minded enough then you might spend a wonderful life there.

## Findings through JUACEP

**Name:** Yusuke Fukui

**Affiliation at home country:** Mechanical Systems Engineering

**Participated program:** Medium 2017

**Research theme:** Developing Immersive Virtual Realities for Human Upper Limb Motor Recovery after Stroke

**Advisor at the visiting university:** Prof. Jacob Rosen

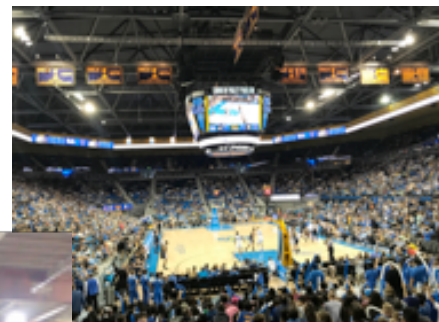
**Affiliation at visiting university:** Mechanical and Aerospace Engineering at UCLA



The Japan-US Advanced Collaborative Education Program (JUACEP) has been one of the most exciting experiences in my career. I really appreciated JUACEP giving me this opportunity because I experienced so many things which are tough and also great. At first the life in LA was very challenging for me because of my English skill, and also because everything is different from Japan. But it has been so good so far and I feel LA is my home city right now. LA has so many diversity and cultures, which give me chances to learn about many countries. Therefore, I have become much more open-minded and I got confidence to live in the English speaking countries. It would be grateful if I have a chance to come back to LA near my future.

Friends in UCLA and in my lab are really competitive and smart. I could learn lots of things from them. Their knowledges are very adorable in wide fields. And they are so friendly that they took me many places for local people even on my first day in the lab. That made me so surprised because I feel it's really different culture and thanks to them, I could get used to LA so fast. And also they gave me some opportunities to enjoy American cultures. For example, my American friend invited me his home to enjoy thanksgiving dinner with his family. I talked with his family a lot and enjoyed the special dinner. That's so sweet and one of the best memory for me. My English skills were not so good, but my lab members were very welcoming. It was great to be in a laboratory environment with hard working staff, I really appreciated them.

The research in UCLA is very attractive and state-of-art, which gave me great experience about VR (Oculus VR) and coding skills (C#). The field of computer science and also VR is getting more popular drastically. It was very grateful for me to study the field in UCLA and in this laboratory. My professor assigned me to a leader position. So I could learn not only computer science skills, but also leadership and how to collaborate with many people including professor of other department and people who work for a company in NY. This experience encourages me to enter IT field after graduation. Overall, the program gave me great opportunity to feel environments studying in US and to meet adorable people who are friendly and open to socialize outside of work.



## Findings through JUACEP

**Name:** Matsubara Fuga

**Affiliation:** Micro-Nano Mechanical Engineering and Science,  
Nagoya University

**Participated program:** Medium course 2017

**Research theme:** Shelf-life testing of bioink-containing tablets  
for 3D Pharming

**Advisor at the visiting university:** Prof. Benjamin M. Wu, DDS, PhD

**Affiliation at visiting university:** Bioengineering, UCLA



I've studied bioengineering in UCLA for 6 months as VGR under supervision of Dr. Benjamin M. Wu. The research life was extremely exciting. In the lab, there are various people who have different nationalities, cultures, values and so on. This diversity that I'd never experienced really inspired my brain because I was a typical Japanese who was born and raised in Japan. At the beginning of the stay, it was very tough to understand them due to my lack of language ability and knowledge of their cultures. But lab members were really helpful and made up my lacks. And now, I'm really missing them. I'd never been boring in such multinational environment any time. I had much fun even in daily conversation with lab members. Previously, I knew only Japanese culture and persisted on it, but now, the way of thinking has been changed completely. I love diversity.

Next, I'd like to talk about research. I was involved in 3D Pharming project and conducted some experiments. 3D Pharming is the use of 3D printing to fabricate personalized medicine. Ordinary pharmaceutical products are defined by the amount of drug. However, it is weird that many people who have different physical and genetic profiles take same medicine. Consequently, this one size fit approach fails. The aim of this project is to invent technology that can fabricate personalized pharmaceutical tablets by using 3D printing. I really impressed by its possibility to bore innovation in pharmaceutical field. This research was brand new for me. Therefore, I had to read many papers to get background knowledge. It was really heavy and I couldn't sleep a couple of days. But such research days were interesting for me because I like learning new things. Fortunately, my supervisor allowed me to design the experiments. So, I could do them as I like. And luckily, I totally succeeded and the results were almost good. I'm honor of having done research as a member of such state of the art project.

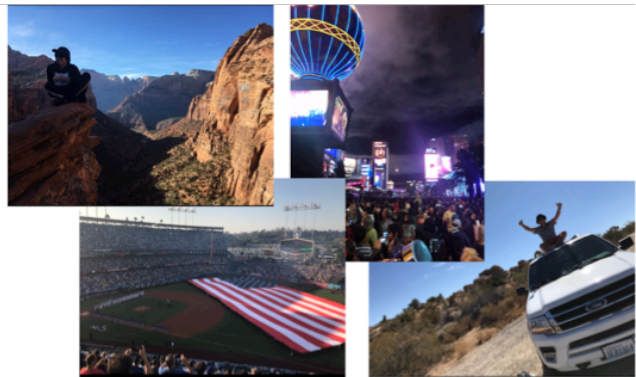
In day off, I traveled many cities such as New York, Las Vegas, San Francisco, San Diego, Boston. In each city, I got unforgettable memories. Every city have their own color and I enjoyed them. National parks were also amazing. I could have visited most of national parks in US and seen absolutely splendid view. I really like nature. Sometimes, we had car trouble or something bad during trip, but they strengthened my mental so much and are good memories now.

Finally, I'd like to say thank you to Dr. Wu and all other lab members for supporting my research and being very kind to me. Without their help, I wouldn't have made nothing. And I appreciate JUACEP for giving me such awesome experience to study in UCLA. This experience changed my life and I'm sure that it'll give positive impact to rest of my life. If I can, I want to come back to LA especially when Japan is in winter.



**Last Meeting**

**Lab Dinner**



## My 6 months in LA LAND

**Name:** Kai Iio

**Department of Molecular Bioengineering Nagoya University**

**Participated program:** Medium course

**Research theme:**

**Advisor at the visiting university:** Prof. Gerard Wong

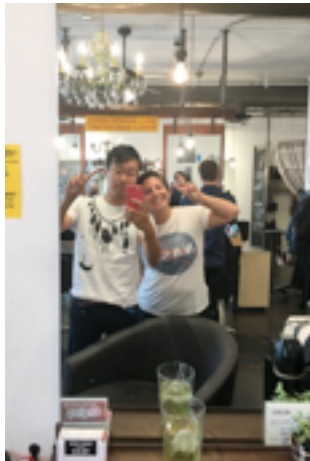
**Department of Bioengineering UCLA**



I am in my second year for my master's. Participating JUACEP program delayed my graduation for 1 year, but I had a wonderful experience in the US. I stayed in LA for 6 months. The best memory in L.A. is that I made a lot of friends all over the world. Los Angeles has many nationalities. So I met people from all over the world in the past 6 months. I hang out with them around Los Angeles, and I traveled in Canada and Mexico with them. We talked about various things such as culture, religion and the image of Japan. I was shy before I went to L.A., but I think it was improved a little bit. Because foreign people basically speak more than Japanese people so I talked more than when I am in Japan. I wish I could go to the countries of my best friend. I really realized that even if the nationality is different, I can make friends. If I can speak English more fluently, I could have more friends. So I will continue to practice English after I return to Japan. Also, I would like to know more about the cultures and histories of the world. Those will help me to communicate with foreign people. So I do recommend L.A. to next JUACEP students. (But things are very expensive.)

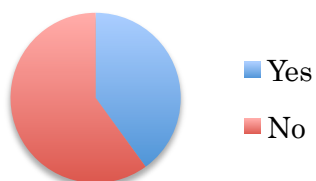
In terms of research in UCLA, I learned the flow of research. First, I make the hypothesis, and then set a proper experiment that can answer the hypothesis precisely. And make new hypothesis from the results of experiments. My research theme was b

acterial biofilm. Using computer programming and a microscopy, we observed bacterial behavior. It was so difficult to research because I didn't study computer programming. But I think it was good experience for me to discuss with my professor and laboratory members and to write JUACEP report in English.

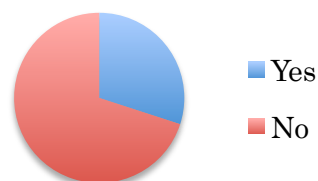


派遣プログラム参加者に行ったアンケート結果  
 <博士課程進学に興味がある>

留学前

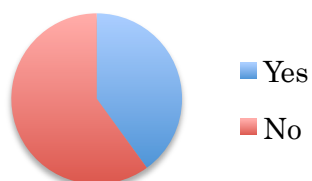


留学後



<外国の大学での博士課程進学に興味がある>

留学前

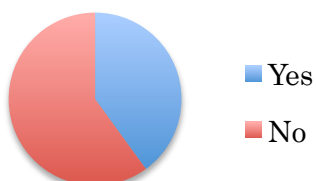


留学後



<日本での外資系企業への就職に興味がある>

留学前



留学後



<外国での日系企業への就職（海外勤務）に興味がある>

留学前



留学後



<外国での日系以外の企業への就職に興味がある>

留学前



留学後



## 1. このプログラムの良かった点

- UCLA という世界トップレベルの環境で研究することが出来たのはとても貴重な経験だった。
- コミュニケーション能力や、異文化に対する理解など、得るものがかなりあり、成長できたという実感がある。
- 奨学金が受けられる点。
- 留学前からのサポートが手厚かったところ（留学中に必要な保険などの情報が得られた）。
- 6ヶ月ともなると一時日本の大学を休学または留年をしないといけない留学プログラムがほとんどですが、それが無いというのが JUACEP 留学を決めた一つのきっかけでした。また、プログラム前に相手先の大学の人たちとの交流の場を設けていただいたおかげで、留学先でも交流が続き、いろいろ助けてもらったりすることでこちらでの生活がしやすくなりました。
- 家を探す、研究室を探すなど自分でやらなくてはならないことが多かった分、国内にいる段階から英語でのメールのやり取りや事務的な作業のプロセスが体験できてよかった。また、実績のあるプログラムなので昨年参加した先輩方からのアドバイスや経験談を聞く機会がありイメージが湧いた状態で渡米できたので短い時間でも有意義に過ごすことができた。
- ミシガン大学・UCLAという優れた大学で、今までと異なる研究分野でも自ら受け入れ先を探すことが可能な点。
- 自分から行きたい研究室にメールで依頼しなければならないところ。（大変だがやりがいがある）
- レポートの提出以外は自由に時間を使えたこと。
- JUACEP のおかげで、大変貴重な経験をすることができました。アメリカの、特にトップ校の一つである UCLA で研究をする機会はこのプログラムでしか得られないものであったと思います。この経験は自分自身を大きく変えてくれたと考えています。良かったことばかりでした。
- 給付型奨学金が参加者全員に支給されたことがとても助かりました。また、滞在する研究室を自分で選ぶ段階で、その研究室の教授から滞在許可を得られるようスタッフの方に支援していただいたおかげで、自分の興味や、研究内容に十分近い研究室を選ぶことができ、充実した研究経験を得ることができました。



## 2. このプログラムで改善してほしい点

- 英語に関してのサポートがもっとあればよかった。(どうにかなりましたが、苦勞もありました)
- 家探しをサポートなしで短期間にすべて自分で行わなくてはいけない点。本当にむずかしい。
- 家が決まるまでのホテル代が出ると助かる。
- 渡航前の必要事項等を伝える説明会がやや遅かったと思う。
- 奨学金が家賃でほとんど消えていく点。
- 8月スタートということで授業が始まっておらず、それに伴い交通サービスが悪く、留学の初めはとて戸惑った。また宿舎を見つける際も、セメスターごとで募集しているところが多くてかなり苦勞した。アメリカのセメスターに合って入れば、それらの点での苦勞が少なくなると思った。
- 航空券の補助をしてほしいと思った。2ヶ月の奨学金は全て航空券の費用となってしまった。
- 半年間で2単位しか付与されない点。
- 評価シートの成績の付け方などを受入先の教授に質問されたが、口頭でうまく説明するのは難しかった。大学から明確な説明を受け入れ先に周知してほしい。
- 授業も少し受けてみたかったので受けられるようなシステムがあるといい。
- 住居費だけで1000ドルはするのでお金がたりなかったこと。
- 英語の講座などを事前にワークショップの形で受ける機会があるとより良いと思う。LAでの生活でやはり大変だったことは英語力に尽きる。英語力は普通以上だと思っていたが、実際にこちらに来てみると、かなり大変さを感じた。英語力について事前に危機感を持たせておくことが重要だと思う。
- 条件の良い滞在宿舎の確保のために支援していただけるとよいと思います。期間中の滞在先は、生活の便だけでなく、留学の満足度に大きく関わってきます。私の場合は研究室のあるキャンパスに近い部屋を見つけることができなかつたため毎日1時間近くかけて研究室まで通わなければならず、少なからず負担になりました。

## 3. その他、自由コメント

- 行く前は不安もありましたが、今は参加してとてもよかったと思います。日本では経験できないようなことばかりだったので、刺激的な毎日でした。研究室の仲間たちは皆研究に関するモチベーションが非常に高く、大いに影響を受けました。この研究留学プログラムを通して、海外でのキャリアや、博士進学の可能性も感じました。修士卒で日本国内の有名企業で働けばいいかなという曖昧なビジョンしかなかったのですが、将来のことを一から考え直すとてもいい機会



にもなりました。

- 奨学金付きで貴重な経験をする機会をいただき誠にありがとうございました。必ず残りの人生にプラスに作用するという確信があります。
- このプログラムは自身にとって大変貴重な体験になりました。私がこのプログラムを知ったきっかけは研究室の先輩に教えてもらったからでしたが、そうでなければ知らないまま終わっていた可能性があります。ぜひもっと多くの人にこのプログラムとその良さを知ってもらいたいと思います。
- 渡米後まもなく所属研究チームのメンバーが自分の宿舍のシェアを無償提供してくれた（約3週間）。その間に家探しをすることができて本当に助かった。
- 滞在した研究チームはほとんど留学生。国際色の豊かさを経験した。
- 説明会や倉林先生と事前に顔をあわせる機会を設けていただくなど渡米、留学に対する不安が少しでも和らぐように色々な気配りをしていただきありがとうございました。
- サポートしていただきありがとうございました。いい6か月を過ごすことができました。
- このJUACEPは本当に自分にとっていい経験でした。様々な面から成長できたと感じています。
- アナバーで出会った人たちはとても優しい人が多く、積極的に色々と助けてくれたおかげで、充実した留学期間を過ごすことができました。
- JUACEPに関わる人々には大変お世話になりました。様々な面からサポートしてくださり、またたくさん相談に乗っていただき、とても感謝しています。ありがとうございました。



Copyright © JUACEP 2018 All Rights Reserved

Published in October 2018

Japan-US-Canada Advanced Collaborative Education Program (JUACEP)

Graduate School of Engineering

Nagoya University

Furo-cho, Chikusa-ku, Nagoya 464-8603, Japan

JUACEP@engg.nagoya-u.ac.jp

<http://www.juacep.engg.nagoya-u.ac.jp>